The Transmembrane Protein Golden Goal Regulates Retinal Axon Guidance In *Drosophila*

Dissertation

der Fakultät für Biologie
der Ludwig-Maximilians-Universität München

Angefertigt am Max Planck Institut für Neurobiologie

Vorgelegt von
Tatiana Tomasi

München, 10. Juni 2008

Erstgutachter:	**Prof. Dr. Rüdiger Klein**
Zweitgutachter:	**PD. Dr. Angelika Böttger**
Tag der mündlichen Prüfung:	**11.08.2008**

Ehrenwörtliche Versicherung

Hiermit, erkläre ich, dass ich die vorliegende Dissertation selbständig und ohne unerlaubte Hilfe angefertigt habe. Ich habe mich dabei keiner anderen als der von mir ausdrücklich bezeichneten Hilfen und Quellen bedient.

Erklärung

Ich erkläre hiermit, daß ich mich nicht anderweitig ohne Erfolg einer Doktorprüfung unterzogen habe. Die Dissertation wurde in ihrer jetzigen oder ähnlichen Form bei keiner anderen Hochschule eingereicht und hat noch keinen sonstigen Prüfungszwecken gedient.

München, Juni 2008

Tatiana Tomasi

Die vorliegende Arbeit wurde zwischen April 2005 und Januar 2008 unter der Leitung von Dr. Takashi Suzuki am Max-Planck-Institut für Neurobiologie in Martinstried durchgeführt.

Table of Contents

Deutsche Zusammenfassung 1
Abstract 3
Publication from the work presented in this dissertation 4
Abbreviations 5

1 Introduction 7
1.1 Molecular mechanism of axon guidance 7
1.2 The visual system of the fly 10
1.3 Visual system development 13
1.4 Known regulators of photoreceptor axon guidance 19
1.5 Screen for novel regulators of R axon guidance 22
1.6 The thesis project 24

2 Materials and Methods 25
2.1 Media 25
2.2 Instruments 26
2.3 Enzymes and Standards 26
2.4 Commercial Kits 26
2.5 Oligonucleotides 27
2.6 Plasmids 28
2.7 Bacteria strains 31
2.8 Antibodies 32
2.9 Cell culture lines 33
2.10 *Drosophila melanogaster* lines 33
2.11 Molecular biology methods 37
2.12 Generation of transgenic flies 43
2.13 Fly genetics 46
2.14 Summary of experimental genotypes 49
2.15 Bioinformatics (performed by Alexander Schleiffer) 51
2.16 Cell culture 52
2.17 Fly maintenance 53
2.18 Biochemistry 54
2.19 Histology 55

3 Results 60
3.1 Gogo is required for R axon pathfinding 60
3.2 Gogo is evolutionary conserved 63
3.3 Gogo requires the GOGO and Tsp1 domain 65
3.4 Gogo requires the cytoplasmic domain for its function 67
3.5 Gogo is dynamically expressed in the developing visual system 68
3.6 *gogo* brain expression is not required for R axon guidance 72
3.7 Identification of the *gogo* enhancer fragment 74
3.8 *gogo* is required for the assembly of lamina cartridges 77
3.9 *gogo* functions in R8 but not in R7 axons 79
3.10 In larvae *gogo*$^-$ R8 axons lose repulsive interactions 81
3.11 R8 target recognition is impaired in *gogo* mutants 85
3.12 Gogo functions in R8 target layer selection 88
3.13 Gogo mediates axon-target recognition at the R8 temporary layer 90
3.14 Gogo overexpression anchors R8s at the M1 layer 94

4 Discussion 97
4.1 Autonomous receptor function in photoreceptor cells 97
4.2 R8 axon-axon interaction 100
4.3 Axon-target interaction 103
4.4 Possible genetical interaction with the cadherin Flamingo 109
4.5 Outlook 111

Bibliography 113
Acknowledgements 122
Curriculum vitae 123

Index of Figures

Figure 1-1 Axon guidance mechanism 8
Figure 1-2 Schematic representation of the Drosophila visual system 11
Figure 1-3 Medulla layering 12
Figure 1-4 Visual system development during 3rd instar larval stage 14
Figure 1-5 Developmental timetable 16
Figure 1-6 Target layer selection of R7 and R8 axons 17
Figure 1-7 *gogo* mutant alleles and protein structure 23
Figure 3-1 Pathfinding defects of *gogo* mutant R axons. 61
Figure 3-2 Onset of developmental defects 62
Figure 3-3 Evolutionary conserved Gogo domains 64
Figure 3-4 Structure-function analysis 65
Figure 3-5 *gogo in situ* staining in eye discs and optic lobes 68
Figure 3-6 Gogo expression during larval development 69
Figure 3-7 Gogo is dynamically presented on R axons during pupal stages 71
Figure 3-8 Gogo is autonomously required in R axons 73
Figure 3-9 *gogo* enhancer fragment bashing 76
Figure 3-10 Lamina cartridge formation in *gogo* mutants 78
Figure 3-11 *gogo* functions in R8 axons, but not in R7 80
Figure 3-12 Schematic summary of methods to generate mosaic animals 81
Figure 3-13 Axon bundling in small *gogo* mutant clones 83
Figure 3-14 Larval *gogo*$^-$ R8 axons lose axon-axon repulsion 84
Figure 3-15 *gogo* mutant R8 axons show target recognition defects 87
Figure 3-16 Gogo functions in R8 axon-target recognition 89
Figure 3-17 *gogo* R8 axons prematurely extend from their temporary targets 92
Figure 3-18 Gogo overexpression phenotype 95
Figure 4-1 Model for competitive axon-axon interactions 101
Figure 4-2 Model for R8 axon-target interaction 105

Index of Tables

Table 1 Oligonucleotides 27
Table 2 Destination vectors 1 29
Table 3 Gogo plasmids used for transgenic flies 29
Table 4 Plasmids used in cell culture 30
Table 5 Destination vectors 2 31
Table 6 *gogo* enhancer Gal4 plasmids 31
Table 7 Fly stocks 33
Table 8 Constructed Fly stocks 35
Table 9 Generated transgenic flies 36

Deutsche Zusammenfassung

Während der Entwicklung des visuellen Systems von Drosophila selektieren Photorezeptor (R) Axone ihre Zielzellen Schritt für Schritt. Dabei treffen R Axone mit unterschiedlichen Identitäten ganz spezifische Entscheidungen zu bestimmten Zeitpunkten während der Entwicklung des visuellen Systems.

Das kürzlich identifizierte Transmembranprotein Golden Goal (Gogo) wird dynamisch in allen R Axonen expremiert und lokalisiert vornehmlich in den Wachstumskegeln von auswachsenden Axonen. Gogo wird dort für die Steuerung der wachsenden Axone während der Entwicklung des visuellen Systems benötigt. In *gogo* Mutanten weisen R1-R6 Axone Fehlprojektionen während der Bildung der Lamina Cartridges auf. Dies läßt darauf schließen, daß Gogo für die Wahl der post-synaptischen Partner benötigt wird. Zusätzlich konnte eine sehr spezifische Funktion von Gogo in R8 Axonen gezeigt werden. Gogo wirkt in diesen Axonen an zwei unterschiedlichen Zeitpunkten während ihrer Entwicklung: Gogo reguliert Axon-Axon Interaktionen und Axon-Zielzellen Interaktionen. Der Gogo Mutanten Phenotyp in Larven suggeriert, daß Gogo abstoßende Axon-Axon Interaktionen zwischen R8 Axonen vermittelt und dadurch angemessene Abstände zwischen den Axonen bewirkt. Während den Puppenstadien hat Gogo eine andere Funktion. Hier reguliert es die Erkennung der temporären Zwischenschicht und die Aufrechterhaltung dieser axonalen Position bis zum zeitlich regulierten Weiterwachsen der Axone. Der Phenotyp bei Verlust der Gogo Funktion läßt darauf schließen, daß Axone nicht mehr richtig mit ihrer temporären Schicht interagieren können und dass diese Interaktion Voraussetzung dafür ist, daß R8 Axone in ihre korrekten Zielsäulen einwachsen können und ihre richtige Zielschicht zu innervieren. Die Überexpression von Gogo hingegen führt dazu, daß R8 Axone permanent an der eigentlich nur temporären Zwischenschicht verankert werden. Die beobachteten Überexpressionsphenotypen und dedektierten Proteinlevel in Antikörperfärbungen lassen darauf schließen, daß Gogo nach der temporären Zwischenphase aus den Axonen verschwinden muss und dadurch erst der letzte Auswachsschritt zur finalen Zielschicht M3 initiert werden kann.

Einzelzell-Mosaik-Analysen haben in Kombination mit Rettungsexperimenten gezeigt, daß Gogo autonom in R Axonen benötigt wird. Eine detailierte Untersuchung der funktionellen Domänen läßt darauf schließen, daß Gogo als Rezeptor fungiert, der an einen bislang unidentifizierten Liganden über die Tsp1 and GOGO Domäne bindet. Bei dem kurzen konservierten zytoplasmatischen Tripeptidmotif, daß allen identifizierten Gogo Orthologen gemeinsam ist, könnte es sich um eine vermeintliche

Regulationsstellen und/oder Interaktionsstelle handeln, die intrazelluläre Signalkaskaden auslöst. Die evolutionäre Konservierung des Proteins in verschiedenen Arten läßt auf eine große funktionale Relevanz des Moleküls schließen.

Abstract

During *Drosophila* visual system development, photoreceptor (R) axons choose their correct paths and targets in a step-wise fashion. R axons with different identities make specific pathfinding decisions at different stages during development.

The novel single transmembrane protein Golden goal (Gogo), which is dynamically expressed in all R neurons and localizes predominantly to growth cones, is required for photoreceptor axon guidance in the developing visual system. R1-R6 missorting defects in *gogo* mutants suggest that Gogo is required for the choice of postsynaptic partners during lamina cartridge formation. In addition, a very specific Gogo function was shown for R8 axons, where it acts in two distinct steps of R8 photoreceptor axon pathfinding: Gogo regulates axon-axon interactions and axon-target interactions in R8 photoreceptor axons. *gogo* loss-of-function phenotypes in larvae suggest that Gogo mediates repulsive axon-axon interaction between R8 axons to maintain their proper spacing. During pupal development *gogo* has a distinct function in R8 temporary layer recognition and position maintenance until the proper extension phase. *gogo* loss-of-function phenotypes indicate that only the proper interaction with the intermediate target layer allows R8 axons to enter their correct target columns and target the correct target layer within the medulla. Overexpression of Gogo in R axons permanently anchors R8s to the temporary layer in the medulla. The observed gain-of function phenotype and protein levels detected by antibody stainings suggest that Gogo has to be absent within the axon after the intermediate targeting phase to allow the initiation of the final targeting step, the extension to the M3 layer.

Single cell mosaic analyses, in combination with rescue experiments have demonstrated the autonomous requirement of Gogo within R axons in axon-axon and axon-target interaction. Detailed structure-function experiments argue for a Gogo function as a receptor that binds an unidentified ligand through its conserved extracellular Tsp1 and GOGO domains. A short conserved cytoplasmic tripeptide motif, which is shared by all Gogo orthologues, may serve as a putative regulatory site and/or protein interaction domain triggering intracellular signaling events. The evolutionary conservation across different species implies a high functional relevance of the molecule and probably conserved role in cell-cell communication.

Publication from the work presented in this dissertation

Tatiana Tomasi*, Satoko Hakeda-Suzuki*, Stephan Ohler, Alexander Schleiffer and Takashi Suzuki (2008).
The Transmembrane Protein Golden Goal Regulates R8 Photoreceptor Axon-Axon and Axon-Target Interactions.
Neuron 57, 691-704
* Equal contribution

Abbreviations

APF	Hours after puparium formation
ato	*atonal*
att	attachment
BMP	bone morphogenetic protein
CAM	cell adhesion molecule
caps	*capricious*
ccdB	*control of cell death*
cMARCM	complementary MARCM
CNS	central nervous system
CUB	complement subcomponents Clr/Cls, Uegf, Bmpl
Df	deficiency
Dscam	Down Syndrome cell adhesion molecule
ECM	extracellular matrix
EGF	epidermal growth factor
EGFR	epidermal growth factor receptor
EM	electron microscopy
EMS	Ethylmethansulfonat
En	Engrailed
Eph	Ephrin receptor
ey	*eyeless*
FGF	fibroblast growth factor
FL	full-length
FLP	Flipase
fmi	*Flamingo*
FRT	Flipase recognition target
Gal	genes induced by galactose
GFP	Green fluorescent protein
GMR	Glass multiple reporter
GOF	gain-of-function
gogo	*golden goal*
hh	*hedgehog*
Ig	Immunoglobulin
L1-L4	lamina monopolar neurons 1-4
LAR	receptor tyrosine phosphatase LAR
LB	Luria-Bertani
LOF	loss-of-function
LPC	lamina precursor cell

M1-M10	medulla layers 1-10
MARCM	mosaic analyses with a repressible cell marker
mKO	monomeric Kusabira Orange
mRNA	messenger RNA
N-Cad	N-Cadherin
NGS	normal goat serum
nls	nuclear localization signal
OE	over expression
OPC	Outer proliferation center
PAGE	polyacrylamid gel electrophoresis
PBS	phosphate buffered saline
PCR	polymerase chain reaction
PTP	receptor tyrosine phosphatase PTP
R	photoreceptor
R1-R8	Photoreceptor R1-R8
RGC	retinal ganglion cell
Rh	rhodopsin
RPTK	receptor protein tyrosine kinase
RPTP	receptor protein tyrosine phosphatase
RT	room temperature
S2	Schneider 2 cell
Sens	*senseless*
SNP	Single nucleotide polymorphism
spi	*Spitz*
TEM	transmission electron microscopy
Tm	transmedulla neuron
Tmtsp	transmembrane molecule with thrombospondin module
TmY	transmedulla Y neuron
Trk	tropomyosin receptor kinase
TSP	Thrombospondin
UAS	upstream activating sequence
unc	uncoordinated
w	*White*
Wnt	Wg and Int
WT	wild type

1 Introduction

1.1 Molecular mechanism of axon guidance

Only the precise formation of appropriate neuronal circuits during development enables sensory perception and behavior in invertebrates and vertebrates. During development differentiating neurons extend their axons with astounding precision, sometimes over long distances, to approach their target field. Within this region axons then choose their specific targets among numerous neurons and assemble stable synapses. How are the axons of neurons guided towards their final destination and how do they recognize their cellular targets and finally form stable synapses?

In the developing nervous system, a precise neuronal network is formed in a step-wise fashion through a series of recognition processes. While axons grow towards their targets, they undergo dynamic changes resulting in various decisions: They turn, selectively fasciculate, halt or extend adjusted with the development of the target field. This complex process of axon guidance is controlled by extracellular guidance cues provided by the surrounding environment over short or long range (Figure 1-1).

Within the growth cone, a highly sensitive and motile structure at the tip of extending axons, guidance receptors detect and integrate multiple specific guidance cues along the pathway, which can either be attractive or repulsive, and translate them into motility. Extracellular cues can emanate from other axons that run in the vicinity involving non diffusible cues like cell surface and extracellular matrix (ECM) proteins to assemble the input connections with correct spacing and location. On the other hand axon guidance is also mediated over long range, for example by the target cells secreting diffusible chemoattractants or chemorepellents. Both, axon-axon interactions and axon-target interactions are important for reaching the target and for the selection of specific synaptic partners (Dickson, 2002).

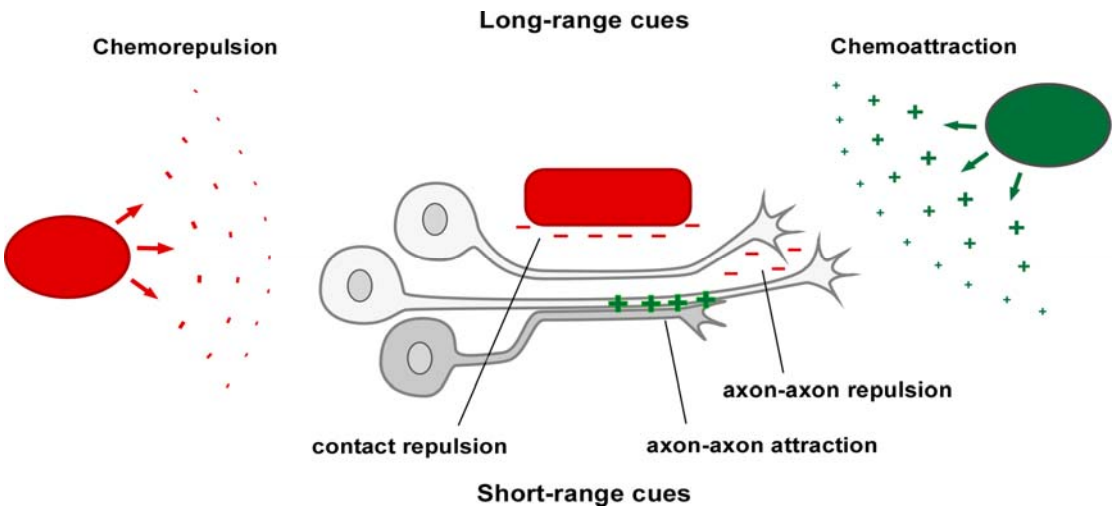

Figure 1-1 Axon guidance mechanism
Different mechanisms contribute to guide growth cones:
Diffusible long-range cues repel (red) or attract (green) axons over a distance (Chemorepulsion or Chemoattraction). In addition, non-diffusible or local cues can be provided to growth cones over short-range. Provided by other axons, repulsive cues (red) result in axon-axon repulsion, whereas attractive cues (green) lead to selective fasciculation (adapted from Tessier-Lavigne and Goodman, 1996).

In recent years several classes of guidance cues and their respective receptors have been identified. Interestingly, they were found to be conserved across different species, showing the evolutionary conservation of axon guidance mechanism.

The first evolutionary conserved diffusible guidance cue identified was netrin (Hedgecock et al., 1990; Mitchell et al., 1996; Serafini et al., 1994). Netrin functions as both chemoattractant and chemorepellent over long range. Attractive and repulsive effects of netrin are mediated by DCC/UNC-40/Frazzeled receptors, whereas UNC-5 receptors act exclusively repulsive (Chan et al., 1996; Keino-Masu et al., 1996; Kolodziej et al., 1996; Leung-Hagesteijn et al., 1992).

Semaphorins form another important family of axon guidance cues. Grouped into eight different classes, this large family encodes both cell-surface and secreted proteins that act either repulsive or attractive upon receptor binding. Semaphorins signal through multimeric receptor complexes, which predominantly include plexin receptors for semaphorin binding and signaling inside the cell. One exception are class 3 semaphorins which require the semaphorin-binding co-receptor neuropilin (Kruger et al., 2005). Studies in flies and mice suggest that semaphorins mainly act over short-range in order to repulse axons from inappropriate targets (Dickson, 2002; Raper, 2000).

The identification of the repellent Slit, a large secreted protein, and its receptor Roundabout (Robo) led to the well-understood models of commissural axon

pathfinding in *Drosophila* and formation of the optic chiasm in vertebrates (Dickson, 2002).

In addition, a variety of receptor protein tyrosine kinases (RPTKs), as FGF, Trk, Derailed/Ryk or Eph receptors and receptor protein tyrosine phosphatases (RPTPs) were found to regulate axon growth and guidance (Barbacid, 1995; Callahan et al., 1995; Desai et al., 1996; McFarlane et al., 1995; Tessier-Lavigne, 1995).

Another important class of axon guidance molecules is formed by cell adhesion molecules (CAMs), which can be divided in the immunoglobulin (Ig) and cadherin subfamilies (Rutishauser, 1993). Cadherins form a large family of transmembrane proteins (Yagi and Takeichi, 2000) mediating strong homophilic interactions (Miyatani et al., 1989). In addition to various roles in nervous system development, they have been proposed to be involved in the regulation of target specificity and synapse formation (Fannon and Colman, 1996).

Recently, several studies have shown that classic morphogens and their molecular gradients can also function as guidance cues, including three classical morphogen families, Wnts, Hedgehogs (Hhs) and BMPs (Schnorrer and Dickson, 2004).

As the examples above show, a variety of extracellular cues and their receptors that guide axons to their targets have been identified (Dickson 2002, Tessier-Lavigne and Goodman, 1996). Nevertheless our understanding of this complex process is still fragmentary. Especially, the high level of specificity underlying neuronal connectivity can still not be explained with the number of known molecules. Therefore it seems likely that additional guidance cues and receptors remain to be discovered in order to further reveal the mechanism of specific axon guidance decisions.

One hallmark of the cellular environment in the nervous system is its tremendous complexity. It is thus particularly challenging to understand the molecular mechanisms that regulate the formation of precise patterns of neuronal connectivity. However, the extraordinary genetic tools available in the model organism *Drosophila melanogaster* allow to analyze single cells within the nervous system and therefore to systematically dissect the complex molecular guidance mechanism. In this study the well described fly visual system was used as a model system.

1.2 The visual system of the fly

It is now 32 years, since the research on the development of the *Drosophila* compound eye began (Ready et al., 1976). Since then the fly visual system has been studied intensively, revealing its beautiful structure and development. The fly visual system comprises the compound eyes (retina) and the optic lobes, the visual processing centers of the brain. The optic lobes constitute about half of the fly's brain and are composed of four neuropils: the lamina, the medulla, the lobula and the lobula plate. The compound eye consists of an array of 800 simple eyes or ommatidia, each composed of eight photoreceptor (R) cell types, R1-R8. R cells can be classified in two subclasses: six outer cells R1-R6 and two inner cells, R7 and R8. Functionally, the outer R cells are responsible for spatial vision, whereas the inner cells, which lie above of each other, function in color vision. Unlike in vertebrates, the retinal axons of the fly directly project into the visual processing centers of the brain. Their precise and complex pattern of neuronal connections has been described at the level of individual neurons (Meinertzhagen and Hanson, 1993).

To reach their proper targets in the optic lobe, photoreceptor axons have to make multiple pathfinding decisions along the way. Based on their spectral sensitivities, R axons target different neuropils within the optic lobe (Figure 1-2A). R1-R6s terminate within the first optic ganglion, the lamina, whereas R7 and R8 axons make layer-specific connections in the second optic ganglion, the medulla (Clandinin and Zipursky, 2002).
In addition to the layer-specific targeting, R axons form a precise topographic map. Both lamina and medulla are composed of columnar units which strictly match the number of ommatidia in the eye. Columnar units targeted by R cells are organized in a strict retinotopic fashion, resulting in an exact map of the visual space reiterated in the optic lobe. R8 and R7 of the same ommatidium, which represent one point in space, project into the same column and each columnar axon maintains a constant distance to neighboring columns (Bazigou et al., 2007; Shinza-Kameda et al., 2006). Therefore, each columnar unit in the medulla represents a single point in space.

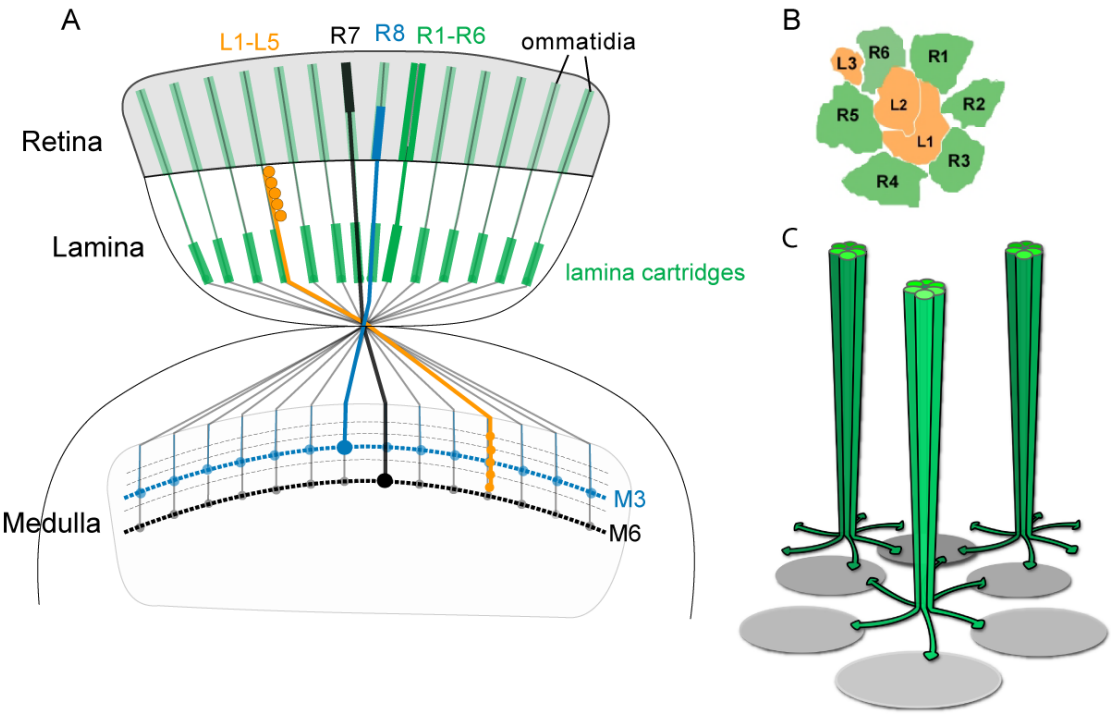

Figure 1-2 Schematic representation of the Drosophila visual system
(A) Adult visual system. R cells in the retina send axons into the brain. Each ommatidium contains 8 photoreceptor cell types. R1-R6 axons (green) terminate in the lamina, where they form lamina cartridges. R7 (black) and R8 (blue) axons extend through the optic chiasm and terminate in two distinct layers in the medulla neuropil, the M6 and M3 layer respectively. Each bundle of R axons is associated with five lamina monopolar axons L1-L5 (orange), which also terminate in different layers within the medulla. Lamina and medulla are composed of columnar units which strictly match the number of ommatidia in the eye. Columnar units targeted by R cells are organized in a strict retinotopic fashion, resulting in a precise map of the visual space reiterated in the optic lobe. **(B)** The lamina cartridge is composed of six photoreceptor cells R1-R6 (green) and their synaptic targets L1, L2 and L3 (orange). **(C)** During lamina cartridge formation, R1-R6 (green) from the same ommatidium defasciculate within the lamina and extend laterally to different cartridges (gray ovals). R1-R6s from different ommatidia but seeing the same point in space converge onto the same cartridge.

In contrast, the connection pattern of R1-R6 has to be more complex in order to represent single points in space. Due to the curvature of the eye the six outer R cells from the same ommatidium 'see' different points in space. According to the principle of superposition, R1-R6 cells deriving from different ommatidia but 'seeing' the same point in space converge onto a single unit within the lamina, the lamina cartridge (Figure 1-2B, C). During lamina cartridge formation R1-R6 cells then form tetradic synapses with the lamina monopolar neurons L1, L2, L3 (Fischbach and Dittrich, 1989; Meinertzhagen and O'Neil, 1991).

As compared to the lamina, the medulla contains more neuronal types and is structurally more complex (Figure 1-3). The mature medulla is subdivided into ten layers (M1-M10) innervated by 50-60 columnar axons (Fischbach and Dittrich, 1989). R8 and R7 axons make layer-specific connections in the M3 and M6 layer,

respectively. In contrast to R1-R6, the postsynaptic targets of R7 and R8 have not been identified yet.

Lamina monopolar neurons (L1-L5) from a single lamina column project via the optic chiasm into specific layers of a single medulla column (Fischbach and Dittrich, 1989). The columnar organization is retained resulting in a one to one correspondence between lamina and medulla columns (Figure 1-2A). As a consequence, each medulla column receives input directly from R7 and R8 and indirectly from R1-R6 via lamina neurons L1-L3. Beside photoreceptor and lamina neurons, a set of higher order neurons can be found, most importantly transmedulla cells (Tm) and transmedulla Y cells (TmY), which also connect to the lobula and lobula plate (Figure 1-3).

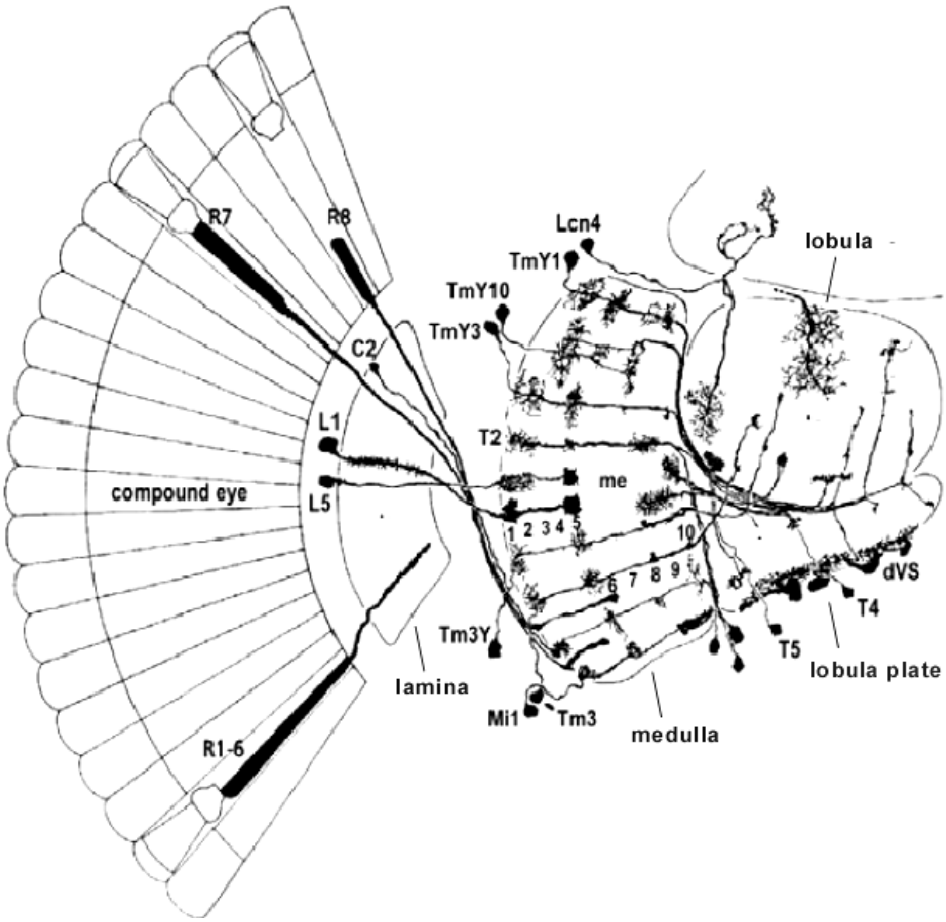

Figure 1-3 Medulla layering

Composite scheme of the left compound eye and optic lobe with camera lucida drawings of Golgi impregnated neurons to illustrate the layering of the medulla. Ten medulla layers are innervated by a large set of columnar axons, each of which showing layer-specific targeting and/or arborizations. Beside retinal and lamina neurons the ten layers of the medulla are innervated by a set of higher order neurons, transmedulla cells (Tm) and transmedulla Y cells (TmY), which also connect to the lobula and lobula plate (adapted from Fischbach and Dittrich, 1989)

1.3 Visual system development

The regular, columnar and layered organization of the visual system in adult flies is the result of a complex developmental program. The development of the *Drosophila* eye takes place in an epithelial bilayer called the eye imaginal disc, or eye disc. Throughout the first and second instar larval stage the eye disc remains unpatterned and grows by cell division. However, in the third or final larval instar, at around 40h before pupation, pattern formation begins (Meinertzhagen and Hanson, 1993).

Sequential photoreceptor differentiation and outgrowth

The differentiation of the photoreceptor cells begins at the posterior of the eye disc and proceeds from posterior to anterior following the morphogenetic furrow (Figure 1-4). Axon outgrowth from the retina occurs sequentially following the wave of cellular differentiation in the eye disc. The first pioneer axons grow out from R8s, which differentiate first and define the trajectories for the following axons, R1-R6 and finally R7, which form fascicles with R8s from the same ommatidium. R axon fascicles first grow towards the base of the eye disc and then turn posterior into the optic stalk, a transient tube-like structure connecting the eye disc with the developing optic lobe. After exiting the stalk they separate again, but they strictly retain their positions according to the retina (Figure 1-4).

R1-R6 axons innervate the first optic ganglion, the lamina, where they select their targets in two temporally distinct steps. Initially, lamina glia cells function as intermediate target cells during larval development by providing a stop signal for arriving R1-R6 axons (Poeck et al., 2001).

R8s continue growing into the medulla, where they form evenly spaced topographic arrays, maintaining ‘inverted-Y-shaped’ growth cones (Senti et al., 2003). As R7s are the last cells to be differentiated and to send axons within each ommatidium, the medulla is mainly innervated by R8 axons during larval development.

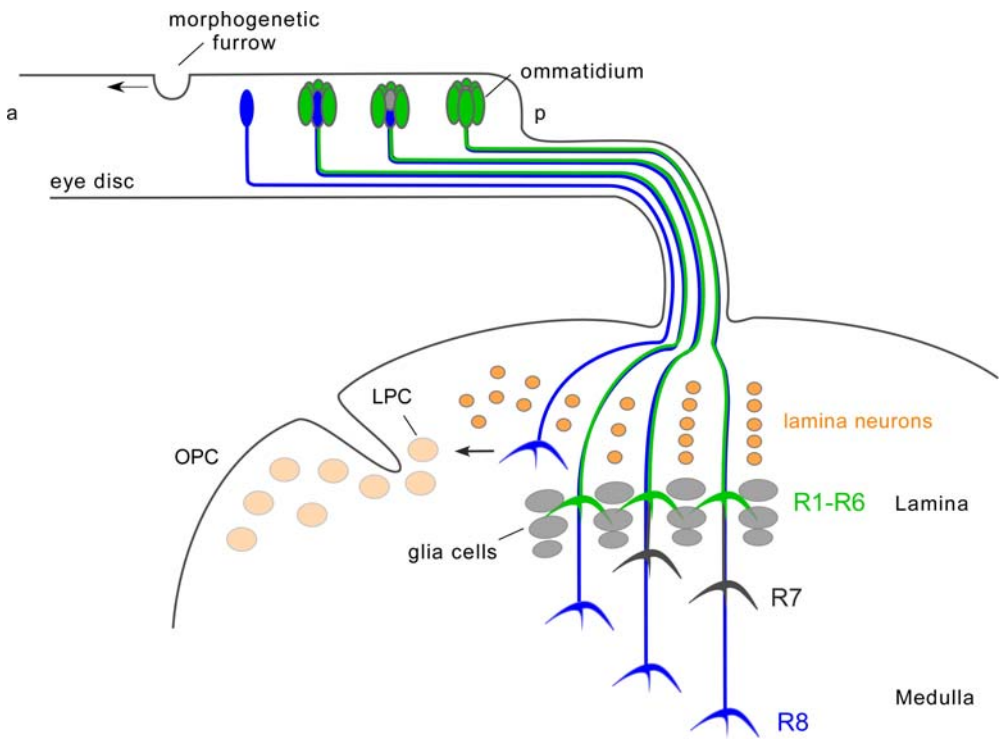

Figure 1-4 Visual system development during 3rd instar larval stage
R cells differentiate within the eye disc following the morphogenetic furrow from posterior (p) to anterior (a). R8 (blue) differentiates first, followed by R1-R6 (green) and finally R7 (black). R1-R6 axons stop between rows of lamina glia cells (grey), their intermediate targets, whereas R8 and R7 continue projecting into the medulla. Successive waves of ingrowing photoreceptors sequentially induce (arrow) and recruit lamina neurons (orange) (adapted from Moses, 2002).

Optic lobe development

While the development of the retina is autonomous (Halder et al., 1995), the development of the optic lobe strongly depends on retinal innervation (Meyerowitz and Kankel, 1978; Steller et al., 1987).

The lamina neurons L1-L5 arise from neuroblasts in the outer proliferation center (OPC) (Figure 1-4) (White and Kankel, 1978). Their precursors, the lamina precursor cells (LPCs) undergo two cell divisions before they differentiate to neurons. After the first division, LPCs arrest in the G1 phase. The arrival of R axons then triggers the second division, thereby inducing the neurogenesis of lamina neurons. Thus, the differentiation of the lamina neurons is directly coupled to the arrival of R axons within the lamina.

As R cell differentiation progresses in a posterior to anterior direction across the eye disc, each row of R cells sends their axons in this order (Figure 1-4). Therefore, R cells trigger the final cell division and terminal differentiation of the LPCs sequentially

in a posterior to anterior direction (Selleck et al., 1992). The molecular basis of this induction is the release of two factors, Hedgehog (Hh) and the EGF family member Spitz (Spi), by the photoreceptor axons (Huang and Kunes, 1996; Huang et al., 1998). The concerted induction of lamina neurons allows to adjust the postsynaptic lamina neuron population to the number of ingrowing photoreceptor axons. After the induction by the photoreceptor axons, lamina monopolar neurons associate with photoreceptor axons to form lamina columns.

In addition, the photoreceptor axons induce the outgrowth of optic lobe cortical axons thereby establishing an axon scaffold that guides glial cell migration (Dearborn and Kunes, 2004). This mechanism coordinates the arrival of photoreceptor axons in the brain with the distribution of glia cells, which are required for axon guidance and neuronal survival.

Consequently, the arriving photoreceptor axons orchestrate the development of the optic lobe. The sequential posterior (older) to anterior (younger) axonal innervations and the concerted recruitment of lamina neurons and glia cells not only adjusts the number of target cells, but also helps establishing the retinotopic columnar organization.

In contrast to the differentiation of lamina neurons that is completely dependent on retinal innervation, the differentiation of medulla and lobula neurons seems to be largely independent of R axons. Medulla and lobula complex show differentiated neurons and retain their columnar organization even in completely eyeless flies. Nevertheless, neuronal survival is impaired, as a massive neuronal degeneration has been described in the absence of photoreceptor axons (Fischbach, 1983; Fischbach and Technau, 1984).

Pupal development

During pupal development, which spans approximately 100h, a massive reorganization takes place. Disc eversion transforms the eye disc into the pupal eye (Meinertzhagen and Hanson, 1993). The forming optic lobes move and center the lamina directly underneath the compound eye. In addition, the medulla neuropil rotates through 90° from its original position, forming the optic chiasm (Meinertzhagen and Hanson, 1993).

But most important, during pupal development the final target layer selection of R1-R8 axons is established followed by synaptogenesis. The stepwise process follows a highly coordinated developmental timetable (Figure 1-5A).

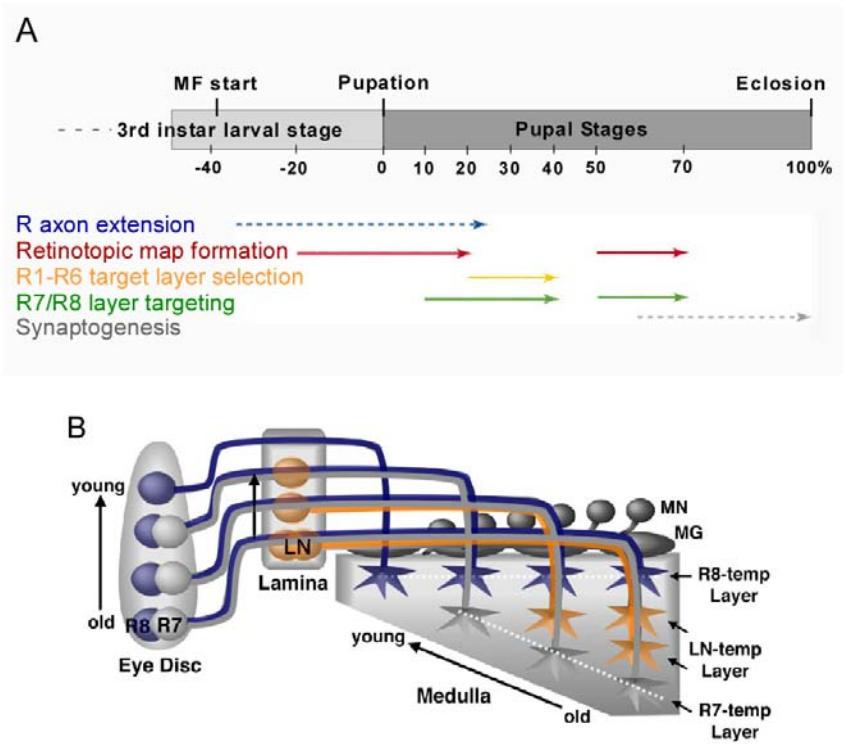

Figure 1-5 Developmental timetable

(**A**) Developmental timetable of the fly visual system. Several key events in the development and various organizational features in visual system development (arrows) are indicated. Pupal stages span approximately 100 h at 25°C (1h ≈ 1%). MF, morphogenetic furrow in the eye disc (adapted from Ting and Lee, 2007) (**B**) A schematic illustrating the order of R-cell and L1-L5 afferents innervating the medulla during early pupal development. The developmental sequences in the eye disc, lamina, and medulla are indicated by arrows. R8 (blue), R7 (light grey), and L1-L5 axons (orange) sequentially innervate the medulla to reach their temporary layers (indicated with dashed lines). LN, L1-L5 neurons; MN, medulla neurons; MG, medulla glia (adapted from Ting et al., 2005).

Initially during larval development, R1-R6 growth cones deriving from the same ommatidia have extended to the lamina as a single fascicle and stopped between rows of lamina glia cells, their intermediate targets (Figure 1-4). After terminating together and forming intermediate connections they still maintain a tight cluster. During pupal development at around 20APF (hours After Puparium Formation) R1-R6 growth cones start to extend out of this cluster and project laterally to 6 different lamina cartridges, in which they form stable synapses with their target neurons, the lamina neurons L1-L3 (Figure 1-2C and orange arrow in Figure 1-5A) (Meinertzhagen and Hanson, 1993).

R7 and R8 axons have extended axons into the developing medulla during larval development. This process of axon extension is still not completed during early pupal stages (blue arrow in Figure 1-5A). The following medulla layer targeting of R7 and R8 involves two selection steps (Ting et al., 2005) (green arrows in Figure 1-5A and

Figure 1-6). During early pupal development the leading R8s temporarily stop at the superficial medulla, later also referred to as M1 layer (R8-temporary layer) (Figure 1-5B). Following R7 growth cones overtake R8s and temporarily terminate at an immediate adjacent layer, the R7-temporary layer (Figure 1-5B). The segregation of R growth cones into two distinct medulla layers is observed at around 17APF (Figure 1-5B, Figure 1-6). Coordinated with the retinal innervation, the first lamina neurons arrive approximately 2-4 hours after the arrival of R7 growth cones and terminate into distinct layers between R8 and R7 growth cones (Figure 1-5B).

During early pupal development, a gradient of R7, R8, and L1-L5 growth cones in the medulla neuropil forms along the anterior-posterior axis between newly arriving axons projecting into the young anterior edge of the medulla and older growth cones in the old posterior edge that has already expanded (Ting et al., 2005) (Figure 1-5B). Thus, the resulting spatial gradient of thickness of the medulla during early pupal development reflects the sequential ingrow of R cells and induction of lamina neurons from posterior (oldest) to anterior (youngest).

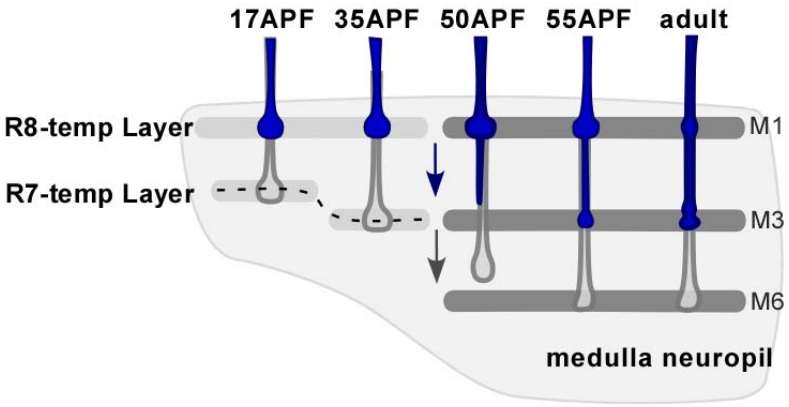

Figure 1-6 Target layer selection of R7 and R8 axons

The layer specific targeting of R7 and R8 axons takes place in two distinct stages. During the first selection stage, R8s (blue) extend axons to a superficial layer in the medulla (R8 intermediate target layer). Following R7 axons (grey) terminate in a deeper layer of the developing medulla neuropil (R7 intermediate target layer).The distance of the two layers increases, whereas the relative position of the axons is maintained (see 35APF). During the second selection stage starting from 50 APF R7 and R8 start extending to their final target layers M6 and M3. During this process R8 send out thin filopodia while a bulb-like structure is maintained around the M1 layer. At 55 APF when thickened R8 terminals can first be observed at the M3 layer, bulb-like structures are still present at the M1 layer. In adult flies this structures have almost completely vanished and mature R8 terminals have formed at the M3 layer.

The temporary layers of R8 and R7 are then more and more pushed apart due to ingrowing neurons during the first 40 hours of pupal development (Figure 1-6). Although the distance between R8 and R7 and the number of observable medulla layers increases, the relative position of R7 to R8 is maintained. In the second selection step starting from 50APF, R7 and R8 axons simultaneously extend to their final target layers, M6 and M3 respectively.

1.4 Known regulators of photoreceptor axon guidance

The developing adult visual system represents an excellent model system to investigate fundamental strategies involved in axon guidance, including topographic map formation, target selection, and selective fasciculation and defasciculation. How are these complex steps of axonal pathfinding decisions determined during visual system development?

In some higher order systems, as known for example for vertebrates, the neurons do require electric activity in order to shape the connections, especially in the final stage of establishing connectivity. However, in the Drosophila visual system it was shown that the establishment of R1-R6 connections does not depend on synaptic vesicle release or electric activity (Hiesinger et al., 2006). This suggests that the choice of synaptic partners of R axons and synaptogenesis are exclusively genetically programmed. Therefore, it is primarily the genes that determine axon wiring in the *Drosophila* visual system.

Several studies on the *Drosophila* visual system attempted to identify the involved regulators. Especially cell surface molecules allowing specific R axon guidance decisions have been of broad interest. Recent genetic studies have revealed roles for several receptors and cell adhesion molecules that control R axonal array establishment and target layer selection, such as the two Cadherin superfamily members, N-Cadherin (N-Cad) and Flamingo (Fmi), two receptor tyrosine phosphatases, LAR and PTP69D, and a cell adhesion molecule, Capricious (Caps) (Clandinin et al., 2001; Garrity et al., 1999; Lee et al., 2001; Lee et al., 2003; Maurel-Zaffran et al., 2001; Newsome et al., 2000; Senti et al., 2003; Shinza-Kameda et al., 2006).

During lamina cartridge formation, the three cell surface molecules N-Cad, LAR and Fmi where shown to play important roles in different aspects of R1-R6 target selection. R1-R6 axons mutant for either gene, *N-cad* or *LAR*, fail to extend from their ommatidial bundle and do not reach their target lamina cartridge during mid-pupal development (Clandinin et al., 2001; Lee et al., 2001), suggesting their involvement in the same process. Furthermore, it was shown in mosaic animals that wild type R axons fail to extend towards *N-cad* mutant lamina neurons (Prakash et al., 2005). The requirement of N-Cad in both pre- and post-synaptic neurons suggests that the homophilic interaction of N-Cads allows this targeting process. Nevertheless N-cad

does not guide the axons directly. However, the results clearly show its function in contact formation and contact stabilization between R1-R6 and their targets.
Flamingo, on the other hand, is required for R cells to reach the appropriate target cartridge. In *fmi* mutants, R1-R6 neurons manage to extend out of the cluster but select spatially inappropriate targets in the lamina. This missorting leads to the formation of lamina cartridges innervated by various numbers of R axons, ranging from 3 to more than 15 axonal termini per cartridge (Lee et al., 2003). It was shown that Flamingo acts in this context as a short-range homophilic signal between specific R cell growth cones to influence their choice of postsynaptic partners. Interestingly, individual growth cones seem to be sensitive to differences in Flamingo activity through opposing interactions between neighboring cells (Chen and Clandinin, 2008), suggesting that the levels of this Cadherins have to be highly regulated and balanced.

In addition to the targeting of R1-R6 in the lamina, *N-cad*, *LAR*, PTP69D and *fmi* also play crucial roles in the target layer selection of R7 and R8 axons. In *N-cad*, *LAR* and *PTP69D* mutants, R7 axons undershoot the correct target layer M6 and terminate prematurely at layer M3, which is normally targeted by R8s (Clandinin et al., 2001; Lee et al., 2001; Maurel-Zaffran et al., 2001; Newsome et al., 2000). In *fmi* mutants, R8 axon targeting is disrupted and R8s are frequently mistargeted to superficial levels of the medulla. Since *fmi* mutants show abnormal spacing between the adjacent axonal tracts in larvae, Fmi has also been implicated in the regulation of axon-axon interactions (Lee et al., 2003; Senti et al., 2003).
From these studies, a Cadherin-based homophilic cell adhesion, possibly controlled by the two receptor tyrosine phosphatises, LAR and PTP69D, has emerged as the key regulating mechanism of axon-axon and axon-target interaction in the *Drosophila* visual system. However, since both N-Cad and Fmi are expressed on all types of R axons and in multiple target layers in the optic lobe, the homophilic interaction of these two Cadherins alone cannot account for the distinct target layer selection of R7 and R8 axons. One of the two phosphatases, LAR, is also broadly expressed in all R axons and multiple target layers. In contrast, the homophilic adhesion molecule Caps, is specifically expressed on R8 axons only. Loss of *caps* function results in R8 target layer selection defects in adult flies and moreover, ectopic expression of *caps* in R7 redirects R7 to the R8 target layer (Shinza-Kameda et al., 2006). These findings strongly support the idea that the combination of homophilic adhesive interactions with additional combinatorial codes may be the key mechanism to create the specificity in layer targeting. A similar mechanism was suggested in vertebrates

where the homophilic adhesion molecules, encoded by the two *sidekicks* genes, control layer specific targeting of retinal neurons (Yamagata et al., 2002). In addition, specificity could be the result of temporal modulations of Cadherin interactions by so far unknown mechanism.

However, for the visual system of *Drosophila*, the set of known molecules is not enough to shape a complete picture of the highly-selective process of R axon connectivity, suggesting that further guidance cues remain to be discovered.

1.5 Screen for novel regulators of R axon guidance

To search for novel players in axon pathfinding, classical forward genetic screens have been performed in the past using the *Drosophila* visual system (Martin et al., 1995). The identification of novel axon guidance molecules, however, involved two major problems in previous screens. First, several genes involved in axon guidance have important additional functions during early development, as for example morphogens (Zou and Lyuksyutova, 2007). Mutations in these genes might result in early lethality and could therefore be missed in screens. Second, mutations in key axon guidance molecules may not produce informative phenotypes in homozygous mutants, as the disruption of the development of target neurons often causes severe secondary defects which can not be properly dissected. These problems can be overcome with the generation of mosaic animals through site-specific mitotic recombination using the FLP/FRT system deriving from yeast (Golic, 1991; Xu and Rubin, 1993). FRT (Flipase Recognition Target) sites which are recognized by the Flipase (FLP) have been introduced on the fly chromosome to induce recombination between homologous chromosomes. In order to induce mosaics for a particular chromosome arm FRT sequences were inserted into the genome near the centromere on each major chromosome arm (Xu and Rubin, 1993).

A large scale saturated genetic screen was performed in the lab of Barry Dickson employing the *ey*FLP system, in which the Flipase is expressed under the eye-specific *ey* (eyeless) promoter fragment. *ey*FLP induced mitotic recombination generates mosaic flies in which virtually the entire retina, but no other tissue, is homozygous for a newly induced mutation (Newsome et al., 2000). Each of the four major autosomal arms was screen for EMS-induced mutations. About 40 different genetic loci that affect the projection pattern of R axons were identified in a screen of 32.000 mosaic lines. So far, 36 of the affected genes were identified (Berger et al., 2008). From the screen one complementation group consisting of three alleles was recovered ([D869], [D1600] and [H1675]). Using the mapping method utilizing single-nucleotide-polymorphisms (SNP) as chromosomal landmarks (Berger et al., 2001), single nucleotide mutations were identified for all three alleles within a single gene (Figure 1-7A), which we named *golden goal* (*gogo*).

Gogo encodes a novel single transmembrane protein with two conserved extracellular domains, a TSP (Thrombospondin) domain and a CUB (complement subcomponents Clr/Cls, Uegf, Bmpl) domain (Figure 1-7B). Both domains are

implicated in directing the migration of growing cells or growth cones in the developing nervous system: e.g. Unc-5 and class 5 Semaphorins contain Tsp1 domains, while A5 and Neuropilin have CUB domains (Adams and Tucker, 2000; Bork and Beckmann, 1993; He and Tessier-Lavigne, 1997; Takagi et al., 1991). As both domains are wide-spread protein-protein interaction domains, Gogo protein structure strongly indicates a function as a cell adhesion molecule or axon guidance receptor, making Gogo a promising candidate for further investigation.

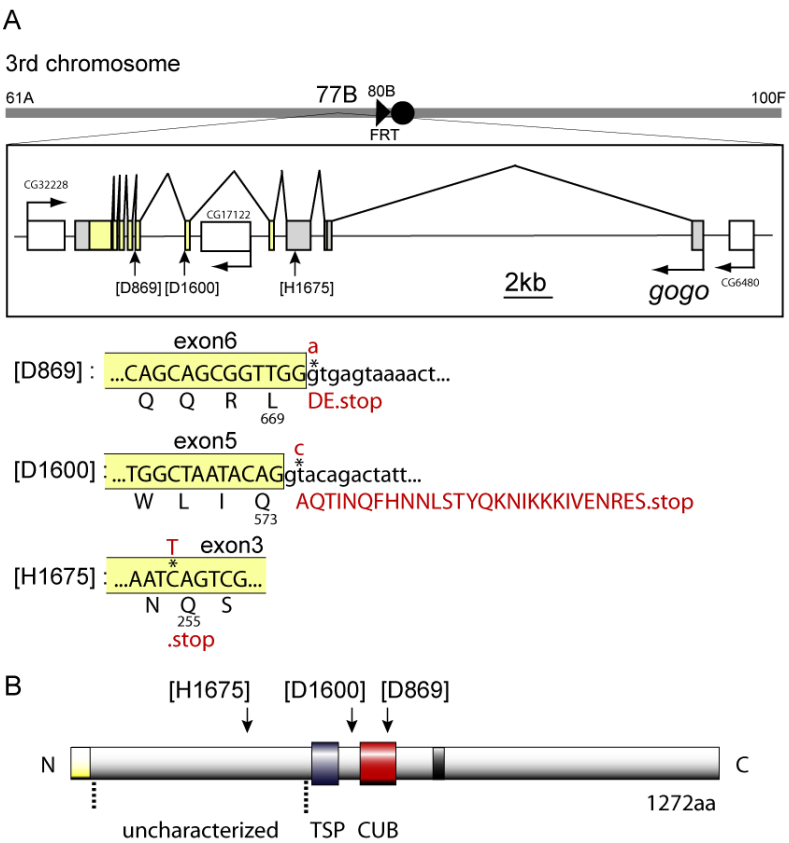

Figure 1-7 *gogo* mutant alleles and protein structure

(**A**) The entire third chromosome is indicated at the top. The *gogo* gene is located at the cytology 77B. Yellow boxes depict the coding region, grey boxes show untranslated regions. Location of the mutation in the respective mutant allele D869, D1600 or H1675 is indicated with arrows. Below: detailed explanation of the mutations. The locations of single nucleotide changes are indicated by asterisks. Changed nucleotides are in red letters. The amino acid changes caused by the mutations are written in the red capital letters. D869 and D1600 carry a mutation in the splice donor site resulting in premature stops. The mutation of H1675 introduces a premature stop.
(**B**) Gogo protein structure and locations of the mutations in the three different alleles are indicated (arrows). The colored boxes and ovals indicate: yellow, signal peptide; purple, Tsp1 domain; red, CUB domain; black, transmembrane domain. An uncharacterized N-terminal, but conserved region is marked by dashed lines.

1.6 The thesis project

The regular, columnar and layered organisation of the visual system is well suited to investigate the genetic determination in nervous system wiring. Although several important axon guidance molecules have been identified in the visual system of *Drosophila*, the specificity in retinal axon guidance can still not be sufficiently explained.

Mutants for Gogo, a novel transmembrane protein, show a strong defect in forming retinal connections suggesting a major role in axon guidance. Due to its structure, Gogo is a strong candidate for functioning as a cell adhesion molecule or axon guidance receptor. This project aims at performing a functional and molecular analysis of Gogo, which will reveal new insights in the developmental mechanisms that underlie the establishment of the neuronal connectivity in the visual system in *Drosophila*.

The main aim of this work is to clarify Gogo's function in photoreceptors. A possible function as a novel axon guidance receptor or merely homophilic cell adhesion can be distinguished by a set of possible mosaic experiments. Especially, the extraordinary genetic tools available in *Drosophila* allow approaching this question by investigating the behavior of single *gogo* mutant axons. The available set of R cell type specific markers also allows a detailed analysis of *gogo* function in single photoreceptor types during different stages of visual system development.
Gogo expression analysis and localization of the Gogo protein during development can also give hints to reveal its function in R axons, but also imply an importance for other neurons or different cell types.
As the combination of the two conserved extracellular domains, the CUB and TSP domain is so fare unknown, detailed structure-function experiments can identify the functional domains and help finding evolutionary conserved proteins in other organism.

2 Materials and Methods

2.1 Media

Media for bacteria

LB medium

Bacto-Tryptone 10g/l
Bacto-Yeast extract 5g/l
NaCl 5g/l
pH 7.5
optional:
75μg/ml Ampicillin
50μg/ml Kanamycin

LB plates

LB medium 1l
Bacto-Agar 15g
optional:
75μg/ml Ampicillin
50μg/ml Kanamycin

Media for *Drosophila* flies

Apple agar plates

7.5 g SELECT Agar was dissolved in 200 ml apple juice (ALDI), boiled in the microwave and poured into petri dishes.

Standard Drosophila medium

For 50 l medium, 585 g Agar was dissolved in 30 l water by heating the mixture to the boiling point; meanwhile 3 kg corn flour and 750 g yeast (Femipan Inc.) were mixed with water to obtain a homogeneous broth. As soon as the agar was dissolved, 4 kg molasses and corn flour/yeast were added. The mélange was filled up with water to

50 l and cooked at 96 °C for 1.5 h. 315 ml Propionic acid and 120 g Methylparaben were added when the temperature had cooled down to 60 °C.

Blue Yeast paste

Instant dry yeast (Femipan Inc.) was mixed with Instant blue Drosophila medium (Fisher Scientific) and water to obtain a paste of the consistency of peanut butter.

2.2 Instruments

Leica SP2 Confocal Microscope	Leica Germany
Leica MZ16 Fluorescent Dissect scope	Leica Germany
Leica MS5 Stereomicroscope	Leica Germany
Leica MZ9.5 Stereomicroscope	Leica Germany
Leica Axioscope 2 plus Fluorescent Microscope	Leica Germany
Zeiss Axiovert S100	Zeiss Germany
Leica DFC 320 digital camera	Leica Germany
Femtojet	Eppendorf Germany
Micro Grinder EG-400	Narishige Japan
Micropipette Puller P-97	Sutter USA

2.3 Enzymes and Standards

iProof High-Fidelity Polymerase Master Mix	Bio RAD Germany
Taq DNA Polymerase	NEB Germany
Gateway BP Clonase II Enzyme Mix	Invitrogen Germany
Gateway LR Clonase II Enzyme Mix	Invitrogen Germany
T3 RNA Polymerase	Roche Germany
T7 RNA Polymerase	Roche Germany
1kb DNA ladder	NEB Germany
PageRuler Prestained Protein Ladder	Fermentas Germany

2.4 Commercial Kits

QIAquick PCR Purification Kit	Qiagen, Germany
QIAquick Gel Extraction Kit	Qiagen, Germany
QIAfilter Plasmid Midi Kit	Qiagen, Germany
QIAprep Spin Miniprep Kit	Qiagen, Germany

2.5 Oligonucleotides

All oligonucleotides were ordered from the company Metabion in Martinsried (Germany).

Table 1 Oligonucleotides

Primer	Sequence	Description
TT1	5`GGGGACAAGTTTGTACAAAAAAGCAGGCTTCGA AGGAGATAGAACCATGCGGAAAAACTCAAAGGA3`	gogo, gateway 5' attB primer from start codon
TT20	5`GGGGACCACTTTGTACAAGAAAGCTGGGTCCA CGGCCACTTCCTTTGACTTC3`	gogo, gateway 3' attB primer, no stop codon
TT3	5`TTGTGGACAACAGAGCGAGTTTTCTTTCGCACC GCCAGCACGT3`	gogo, overlap 3' SP with 5' TM domain
TT4	5`ACGTGCTGGCGGTGCGAAAGAAAACTCGCTCT GTTGTCCACAA3`	gogo, overlap 3' TM with 5' SP domain
TT5	5`TCGCTCCAAGGTCCCCAGCCCTTTCGCACCGC CAGCACGT3`	gogo, overlap 3' SP with 5' TSP domain
TT6	5`ACGTGCTGGCGGTGCGAAAGGGCTGGGGACC TTGGAGCGA3`	gogo, overlap 3' TSP with 5' SP domain
TT7	5'ACGACATCCTGGTCCAATTTCACCGGTATCCGA GTCGCTGA3`	gogo, overlap 3' GOGO with 5' CUB domain
TT8	5`TCAGCGACTCGGATACCGGTGAAATTGGACCA GGATGTCGT3`	gogo, overlap 3' CUB with 5' GOGO domain
TT9	5`TTGTGGACAACAGAGCGAGTTTTCTGGCTCAC CTCGGTGCTATT3`	gogo, overlap 3' TSP with 5' TM domain
TT10	5`AATAGCACCGAGGTGAGCCAGAAAACTCGCTC TGTTGTCCACAA3`	gogo, overlap 3' TM with 5' TSP domain
TT11	5 `TTGTGGACAACAGAGCGAGTTTTACCGGTATC CGAGTCGCTGA3`	gogo, overlap 3' GOGO with 5' TM domain
TT12	5`TCAGCGACTCGGATACCGGTAAAACTCGCTCT GTTGTCCACAA3`	gogo, overlap 3' TM with 5' GOGO domain
TT15	5`ACGACATCCTGGTCCAATTTCCTTTCGCACCG CCAGCACGT3`	gogo, overlap 3' SP with 5' CUB domain
TT16	5`ACGTGCTGGCGGTGCGAAAGGAAATTGGACC AGGATGTCGT3`	gogo, overlap 3' CUB with 5' SP domain
TT31	5'CTGCGCGGGCACCAATGTGGTCTTTCGCACCG CCAGCACGT3`	gogo, overlap 3' SP with 5' GOGO domain
TT32	5`ACGTGCTGGCGGTGCGAAAGACCACATTGGT GCCCGCGCAG3'	gogo, overlap 3' GOGO with 5' SP domain

TT33	5`CACTAGTTGGGGTTATATTCCGATTCTTTCGC ACCGCCAGCACGT3`	gogo, overlap 3' SP with 5' partial GOGO domain
TT34	5`ACGTGCTGGCGGTGCGAAAGAATCGGAATAT AACCCCAACTAGTG3`	gogo, overlap 3' partial GOGO with 5' SP
TT49	5`GGGGACAAGTTTGTACAAAAAAGCAGGCTAC CGACGCGAAGTGTTCATCATTCATTA3`	gogo, gateway 5`attB, intergenic Fragment 1
TT50	5`GGGGACCACTTTGTACAAGAAAGCTGGGTGA TTGCCACGCGACTTTGAGCCAC3`	gogo, gateway 3`attB + intergenic Fragment 1
TT58	5`GGGGACAAGTTTGTACAAAAAAGCAGGCTTG CTCAGTGAACTACTCATCAACAGAATAATCG3`	gogo, gateway 5`attB + 1st Intron Fragment 2
TT59	5`GGGGACCACTTTGTACAAGAAAGCTGGGTAC GAGGATGAAGCCTAAATTCGAGCAG3`	gogo, gateway 3`attB + 1st Intron Fragment 2
TT53	5'GGGGACAAGTTTGTACAAAAAAGCAGGCTGCC GTTCGTAAATGTTTTTAGTTCGGC3`	gogo, gateway 5`attB + 1st Intron Fragment 3
TT54	5`GGGGACCACTTTGTACAAGAAAGCTGGGTGGAC AAACACACTAAATACCCATGGAAC3`	gogo, gateway 3`attB + 1st Intron r Fragment 3
TT55	5`GGGGACAAGTTTGTACAAAAAAGCAGGCTAAGC TGTCTCTTGCTTGTCAATAGCC3`	gogo, gateway 5`attB + 1st Intron Fragment 4
TT56	5`GGGGACCACTTTGTACAAGAAAGCTGGGTCTGC AAAAAAGAAAAAAGTTGACTTTACTG3`	gogo, gateway 3`attB + 1st Intron Fragment 4
T1B UAS	5`GCAGAAGCTTTGCGTACTCGC3`	Degenerative PCR
AD3	5`WGTGNAGWANCANAGA3`	Degenerative PCR
T2D	5`ATTCAAACCCCACGGACATG3`	Degenerative PCR

2.6 Plasmids

Gogo constructs

All constructs were generated using the Gateway Recombination Cloning (Invitrogen). Gogo full-length (Gogo-FL) and truncated Gogo fragments were obtained by overlapping PCR using cDNA clone RE53634. Except for the plasmids GMR-*gogo*Δ N-G::myc and GMR-*gogo*Δ N-H::myc. For these two plasmids GMR-*gogo*Δ N-F::myc was used as a PCR template. attB sites were added directly to PCR primers. Fragments were recombined into pDONR221 (Invitrogen) via BP reaction to

receive Entry clones. Entry clones were then recombined in the LR reaction with the respective Destination Vector to obtain the final plasmid.

Destination vectors used:

Table 2 Destination vectors 1

Vector name	Description	source
pGMR-myc	Casper based Promoter: GMR C-terminal fusion of 4x c-myc epitopes	Stephan Ohler
pUAST-myc	Casper based Promoter: UAS C-terminal fusion of 4x c-myc epitopes	Stephan Ohler
pUAST-gfp	Casper based Promoter: UAS C-terminal fusion of GFP	Stephan Ohler

Plasmids used for the generation of transgenic flies:

Table 3 Gogo plasmids used for transgenic flies

Plasmid name	Encoded Gogo domains	source	primers
pGMR-*gogo*FL::myc	full-length protein	Stephan Ohler	-
pGMR-*gogo*ΔN::myc	$[SP]_{1-54}$ $[Cterm]_{689-1272}$	cloned	TT1, TT3, TT4, TT20
pGMR-*gogo*ΔC::myc	$[Nterm]_{1-745}$	Stephan Ohler	-
pGMR-*gogo*ΔN-A::myc	$[SP]_{1-54}$ $[CUB+Cterm]_{535-1272}$	cloned	TT1, TT15, TT16, TT20
pGMR-*gogo*ΔN-B::myc	$[SP+GOGO]_{1-457}$ $[Cterm]_{689-1272}$	cloned	TT1, TT11, TT12, TT20
pGMR-*gogo*ΔN-C::myc	$[SP]_{1-54}$ $[Tsp1]_{458-534}$ $[Cterm]_{689-1272}$	cloned	TT1, TT5, TT6, TT9, TT10, TT20
pGMR-*gogo*ΔN-D::myc	$[SP]_{1-54}$ $[Tsp1+CUB+Cterm]_{458-1272}$	cloned	TT1, TT5, TT6, TT20

pGMR-*gogo*ΔN-E::myc	[SP+GOGO] $_{1-457}$ [CUB+Cterm]$_{535-1272}$	cloned	TT1, TT7, TT8, TT20
pGMR-*gogo*ΔN-F::myc	[SP+GOGO+Tsp1]$_{1-534}$ [Cterm]$_{689-1272}$	cloned	TT1, TT9, TT10, TT20
pGMR-*gogo*ΔN-G::myc	[SP]$_{1-54}$ [GOGO+Tsp1]$_{204-534}$ [Cterm]$_{689-1272}$	cloned	TT1, TT31, TT32, TT20
pGMR-*gogo*ΔN-H::myc	[SP] $_{1-54}$ [partial-GOGO+Tsp1]$_{278-534}$ [Cterm]$_{689-1272}$.	cloned	TT1, TT33, TT34, TT20
pUAS-*gogo*FL::myc	full-length protein	Stephan Ohler	-
pUAS- *gogo*ΔC	[SP]$_{1-54}$ +[Cterm]$_{689-1272}$	Stephan Ohler	-

Plasmids used for S2 cell transfection

Table 4 Plasmids used in cell culture

Plasmid name	Encoded Gogo domains	source
pActin-*gal4*	Gal4 expression	Jürgen Knoblich
pUAS-*gogo*FL::GFP	Gogo full-length protein	Stephan Ohler
pUAS-*gogo*ΔC::GFP	Gogo [Nterm]$_{1-745}$	Stephan Ohler
pUAS-*fmi*	Fmi expression	T. Uemura
UAS-*citrine*	Co-Transfection marker	T. Uemura

***gogo* enhancer fragments**

All constructs were generated using the Gateway Recombination Cloning (Invitrogen). PCR products were obtained using genomic DNA from wild type flies (W^{1118}). Fragments were recombined into pDONR221 (Invitrogen) via BP reaction to receive Entry clones. Entry clones were then recombined with the Destination Vector pCaSpeR-DEST6.

Destination vector used

Table 5 Destination vectors 2

Vector name	Description	source
pCaSpeR-DEST6	core hs-> GAL4-SV40	Frederik Wirtz-Peitz

Plasmids used for the generation of transgenic flies

Table 6 *gogo* enhancer Gal4 plasmids

Plasmid name	Region of *gogo* locus	source	primers
p*gogo*1-Gal4	700bp intergenic	cloned	TT49, TT50
p*gogo*2-Gal4	6kb 1st intron	cloned	TT58, TT59
p*gogo*3-Gal4	6kb 1st intron	cloned	TT53, TT54
p*gogo*4-Gal4	6kb 1st intron	cloned	TT55, TT56

2.7 Bacteria strains

DH5α

Genotype: F^- φ80*lac*ZΔM15 Δ(*lac*ZYA-*arg*F) U169 *rec*A1 *end*A1 *hsd*R17 (r_k-, m_k+) *pho*A *sup*E44 λ^- *thi*$^-$1 *gyr*A96 *rel*A1

Use: cloning

Sure

Genotype: *e14*$^-$ *(McrA*$^-$*)* *(mcrCB-hsdSMR-mrr)171 endA1 supE44 thi*$^-$*1 gyrA96 relA1 lac recB recJ sbcC umuC::Tn5* (Kan^r) *uvrC* [F' *proAB lacI*^{q}*ZΔM15 Tn10* (Tet^r)]

Use: cloning

DB3.1

Genotype: F^- *gyr*A96 *end*A1 Δ(*sr*1-*rec*A) *mcr*B *mrr hsd*S20(r_B-, m_B-) *sup*E44 *ara*14 *gal*K2 *lac*Y1 *pro*A2 *rps*L20(Sm^r) *xyl*5 Δ*leu mtl*1

Use: Amplification of *ccdB* containing plasmids, as DB3.1 is not sensitive to CcdB effects

2.8 Antibodies

Gogo antibody

Anti-Gogo antiserum was obtained from rabbit immunized with a 6xHis tagged protein containing 412 amino acids (48-459) of the extracellular domain. The antiserum was purified with the Melon Gel IgG Purification Kit (Pierce), and used at a dilution of 1:1000.

Other primary antibodies

rabbit anti-GFP (Torrey Pines Biolabs, 1:300)
rabbit anti-GFP Alexa Fluor488-conjugated (Molecular Probes, 1:300)
rabbit anti-β-gal (Cappel, 1:5000)
mouse anti-β-gal (Promega, 1:300)
chicken anti-β-gal (Abcam, 1:1000)
mouse anti-Myc (9E10; Santa Cruz, 1:300)
mouse anti-CoralHue Kusabira-Orange (MBL clone 2G9, 1:300)
mouse Ab24B10 (DSHB, 1:50)
rat anti-Elav (DSHB 7E8A10, 1:100)
mouse anti-Tau (Sigma, 1:200)
rat anti-mCD8 (Caltag, 1:300)
rabbit anti-Repo (gift from J. Urban, 1:500)
guinea pig anti-Senseless (gift from H. Bellen, 1:1000)
sheep anti-Digoxigenin-AP, Fab fragments (Roche 1:2000)

Secondary antibodies

Alexa Fluor-conjugated secondary antibodies (488, 568, 633; Molecular Probes) were used at 1:300-1:1000.

2.9 Cell culture lines

Drosophila Schneider 2 cells (S2) (Invitrogen) were grown in cell culture. The S2 cell line derived from a primary culture of late stage (20-24 hours old) *Drosophila melanogaster* embryos (Schneider, 1972). Many features of the S2 cell line suggest that it is derived from a macrophage-like lineage. S2 cells grow at room temperature without CO_2 as a loose, semi-adherent monolayer in tissue culture flasks and in suspension in spinners and shake flasks.

2.10 *Drosophila melanogaster* lines

Fly stocks

Table 7 Fly stocks

genotype	Description/use	source
w^{1118}	w^- flies	Bloomington Stock Center
yw X; Pin/CyOy$^+$ II	balancer 2nd	Barry Dickson
yw/Yhshid X; Pin/CyOy$^+$ II	balancer 2nd virgin collection	Barry Dickson
yw X; MKRS/TM6By$^+$ III	balancer 3rd	Barry Dickson
yw/Yhshid X; MKRS/TM6By$^+$ III	balancer 3rd virgin collection	Barry Dickson
yw X; Elp/CyO Kr-G U-GFP II; Ki/TM3 Kr-G U-GFP III	double balancer	Gaia Tavosanis
w/Yy$^+$ X; nub b Sco lt stw/CyO II; MKRS/TM6B III	double balancer	Bloomington Stock Center
yw eyFLP2 C-lacZ X; M(3)i[55] FRT80B/TM6By$^+$ III	3rd left, cell lethal	Barry Dickson
yw eyFLP2 Rh1-τlacZ X; M(3)i[55] FRT80B/TM3Sery$^+$ III	Rh1: R1-R6 marker	Barry Dickson
w eyFLP2 Rh6-mCD8GFPmyc X; M(3)i[55] FRT80/TM3 III	Rh6: adult R8 marker, stains 70%	Barry Dickson
w eyFLP2 Rh4-mCD8GFPmyc X; M(3)i[55] FRT80/TM3 III	Rh4: R7 marker stains 70%	Barry Dickson
yw eyFLP2 C-lacZ X; *gogo*[D869]/TM6By$^+$ III	*gogo* mutant allele	Takashi Suzuki
yw eyFLP2 C-lacZ X; *gogo*[D1600]/TM6By$^+$ III	*gogo* mutant allele	Takashi Suzuki
yw eyFLP2 C-lacZ X; *gogo*[H1675]/TM6By$^+$ III	*gogo* mutant allele	Takashi Suzuki

yw eyFLP2 C-lacZ X; FRT80 tub-GAL80 GMR-mKO M(3)i[55]/TM6By^{+} III	GMR-mKO: R1-R8 marker, Gogo AB staining	Satoko Suzuki
elav-Gal4 hsFLP UAS-mCD8GFP X; GMR-KO tub-Gal80 FRT80/TM6By^{+} III	cMARCM	Satoko Suzuki
yw X; ey1xFLP/CyO II; *gogo*[D869] FRT80 III	cMARCM	Satoko Suzuki
yw X; ey1xFLP/CyO II; *gogo*[D869] FRT80 UAS-gogoFL-3B/ TM6By^{+} III	cMARCM	Satoko Suzuki
yw X; ey1xFLP/CyO II; *gogo*[D869] FRT80 UAS-gogoΔC-3B/ TM6By^{+} III	cMARCM	Satoko Suzuki
yw X; 1xeyFLP/CyO; GMR-KO tub-Gal80 FRT80/TM6By^{+} III	R8 bundling phenotype in larvae, small mutant clones in pupae	Satoko Suzuki
yw GMR-FLP X; Gla/CyO II	MARCM clones in R7	Larry Zipursky
w eyFLP2 Rh6-mCD8GFPmyc X ; GMR-KO Gal80 FRT80/TM3 III	making small clones, label R8 and WT cells in adults	Takashi Suzuki
w eyFLP2 Rh6-mCD8GFPmyc X; M(3)i[55] cl GMR-KO Gal80 FRT80/TM3 III	making large clones, label R8 and WT cells inadults	Takashi Suzuki
yw PM181-Gal4 X	R7 specific Gal4	Bloomington Stock Center
Yw X; Pin/Cyo II; UAS-mCD8GFP III	expression of GFP localized to axons	Bloomington Stock Center
UAS-GFP:lacZnls II	*gogo*-Gal4 expression analysis	Bloomington Stock Center
UAS-GFP:lacZnls III	*gogo*-Gal4 expression analysis	Bloomington Stock Center
GMR-gogo-FLmyc II	rescue experiments	Stephan Ohler
GMR-gogo-ΔCmyc II	rescue experiments	Stephan Ohler
UAS-gogo-FLmyc-T1 II	Gogo OE	Barry Dickson
UAS-gogo-FLmyc-T2 II	R8 rescue, *gogo*2-Gal4 rescue, Gogo OE, Western	Stephan Ohler
UAS-gogo-FLmyc-2B II	Gogo OE, Western	Stephan Ohler
UAS-gogo-FLmyc-3A III	Gogo OE, Western	Stephan Ohler
UAS-gogo-FLmyc-3B III	cMARCM, R7 rescue, Gogo OE, Western	Stephan Ohler
UAS-gogo-FLmyc-3C III	Gogo OE, Western	Stephan Ohler
UAS-gogo-ΔCmyc-3B III	cMARCM	Stephan Ohler

Constructed Fly stocks

Table 8 Constructed Fly stocks

genotype	Description/use
yw/yw eyFLP2 C-lacZ X; ato-τ-myc II; *gogo*[D869] FRT80/TM6By^{+} III	ato: R8 marker, mutant R8 phenotype analysis in larvae
yw eyFLP2 C-lacZ X; GMR-gogo-FL II; *gogo*[D869] FRT80/TM6By^{+} III	transheterozygous rescue
yw eyFLP2 C-lacZ X; GMR-gogo-ΔC II; *gogo*[D869] FRT80/TM6By^{+} III	transheterozygous rescue
w X; ato-τ-myc *gogo*[D1600] FRT80/TM6By^{+} III	transheterozygous rescue
ey3.5FLP II; M(3)i[55] FRT80/TM6By^{+} III	clean ey3.5FLP from Iris Salecker, no brain clones, EM
yw eyFLP2 C-lacZ X; 109-68Gal4/Cyo; M(3)i[55] FRT80/TM6By^{+} III	R8 rescue
yw/yw eyFLP2 C-lacZ X; Caps-Gal4 *gogo*[D869] FRT80/TM6By^{+} III	R8 rescue
yw/yw eyFLP2 C-lacZ X; UAS-Gogo-FLT2/Cyo II; Caps-Gal4 *gogo*[D869] FRT80/TM6By^{+} III	R8 rescue
yw X; GMR-Gal4/CyO II; *gogo*[D869] FRT80/TM6By^{+} III	positive control for *gogo* enhancer fragment rescue
yw X; UAS-gogo-FL-T2/Cyo II; *gogo*[D1600] FRT80/TM6By^{+} III	*gogo* enhancer fragment rescue
yw X; *gogo*2-Gal4-T1 II; *gogo*[D869] FRT80/TM6By^{+} III	*gogo* enhancer fragment rescue
yw eyFLP2 C-lacZ X; Gal80 FRT80/TM6By^{+} III	Replacement of non-functional stock in Bloomington stock collection
w X; PanR7-Gal4 UAS-SybGFP/CyO II; Gal80 FRT80/TM6B III	R7 mutants
yw X; UAS-Gogo–ΔC-3B *gogo*[D869] FRT80/TM6By+	cMARCM
yw X; UAS-Gogo–FL-3B *gogo*[D869] FRT80/TM6By+	R7 rescue, cMARCM
yw eyFLP2 C-lacZ X; ato-t-myc *gogo*[D869] FRT80/TM6By+	pupal stages R8, R8 bundling in larvae
yw eyFLP2 C-lacZ X, ato-t-myc FRT80/TM6By+	pupal stages R8, R8 bundling in larvae

Generated Transgenic fly lines

Table 9 Generated transgenic flies

Transgenic line	Injected Plasmid	Description
GMR-*gogo*ΔN::myc-T1 II	pGMR-*gogo*ΔN::myc	Gogo expression in R1-R8
GMR-*gogo*ΔN::myc-T2 II		$[SP]_{1-54}$
GMR-*gogo*ΔN::myc-T3 II		$[Cterm]_{689-1272}$
GMR-*gogo*ΔN-A::myc-T1 II	pGMR-*gogo*ΔN-A::myc	Gogo expression in R1-R8
GMR-*gogo*ΔN-A::myc-T2 II		$[SP]_{1-54}$
GMR-*gogo*ΔN-A::myc-T3 II		$[CUB+Cterm]_{535-1272}$
GMR-*gogo*ΔN-B::myc-T1 II	pGMR-*gogo*ΔN-B::myc	Gogo expression in R1-R8
GMR-*gogo*ΔN-B::myc-T2 II		$[SP+GOGO]_{1-457}$
GMR-*gogo*ΔN-B::myc-T3 II		$[Cterm]_{689-1272}$
GMR-*gogo*ΔN-C::myc-T1 II	pGMR-*gogo*ΔN-C::myc	Gogo expression in R1-R8
GMR-*gogo*ΔN-C::myc-T2 II		$[SP]_{1-54}$
GMR-*gogo*ΔN-C::myc-T3 II		$[Tsp1]_{458-534}$
		$[Cterm]_{689-1272}$
GMR-*gogo*ΔN-D::myc-T1 II	pGMR-*gogo*ΔN-D::myc	Gogo expression in R1-R8
GMR-*gogo*ΔN-D::myc-T2 II		$[SP]_{1-54}$
GMR-*gogo*ΔN-D::myc-T3 II		$[Tsp1+CUB+Cterm]_{458-1272}$
GMR-*gogo*ΔN-E::myc-T1 II	pGMR-*gogo*ΔN-E::myc	Gogo expression in R1-R8
GMR-*gogo*ΔN-E::myc-T2 II		$[SP+GOGO]_{1-457}$
GMR-*gogo*ΔN-E::myc-T3 II		$[CUB+Cterm]_{535-1272}$
GMR-*gogo*ΔN-F::myc-T1 II	pGMR-*gogo*ΔN-F::myc	Gogo expression in R1-R8
GMR-*gogo*ΔN-F::myc-T2 II		$[SP+GOGO+Tsp1]_{1-534}$
GMR-*gogo*ΔN-F::myc-T3 II		$[Cterm]_{689-1272}$
GMR-*gogo*ΔN-G::myc-T1 II	pGMR-*gogo*ΔN-G::myc	Gogo expression in R1-R8
GMR-*gogo*ΔN-G::myc-T3 II		$[SP]_{1-54}$
GMR-*gogo*ΔN-G::myc-T4 II		$[GOGO+Tsp1]_{204-534}$
		$[Cterm]_{689-1272}$
GMR-*gogo*ΔN-H::myc-T3 II	pGMR-*gogo*ΔN-H::myc	Gogo expression in R1-R8
GMR-*gogo*ΔN-H::myc-T4 II		$[SP]_{1-54}$
GMR-*gogo*ΔN-H::myc-T5 II		$[partial\text{-}GOGO+Tsp1]_{278-534}$
		$[Cterm]_{689-1272}$
*gogo*1-Gal4-T2	p*gogo*1-Gal4	Potential *gogo* enhancer
*gogo*1-Gal4-T3		fragment fused to Gal4
*gogo*1-Gal4-T5		*gogo* locus: intergenic

*gogo*2-Gal4-T1 II (closer examined in experiments)	p*gogo*2-Gal4	Potential *gogo* enhancer fragment fused to Gal4 *gogo* locus:1st intron
*gogo*2-Gal4-T4 II		
*gogo*2-Gal4-T11 II		
*gogo*3-Gal4-T2	p*gogo*3-Gal4	Potential *gogo* enhancer fragment fused to Gal4 *gogo* locus:1st intron
*gogo*3-Gal4-T3		
*gogo*3-Gal4-T4		
*gogo*4-Gal4-T2	p*gogo*4-Gal4	Potential *gogo* enhancer fragment fused to Gal4 *gogo* locus:1st intron
*gogo*4-Gal4-T3		
*gogo*4-Gal4-T4		

2.11 Molecular biology methods

Transformation

After thawing 100µl competent bacteria from a -80°C stock on ice, the bacteria were incubated with 100-150ng of DNA on ice for 30min. The cells were heat-shocked at 42°C for 90sec and immediately returned on ice for 1-2min. To allow expression of resistance genes in transformed bacteria, the cells were shaken for 1h at 37°C after the addition of 1ml of LB medium. Afterwards, they were plated on LB plates containing selective antibiotics and incubated overnight at 37°C

DNA gel electrophoresis

DNA is negatively charged and therefore can be separated by electrophoresis according to its size (Maniatis, 1986). Depending on the fragment size of the DNA the agarose concentration in TAE buffer ranged from 0.5%-2.0%. Ethidium bromide was added to the melted agarose to a final concentration of 0.5µg/ml before pouring. 1xTAE was used as running buffer.

6x loading buffer

0.25% Bromphenol blue
0.25% Xylene Cyanol
30% Glycerol
100mM Tris pH 7.5
100mM EDTA pH 8.0
H_2O

50xTAE (2l)

484g Tris base
50mM EDRA pH 8.0
114.2ml glacial acetic acid
H_2O
adjust pH 8.5 with gl. ac. acid

Gel extraction of DNA

To purify specific DNA fragments, DNA was separated on an agarose gel. The band of interest was cut out of the gel using a sterile razor blade and purified using Qiagen Gel Extraction Kit as described in the company's manual. DNA was eluted with 30µl H_2O.

Plasmid preparations

Bacterial plasmids were purified using the corresponding Qiagen Kits as described in the respective manual provided from the company. For Mini-Preps 5ml of overnight bacteria culture in LB (containing selective antibiotics) was used. For Midi-Preps 200ml of overnight culture was used. After plasmid preparation the DNA concentration was determined using a photometer.

Polymerase chain reaction (PCR)

Standard PCR reactions were performed as described in the following protocol

25µl assay using Taq Polymerase

2.5µl 10x reaction buffer (containing 25mM $MgCl_2$)

0.4µl dNTPs (10mM)

0.6µl primer sense (10mM)

0.6µl primer antisense (10mM)

0.25µl Taq Polymerase

0.5µl DNA (50ng/µl)

H_2O

Standard PCR program using Taq Polymerase

1. 94°C 2min
2. 92°C 30sec
3. 58°C 30sec
3. 72°C 30sec/500bp
5. Step 2 to 4 for 34 more cycles
6. 72°C 5min

25µl assay using iProof Polymerase

12.5µl 2x iProof Master Mix

0.6µl primer sense (10mM)

0.6µl primer antisense (10mM)

(0.75 DMSO for genomic DNA)

0.5µl DNA (50ng/µl)

H_2O

Standard PCR program using Taq Polymerase

1. 98°C 30sec
2. 98°C 10sec
3. 58°C 30sec
3. 72°C 30sec/kb
5. Step 2 to 4 for 34 more cycles
6. 72°C 5min

Gateway Recombination Cloning

Invitrogen's Gateway technology uses the well-characterized bacteriophage lambda site-specific recombination pathway (Landy, 1989). After infection, the lambda DNA recombines with the corresponding bacterial DNA via *att* (attachment) sites. The attachment site in *E. coli* called *att*B, (B for bacteria) is recombined with the phage site called *att*P (P for phage) using a phage-encoded enzyme. The integrated phage DNA is now flanked by two variant *att* sites, *att*L and *att*R sites. The reverse reaction between *att*L (L for left) and *att*R (R for right) results in excision of the phage DNA, and regenerates the original *att*B and *att*P sequences.

For Gateway cloning the DNA fragment or gene of interest is flanked by two *att*B sites, by simply adding the sites to PCR primers. The *att*B flanked fragment is then recombined with the donor vector carrying two *att*P sites in a so called BP reaction. The recombination creates *att*L and *att*R sites. Recombinant entry clones selectively grow, as the lethal *ccd*B (control of cell death) gene, carried by the donor vector, is lost due to the recombination. The *ccd*B protein poisons bacterial DNA gyrase, causing degradation of the chromosome and cell death (Bernard P 1992, 1993). The obtained entry clone can then be recombined with various destination vectors in the LR reaction. The variety of destination vectors allows adding easily N-terminal and C-

terminal tags to the gene of interest or to express the gene under the control of different promoters just by performing one recombination step.

Generation of *gogo in situ* probes (performed by Satoko Suzuki)

Digoxigenin-labeled *gogo* RNA riboprobes were generated from EST clone RE53634 containing T7 and T3 RNA polymerase sites upstream and downstream of the cDNA. 10μg of template DNA was digested with restriction enzymes cutting downstream (for sense probe) or upstream (for antisense probe) to linearize the plasmid. The linearized DNA was purified using Qiagen PCR purification kit and used as a template for *in* vitro transcription. The reaction mix was incubated at 37°C for 2h and then stopped by adding 2μl of 0.5M EDTA. The transcripts (1μl) were checked on an agarose gel. Transcripts were hydrolyzed to obtain short RNA probes. 60μl of Hydrolysis buffer was added to the transcripts and incubated at 60°C for 10-60min [Incubation time in min = (Probe length in kb – 0.15) / 0.0165 x Probe length in kb]. Before precipitation with 300μl of chilled 100% EtOH, 8μl of 3M NaOAc (pH 5.2) and 1ml of 10mg/ml ssDNA was added. After 30min centrifugation the pellet was washed with 70% EtOH and air dried. The RNA was resuspended in 20μl H_2O and 80μl of Hybridization buffer was added. Probes were stored at -20°C.

In vitro transcription mix (20μl assay) (Roche)

2μl DIG RNA labeling mix
2μl 10x Transcription buffer
6μl linearized template DNA
1μl RNAse inhibitor
1μl T3 or T7 RNA Polymerase
H_2O

Hydrolysis buffer

60mM Na_2CO_3
40mM $NaHCO_3$ pH 10.2

Hybridization buffer

5x SSC (for eye disc pH 7.0)
50% Formamide
0.1% Tween20
50μg/ml Heparin
100μg/ml sonicated denaturized salmon sperm DNA

Isolation of genomic Drosophila DNA

Flies were collected in a 1.5ml eppendorf tube on ice. After adding Solution A to flies, they were homogenized using a 200µl pipette tip.

Added solution A:	1-5 flies	100µl
	6-10 flies	200µl
	-50 flies	400µl

Homogenized flies were incubated at 70°C for 30min, 14µl of 8M KAc was added per 100µl of solution A. The samples were then put on ice for 30min. After spinning for 15min at room temperature (RT) at 13,000rpm, the supernatant was transferred to a new tube. The same volume of phenol/chloroform as solution A was added. After mixing and spinning at 13,000rpm for 5min at RT, the upper aqueous phase was transferred to a new tube. As before, the same volume of phenol/chloroform as solution A was added. After mixing and spinning at 13,000rpm for 5min at RT, the upper aqueous phase was transferred to a new tube as before. DNA was precipitated by the addition of isopropanol (0.5 volume of solution A) and spin at 13,000rpm for 5min at RT. After washing the pellet in 70% EtOH, the pellet was dried and resuspended in 100µl of TE.

Solution A
0.1M Tris Hcl pH 9.0
0.1M EDTA pH 8.0
1% SDS
H_2O

TE
10mM Tris base pH 7.5
1mM EDTA pH 8.0
H_2O

Degenerative PCR

Degenerative PCR is used to map the insertion sites of P elements within the genome of *Drosophila melanogaster*. In this work P-element insertion was used to generate transgenic flies. In order to recombine the inserted transgenes with other transgenes or mutations the exact localization of the transgene has to be determined in order to calculate the expected recombination frequency, as well as the dimension of the required fly cross. Degenerative PCR is a sequence of two to three PCR reactions using genomic DNA isolated from a specific transgenic fly line. In the first PCR reaction one determined primer, specific for the used P-element is used in combination with a degenerate primer. The PCR reaction results in the formation of

PCR fragments of variable size with one defined and one variable end. These fragments are then used in a second or third PCR reaction to enrich the fragments. The obtained fragments are directly sequenced using the determined primer as a sequencing primer.

In this work, I searched for the insertion sites of UAS-Gogo-ΔC and UAS-Gogo-FL transgenes inserted on the 3rd chromosome to recombine them with a *gogo* mutant allele. Genomic DNA of the transgenic fly lines was isolated as described above as a template for the 1st PCR reaction. After the 2nd PCR bands of variable size could be visibly detected on agarose gel. The 2nd PCR sample was purified from PCR primers using EXOSAP (GE Healthcare Germany) and directly sequenced.

1st PCR (20µl assay)

2.0µl 10x reaction buffer (containing 25mM $MgCl_2$)

0.4µl dNTPs (10mM)

0.4µl T1BUAS primer (10mM) (binds to 3`of P element but is vector specific)

0.8µl AD3 primer (100mM) (degenerative primer)

0.25µl Taq Polymerase

0.8µl DNA

H_2O

1st PCR Programm

1. 93°C 1min
2. 95°C 1min
3. 94°C 1min
4. 62°C 1min
5. 72°C 2min30sec
6. Step 3 to 5 for 5 more cycles
7. 94°C 1min
8. 25°C 3min

Ramp to 72°C at 0.2°C/sec

9. 72°C 2min30sec
10. 94°C 30sec
11. 68°C 1min
12. 72°C 2min30sec
13. 94°C 30sec
14. 68°C 1min

15. 72°C 2min30sec
16. 94°C 30sec
17. 44°C 1min
18. 72°C 2min30sec
19. Step 10 to 18 for 15 more cycles
20. 72°C 5min

2nd PCR (20µl assay)

2.0µl 10x reaction buffer (containing 25mM $MgCl_2$)
0.4µl dNTPs (10mM)
0.4µl T2D primer (10mM) (binds to 3`of any P element)
0.4µl AD3 primer (100mM) (degenerative primer)
0.25µl Taq Polymerase
1µl of 1st PCR
H_2O

2nd PCR Programm

1. 94°C 1min
2. 94°C 30sec
3. 64°C 1min
4. 72°C 2min30sec
5. 94°C 30sec
6. 64°C 1min
7. 72°C 2min30sec
8. 94°C 30sec
9. 44°C 1min
10. 72°C 2min30sec
11. Step 2 to 10 for 11 more cycles
11. 72°C 5min

2.12 Generation of transgenic flies

P-element mediated transformation

The constructed DNA was inserted into the fly genome via P-element insertion. A P-element is a native Drosophila-specific transposon. Its excision and insertion in the

genome is catalyzed by the transposase which is encoded by the P-element. The P-element is flanked by inverted repeats containing the transposase recognition site. The P-element used for the generation of transgenic flies lacks the transposase gene. An additional helper plasmid containing the required enzyme has to be co-injected into the fly. The injected plasmid contains a P-element with a promoter and the cDNA of the gene of interest plus a marker gene to identify transgenic flies, everything flanked by the inverted repeats. In this work the used P-element contained the *w*+ (*white*) reporter gene to identify transgenic flies. Homozygous w^{1118} flies were injected. The w^{1118} allele causes a white eye phenotype.

Germline Transformation

The syncytial blastoderm of *Drosophila* embryos is an excellent target for gene transfer. In order to transform the germline the DNA is microinjected into the syncytium at posterior side of the embryo before pole cell formation. These cells will later form the germline of the fly. In this way, “new” DNA can be internalized by P-element insertion during cell formation and is integrated into the genome of the pole cells. This is only possible during the first 1.5 hr after fertilization, as during this time the embryo forms a syncytium of dividing nuclei (Campos-Ortega, 1997).

DNA preparation

Plasmid DNA and also the helper plasmid containing the transposase pP(Δ2-3) were centrifuged with for 10 min at full speed to avoid dust and dirt clogging the injection needle.

Injection mix (20 µl)

P-element plasmid	12 µg
pP(Δ2-3)	2 µg
dH_2O	

Preparation of fly embryos

To collect well-staged embryos from w^{1118} flies, young flies were put 2 days in advance to the injection into a population cage on apple agar plates with yeast paste and were incubated at 25ºC. The apple agar plates were several times a day. Embryos were collected on apple agar plates for 30 min and dechorinated in 50 % bleach solution for 2 min. Afterwards they were poured from the apple agar plates

onto a membrane filter on a vacuum flask. Then, the embryos were rinsed with H2O at least 5 times. Dechorinated embryos were lined up in posterior to anterior orientation using a brush with 3 fine bristles. The aligned embryos were then transferred to a glass slide greased with Scotch heptane glue and dried in silica gel filled box for 13-15min and then covered with Halocarbon oil.

Scotch heptane glue

Heptane and double-sided Scotch tape (Scotch #665) were put together in a 250 ml bottle. Heptane dissolved the glue from the tape resulting in quick evaporating glue.

Microinjection

The embryos were injected under the microscope with the prepared clean Injection mix. A pulled and grinded needle, which was connected to an Eppendorf FemtoJet micromanipulator, injected the DNA into the posterior end of the embryos. After injection the embryos were incubated at 18 ºC in a wet chamber. Hatched larvae were collected after two days and transferred into a fresh fly vial.

Eppendorf FemtoJet parameters:

Constant pressure (Pc): 60 hPa

Pressure of injection (Pi): ~100 hPa

Time of injection (Ti): ~0.5 sec

Identification and linkage of transgenic insertions

Flies developing from the injected embryos do not show visible signs for successful germline transformation. Therefore every hatched fly has to be crossed clonally to a w^- fly in order to select for marker gene expression in the next generation. Transgenic F1 generation flies contained a single copy of the dominant white$^+$ marker and could therefore be selected through their orange eye color.

In order to prevent transgenic flies from recombination and to link the transgenic insertion to a certain chromosome the flies were balanced. A balancer chromosome is characterized by a recessive lethality, multiple inversions and a dominant marker. Each transgenic fly line was individually crossed to balancers for the second or third chromosome. Heterozygous progeny containing one dominant marker and the transgene were again crossed. According to Mendel law correctly balanced flies did not show any w^- progeny in the next generation. Of each construct several independent lines were generated and tested. Depending on the expression level,

which usually correlates with darkness of eye color, intermediate lines were selected and added to the stock collection.

2.13 Fly genetics

Reporter/Gene expression in photoreceptors

***ey*FLP**

Different *ey* (*eyeless*) enhancer fragments were used. Detailed description can be found in the description of the FLP/FRT system (see next chapter)

***glass*-lacZ**

The *glass* protein is present in the nuclei of all cells posterior to the morphogenetic furrow in the eye-imaginal disc (Moses and Rubin, 1991). In addition expression was also observed in the Bolwig's organ and in some cells of the embryonic and third-instar larval brain. *glass* protein positively regulates its own expression. For creating a *glass*-lacZ reporter a *lacZ* enhancer-trap element was inserted at the *glass* locus (Moses and Rubin, 1991).

***gmr* (*glass multiple reporter*)**

gmr enhancer is composed of five copies of a Glass response element from the Rh1 gene and drives expression in all cells behind the morphogenetic furrow (Freeman, 1996; Hay et al., 1994).

***rh*1-lacZ**

*rh*1 (*rhodopsin*1) enhancer fragment which is specifically expressed in R1-R6 fused to lacZ (Mismer and Rubin, 1987; Newsome et al., 2000)

***rh*4-mCD8GFPmyc**

*rh*4 (rhodopsin4) enhancer fragment which is specifically expressed in 70% of adult R7 (Fortini and Rubin, 1990; Newsome et al., 2000) was subcloned upstream of mCD8GFPmyc (Georg Dietzl, unpublished)

ato-τmyc

ato (*atonal*) is expressed anterior to the morphogenetic furrow and is strongly expressed in R8 after its formation beyond the furrow (Jarman et al., 1994).

Expression lasts only in 2-3 rows of R8s corresponding to 4-6h of development. *ato*-Gal4 expression can be detected until mid-pupal stages (at least until 55APF). A 2-kb R8-specific enhancer fragment derived from the atonal locus was used for the *ato*-τmyc reporter (Senti et al., 2003).

***rh*6-mCD8GFPmyc**

*rh*6 (*rhodopsin*6) enhancer fragment which is specifically expressed in 70% of adult R8 (Papatsenko et al., 2001) was subcloned upstream of mCD8GFPmyc (Georg Dietzl, unpublished).

***PM181*-Gal4**

PM181-Gal4 is specifically expressed in R7 (Lee et al., 2001)

PANR7-Gal4

R7-specific driver (Lee et al., 2001)

***109-68*Gal4**

*109-68*Gal4 is an enhancer trap insertion on the second chromosome (Jarman and Ahmed, 1998; White and Jarman, 2000) and is specifically expressed in R8s starting from the 3rd larval stage. Takashi Suzuki examined the expression during pupal stages. There is no expression in R7 at any time.

***caps*-Gal4**

caps-Gal4 is an enhancer trap insertion. *caps*-Gal4 expression was detected specifically in R8 in third instar larvae and throughout pupal stages (Shinza-Kameda et al., 2006).

FLP/FRT system

Different *ey* enhancer fragments were used to induce mitotic recombination upon Flipase expression. Depending on the used *ey* enhancer fragment different clone sizes and slightly different expression patterns were obtained. In addition, mutant clone size was increased by inserting the *Minute* mutation M(3)i[55] (RpS17) onto the left arm of the 3rd chromosome in trans to the *gogo* mutant alleles. *Minute* mutations prevent the proliferation or survival of homozygous cells, and retard the proliferation of heterozygous cells (Morata and Ripoll, 1975).

*ey*FLP2 (referred to as *ey*FLP)

*ey*FLP is a 258bp eye-specific enhancer fragment from the *ey* gene upstream of the FLPcDNA (Newsome et al., 2000). *ey*FLP2 represents the transgene which is inserted on the X chromosome in a *yw* background. The *ey* enhancer fragment used in this *eyFLP* construct does not recapitulate the entire expression pattern of the *ey* gene, but is almost exclusively expressed in the visual system (Hauck et al., 1999). Expression begins in the 6-23 cell eye disc primordium in stage 15 embryos and is maintained until the final cell divisions in the approx. 15000-cell disc of the late third instar larvae. A lower level of expression can also be detected in the optic lobes, resulting in the generation of small mutant brain clones in mosaic animals. Mutant clone size in the retina without cell lethal mutation ranges from 20-30%. Using a cell lethal mutation, almost the entire retina 90% is homozygous mutant (Newsome et al., 2000).

ey$^{3.5}$FLP

ey$^{3.5}$FLP is a 3.5kb eye-specific enhancer fragment from the *ey* gene cloned from *ey*tTA vector (Bazigou et al., 2007). This clean *ey* enhancer does not show any brain expression

*ey*1x-FLP.Exel

*ey*1x-FLP.Exel expresses FLP recombinase in the pattern of the *eyeless* gene. One copy of the *ey* enhancer drives FLP expression (Exelixis, Inc.). Obtained mutant mosaics are distinctly smaller then using *ey*FLP without cell lethal mutation. Our personal impression is that less than 5% of photoreceptors are mutant.

MARCM (Mosaic analyses with a repressible cell marker)

MARCM (Mosaic analyses with a repressible cell marker) is a widely used technique in *Drosophila* which allows the generation of labeled mutant cells in mosaic tissues (Lee and Luo, 1999). Heterozygous or WT cells remain unlabeled. To achieve this, the yeast Gal80 protein was introduced into the GAL4-UAS expression system in *Drosophila*. The Gal80 protein inhibits the activity of the transcription factor GAL4 (Brand and Perrimon, 1993). Heterozygous cells contain the transgene for GAL80 *in trans*, but on the same chromosomal arm, to the mutated gene of interest. Following FLP/FRT-mediated mitotic recombination, the GAL80

transgene is removed from the homozygous mutant daughter, allowing expression of a GAL4-driven UAS-GFP reporter gene specifically in this mutant cell and its progeny.

cMARCM (complementary MARCM) (established by Satoku Suzuki)

In a normal MARCM situation, homozygous and heterozygous WT cells remain unlabeled making it impossible to examine the behavior of mutant and WT cells in respect to each other. To circumvent this problem an additional marker mKOrange under the control of the promoter GMR was inserted on the Gal80 containing chromosomal arm. The monomeric Kusabira Orange (mKOrange) gene was obtained from the vector pmKO1-MN1 (MBL). The mKOrange gene fused in frame to the 3' end of mCD8 was tagged with myc epitopes and inserted into the GMR vector to generate a GMR-mCD8mKOrange construct and used for generation of transgenic flies. Following FLP/FRT-mediated mitotic recombination in cMARCM flies, the mKO marker is specifically lost from mutant cells but retained in homozygous and heterozygous WT cells, allowing a clear distinction between differentially labeled WT and mutant cells.

2.14 Summary of experimental genotypes

Figure 3-1:

A´) *yw ey*FLP C-lacZ; *gogo*[D869] FRT80B / M(3)i[55] FRT80B

B´) *yw ey*FLP *Rh1*-τlacZ; *gogo*[D869] FRT80B / M(3)i[55] FRT80B

C´) *yw ey*FLP *Rh4*-mCD8GFPmyc; *gogo*[D869] FRT80B / M(3)i[55] FRT80B

D´) *yw ey*FLP *Rh6*-mCD8GFPmyc; *gogo*[D869] FRT80B / M(3)i[55] FRT80B

Figure 3-2:

B) *yw ey*FLP C-lacZ; *ato-τmyc gogo*[D869] FRT80B / M(3)i[55] FRT80B

D) *yw ey*FLP C-lacZ; *gogo*[D869] FRT80B / M(3)i[55] FRT80B

F) *yw ey*FLP C-lacZ; *gogo*[D1600] FRT80B / M(3)i[55] FRT80B

Figure 3-4:

ii) *yw ey*FLP C-lacZ; *gogo*[D869] FRT80B / M(3)i[55] FRT80B

iii) *yw ey*FLP C-lacZ; GMR-*gogo*FL/+; *gogo*[D869] FRT80B / M(3)i[55] FRT80B

…

Figure 3-8:

A, D) *yw ey*FLP C-lacZ; *gogo*[D869] FRT80B / *gogo*[1600] FRT80B

B, E) *yw ey*FLP C-lacZ; *GMR-gogo*FLmyc/+; *gogo*[D869] FRT80B / *gogo*[1600] FRT80B

C, F) *yw ey*FLP C-lacZ; *GMR-gogo*FLmyc/+; *gogo*[D869] FRT80B / M(3)i[55] FRT80B

Figure 3-9:

F) *yw ey*FLP C-lacZ; *GMR*-Gal4 / UAS-*gogo*FLmyc-T2; *gogo*[D869] FRT80B / *gogo*[1600] FRT80B

G) *yw ey*FLP C-lacZ; *gogo*2-Gal4 / UAS-*gogo*FLmyc-T2; *gogo*[D869] FRT80B / *gogo*[1600] FRT80B

Figure 3-10:

A) *yw ey*FLP C-lacZ; *gogo*[D1600] FRT80B / M(3)i[55] FRT80B

B, C, D) *yw ey*FLP C-lacZ; *gogo*[D1600] FRT80B / M(3)i[55] FRT80B

D) $ey^{3.5}$FLP; *gogo*[DH1675] FRT80B / M(3)i[55] FRT80B

Figure 3-11:

B) GMR-FLP; PanR7Gal4 UAS-*nsyb*::GFP/+; *gogo*[D869] FRT80B/ *tub*-Gal80 FRT80B

C) *PM181*-Gal4 / *yw ey*FLP C-lacZ; *gogo*[D869] FRT80B UAS-*gogo*FLmyc-3B/ M(3)i[55] FRT80B

D) *yw ey*FLP C-lacZ; 109-68Gal4 / UAS-*gogo*FLmyc-T2; *caps*-Gal4 *gogo*[D869] FRT80B / M(3)i[55] FRT80B

Figure 3-13: (without heat shock!)

A) *hs*FLP *elav*-Gal4 UAS-mCD8GFP; *ey*1xFLP.Exel/+;
FRT80B / GMR-mCD8mKOmyc *tub*-Gal80 FRT80B

B, C) *hs*FLP *elav*-Gal4 UAS-mCD8GFP; *ey*1xFLP.Exel/+; *gogo*[D869] FRT80B / GMR-mCD8mKOmyc *tub*-Gal80 FRT80B

D) *hs*FLP *elav*-Gal4 UAS-mCD8GFP; *ey*1xFLP.Exel/+; *gogo*[D869] FRT80B UAS-*gogo*FLmyc-3B / GMR-mCD8mKOmyc *tub*-Gal80 FRT80B

E) *hs*FLP *elav*-Gal4 UAS-mCD8GFP; *ey*1xFLP.Exel/+; *gogo*[D869] FRT80B UAS-*gogo*ΔCmyc-3B / GMR-mCD8mKOmyc *tub*-Gal80 FRT80B

Figure 3-14:

A) *yw*; *ey*1xFLP.Exel/+; *ato*-τ*myc* FRT80B / GMR-mCD8mKOmyc *tub*-Gal80 FRT80B

B, C) *yw*; *ey*1xFLP.Exel/+; *ato*-τ*myc gogo*[D869] FRT80B / GMR-mCD8mKOmyc *tub*-Gal80 FRT80B

Figure 3-15:

A, D) *yw ey*FLP *Rh6*-mCD8GFPmyc; FRT80B / M(3)i[55] GMR-mCD8mKOmyc *tub*-Gal80 FRT80B

B, E) *yw ey*FLP *Rh6*-mCD8GFPmyc; *gogo*[D869] FRT80B / M(3)i[55] GMR-mCD8mKOmyc *tub*-Gal80 FRT80B

F) *yw ey*FLP *Rh6*-mCD8GFPmyc; *gogo*[D869] FRT80B / GMR-mCD8mKOmyc *tub*-Gal80 FRT80B

Figure 3-16:

A) *yw*; *ey*1xFLP.Exel/+; *ato*-τ*myc* FRT80B / GMR-mCD8mKOmyc *tub*-Gal80 FRT80B

B-D) *yw*; *ey*1xFLP.Exel/+; *ato*-τ*myc gogo*[D869] FRT80B / GMR-mCD8mKOmyc *tub*-Gal80 FRT80B

E-G) *yw ey*FLP *Rh6*-mCD8GFPmyc; *gogo*[D869] FRT80B / GMR-mCD8mKOmyc *tub*-Gal80 FRT80B

Figure 3-17:

A-D) *yw ey*FLP C-lacZ; *ato*-τ*myc* FRT80B / M(3)i[55] FRT80B

E-G) *yw ey*FLP C-lacZ; *ato*-τ*myc gogo*[D869] FRT80B / M(3)i[55] FRT80B

H) *yw*; *ey*1xFLP.Exel/+; *ato*-τ*myc gogo*[D869] FRT80B / GMR-mCD8mKOmyc *tub*-Gal80 FRT80B

Figure 3-18:

A) *Rh6*-mCD8GFPmyc; GMR-Gal4/+

B) *Rh6*-mCD8GFPmyc; GMR-Gal4/UAS-*gogo*FLmyc-T1

C) *Rh6*-mCD8GFPmyc; GMR-Gal4/UAS-*gogo*FLmyc-T2

2.15 Bioinformatics (performed by Alexander Schleiffer)

The GOGO conserved domain was characterized using iterative PSI-BLAST searches (Altschul and Koonin, 1998) within the NCBI non redundant database (May

2007). The Drosophila N-terminal uncharacterized region (54-458) was used to collect proteins from insect genomes. A search with the homologous *A.aegypti* sequence (amino acids 3-357) converges with insect proteins, but in addition, there was a subsignificant hit to a *Canis familiaris* (dog) protein. Interestingly, the *C.familaris* protein contains a TSP1 domain (344-394). Using the dog hit to the GOGO domain, other Deuterostomia could be identified. NCBI-BLASTp searches within the *Ciona intestinalis* proteome (Dehal et al., 2002) and the *Strongylocentrotus purpuratus* proteome (Sodergren et al., 2006) revealed one ortholog in each proteome. The *Caenorhabditis elegans* GOGO protein F09F9.4 was identified in a HMMer search (Eddy, 1998) using a multiple alignment of GOGO domain proteins (Bailey and Gribskov, 1998; Do et al., 2005). The cytoplasmic motif shared by insects, worms, and Deuterostomia, was identified within a set of 15 C-termini of Gogo orthologues using Meme (Bailey and Gribskov, 1998).

2.16 Cell culture

Culturing of S2 cells

Cells were grown at 25°C in 12ml S2 growth medium in 50ml tissue culture flasks (Falcon). When cell density reached 6 to 20 x10^6 cells/ml (determined using a Neubauer counting chamber), they were split in a 1:5 dilution. Before splitting cells were gently resuspended by washing the surface of the flask with a 5ml pipette. Clump of cells were broken by briefly pipetting up and down after the cells have detached.

S2 growth medium
Schneider's Drosophila Medium (Promocell)
1% L-Glutamine (Promocell)
10% FCS (Promocell)
1% 100x PenStrep (Sigma-Aldrich)

Transfection of S2 cells

The cells should reach a density of 5x 10^5 -1x 10^6 cells/ml before transfection. Cells were gently resuspended by washing the surface of the flask with a 5ml pipette.

Clump of cells were broken by briefly pipetting up and down after the cells have detached. 2ml of cell suspension was placed into each well of a 6-well-plate (Falcon). The cells were allowed to settle down for 6-12h. The growth medium was removed from the cells and replaced with 1ml serum-free media. In the meantime the transfection mix was prepared: In an eppendorf tube 2μg of pActin-Gal4 and 2-8 μg of the respective pUAS vector were added to 100μl of serum-free media. In a second eppendorf tube 10μl of Cellfectin (Invitrogen) was added to 100μl of serum-free media. The content of the two eppendorfs was merged and carefully mixed by tapping the tube and then incubated for 30min at RT. After adding 800 μl of serum-free media the transfection mix was put on the cells. 16h after transfection serum-free transfection mix was removed from the cell and replaced with S2 growth medium. The cells were allowed to grow for 24h before further examination.

Cell aggregation assay (performed by Xiuye Chen)

GFP-tagged *gogo* constructs (UAS-*gogo*FL::GFP, UAS-*gogo*ΔC::GFP) were transiently expressed in S2 cells by cotransfection with p*Actin*-Gal4 using Cellfectin (Invitrogen). As a positive control, pUAS-*fmi* was cotransfected with *Actin*-Gal4 and UAS-*citrine*. The aggregation assay was performed for three times starting from transfection as described (Matthews et al., 2007). After transfection cells were resuspended and diluted to a density of 2x 10^6 cells/ml. Suspended cells were transferred to a 2ml eppendorf tube and rotated at RT at 150RPM for 6h. An aliquot of cells (100μl of a 1:5 dilution) was spotted for aggregation.

2.17 Fly maintenance

Flies were cultured in vials or, for expansion, in bottles with ~2 cm of fly food covering the bottom. Vials/bottles were put into cardboard boxes and stored in incubators controlling temperature and humidity. Humidity was held constantly between 60 and 70%, while the temperature was set to 25 ºC for expanding flies, including crossings, and to 18 ºC for maintaining the stock. For R7 specific GMR-FLP MARCM, flies were shifted down from 25°C to 18°C for three days after eclosion. For examination the flies were anaesthetized with CO_2 and put on a CO_2 pad underneath a stereo microscope.

2.18 Biochemistry

Lysis

Dissected larval brains or whole pupae were smashed in 25µl loading buffer using a glass homogenizer (Kontes Glass Co. 398) for exactly 1min. Another 25µl loading buffer was added and the cell lysat was transferred to an eppendorf tube and stored on ice. Protein samples were cooked for 10min at 98°C and subsequently centrifuged for 2min at 13.000rpm. The supernatant was transferred to a fresh eppendorf tube and either stored at -4°C or directly used for SDS-PAGE.

Immunoblotting

Protein samples were cooked for 10min at 98°C and subsequently centrifuged for 2min at 13.000rpm. 20µl of the supernatant were separated by SDS-PAGE on a 7.5% resolving gel Tris-HCl (Bio- Rad Laboratories GmbH). After protein separation the bands were blotted to a Hybond ECL Nitrocellulose membrane (Amersham) for 2h. Membranes were washed briefly with water and incubated with blocking solution (5% milk powder in PBS) for 1h. Primary antibody was applied in blocking solution o/n at 4°C while rocking in a wet chamber on a shaker. The membrane was washed 3 x 10 min with PBS. Secondary antibody was applied in PBS for 2-3h at RT on a shaker. The membrane was washed 3 x 10 min with PBS and 1x10min in 0.1% PBTw (0.1% Tween in PBS). The membrane was incubated in 14ml of ECL solution (GE Healthcare) and exposed to Hyperfilm ECL (Amersham).

Running buffer
25mM Tris
250mM Glycin
0.1% SDS

Blotting buffer
25mM Tris
250mM Glycin
0.02% SDS
30% Methanol

Loading buffer
100mM Tris pH 6.8
40g/l SDS
20% Glycerol
0.25g/l Bromphenol Blue
200mM β-Mercaptoethanol

2.19 Histology

S2 cell surface labeling

GFP-tagged constructs (UAS-*gogo*FL::GFP, UAS-*gogo*ΔC::GFP and UAS-mCD8::GFP) were transiently expressed in S2 cells by co-transfection with *Actin*-Gal4 using Cellfectin (Invitrogen).48h after transfection, cells were plated on μ-Slide VI, Poly-L-Lysine coated slides (Ibidi), as described in the users manual. Fixation was done for 30min at 37 degree with 4% Paraformaldehyde. For permeabilization, cells were treated with (+Triton) 0.4%Trition or without Triton (-Triton) in PBS for 10min. After washing, cells were blocked with 5%NGS in PBS and stained with primary antibody α-Gogo over night at 4°C. After washing 4x2min with PBS the secondary antibody α-rabbit Alexa 568 was applied for 2h at RT. After washing with PBS, Vectashield Mounting Medium (Vector Laboratories Inc.) was added to the cells. GFP signal was observed directly without immunostaining.

Whole mount brain antibody staining

Whole mount brain antibody stainings were performed of 3rd instar larvae, pupae and adult flies. Larval and pupal brains were directly dissected in PBS. For staging of pupal development, white pupae that have enclosed shortly were transferred into a new vial (representing time point 0 of pupal development = 0APF) and were incubated at 25°C for a certain time and then immediately dissected. Pupal cases had to be carefully removed around the head region before dissection. Adult female or male *Drosophila* flies were anesthetized with CO_2 and transferred into 70% EtOH for 30s in order to remove the wax that covers the cuticles. Then the flies were dissected in PBS solution. Tracheas that normally cover adult brains were removed.
All brains were transferred in 100μl of PBS on ice after dissection. 10 μl of 37% Formaldehyde were added and the brains were fixed on a shaker for 25min. Then brains were washed 3x10min in 0.2% PBT (0.2% Triton-X in PBS). The brains were blocked for 30min in 0.2% PBT with 5% NGS and then stained on a shaker from over night up to 2 days at 4°C. Antibody solution contained 1st antibody in 0.2% PBT with 5% NGS. After washing the brains 3x10min in 0.2% PBT the 2nd antibody in 0.2% PBT with 5% NGS was applied. Again, the brains were incubated on a shaker from over night up to 2 days at 4°C. After washing the brains 3x10min in 0.2% PBT, brains

were mounted on microscope slides using Vectashield Mounting Medium (Vector Laboratories Inc.)

Whole mount LacZ staining

3rd instar larval brains were dissected in PBS and transferred in PBS on ice. Brains were fixed at RT in 0.5% Glutaraldehyde in PBS. After fixation brains were washed once in PBS and then incubated in Staining solution at 37°C. The reaction was stopped by washes in PBS. Brains were mounted in 70% Glycerol in PBS.

Buffer B	Staining solution
10mM Sodium Phosphate buffer pH 7.0	500µl Buffer B
1mM $MgCl_2$	5µl 0.3M Ferricyanide
150mM NaCl	5µl 0.3M Ferrocyanide
H_2O	5µl 10% Triton X-100
	5µl 10% X-Gal solution
	(0.1g X-Gal/1ml DMF)

Cryostat section antibody staining

Adult *Drosophila melanogaster* flies were anesthetized with CO_2. On the fly pad *Drosophila* heads were cut off using straight and sharp Spring scissors Cohan-Vannas (Fine Science Tools). After removing the proboscis, the heads were transferred into 2% Formaldehyde in PBS containing 0.05% TritonX-100 and fixed for 60-90min at 4°C. After washing the heads in PBS, they were transferred in 12% Sucrose in PBS at 4°C for 16h. The heads were removed from the sucrose and submerged in a drop of Sakaura Tissue-Tek O.C.T. Compound (Vogel GmbH & Co. KG). The heads were allowed to be permeated by the O.C.T. compound for 10-30min at RT and then embedded in O.C.T in Peel-a-way embedding molds T8 (Polysciences) and frozen on dry ice. 10-14µm horizontal sections were made using the cryostat and loaded onto SuperFrost Plus microscope slides (Menzel). After drying the sections for 5min at RT they were fixed in 0.5% Formaldehyde in PBS for 20-60min at RT and washed in PBS 3x3min. Slides were blocked in 0.3% PBT (0.3% Triton-X in PBS) with 1% BSA for 30min. After washing 3x10min in 0.3% PBT, 200µl of 1st antibody solution was added to each slide in a wet chamber and incubated over night at 4°C. Antibody solution contained 1st antibody in 0.3% PBT with 5% NGS.

After washing the slides two times each 3x10min, HRP conjugated secondary antibody in 0.3% PBT with 5% NGS was added to the slides in a wet chamber and incubated for 4h at RT. Slides were washed through several changes of 0.3% PBT and then incubated in DAB staining solution for 15-30min at RT. DAB staining solution consists of 0.03% H_2O_2 in DAB. When reaction has completed, the reaction was stopped by washing the slides with PBS. Microscope slides were covered with 70% Glycerol in PBS and cover slips.

In situ hybridization of larval eye discs

Larval disc preparation

20-40 larval eye discs were dissected in PBS and transferred in PBS on ice. They were fixed in 4% Formaldehyde in PBS for 40-60min and then washed in PBT. The discs were dehydrated through a gradually increasing EtOH series (30-100% in H_2O). After transferring the discs to a glass vial, they were rinsed with EtOH:Xylene (1:1), then soaked in pure Xylene for 1h and again rinsed first with EtOH:Xylene (1:1) and second with MtOH. Discs were rehydrated through a gradually increasing MtOH series (80-0% in H_2O). After permeabilizing the discs in 80% Acetone in H_2O for 10min at -20°C, the Acetone was removed and 1ml of PTw added. The discs were transferred to eppendorf tubes. After washing the discs 2x10min in PTw, they were postfixed for 20min in 4% Formaldehyde and again washed 2x10min in PTw.

Hybridization

Discs were washed for 10min in Hybridization buffer:PTw (1:1) and in Hybridization buffer. Discs in 100µl Hybridization buffer were prehybridized for more then 30min at 55°C. The Hybridization solution, containing 100µl Hybridization buffer, 1µl denaturated salmon sperm DNA (10mg/ml) and 1-5µl of the riboprobe, was denaturated at 95°C for 5min and immediately cooled on ice. After preheating the Hybridization solution at 55°C it was added to the prepared eye discs. Samples were hybridized over night at 55°C. Hybridization was followed by a series of washing steps: 1) wash 2x20min in 500µl Hybridization buffer at 55°C; 2) wash 10min in 500µl Hybridization buffer at RT; 3) after 5min add 250µl Hybridization buffer/PTw (2:1); 4) again after 5min add 250µl Hybridization buffer/PTw (1:1); 5) Remove 500µl of liquid; 6) add 250µl Hybridization buffer/PTw (1:2) and wash for 5min; 6) wash 10min in PTw; 7) wash 10min in PBT

Detection

Samples were blocked in PBT with 5% NGS. Discs were incubated with anti-DIG AP antibody in PBT over night at 4°C. After washing 2x20min in PBT, discs were rinsed in AP buffer and washed in 1ml of AP buffer for 30min. Most of the liquid was removed and the Staining solution added to discs. The sample was allowed to develop in the dark at RT for 30-60min. Afterwards the reaction was stopped by washing 2x15min in PBT. Samples were stored in PBS.

For double staining, *in situ* hybridization was performed first and detected with HNPP Fluorescent Detection Set (Roche), followed by antibody staining.

AP buffer
100mM NaCl
50mM $MgCl_2$
Tri-HCl pH 9.5

PTw
PBS 0.1% Tween

PBT
PBS 0.1% TritonX

Hybridization buffer
5xSSC (for eye disc pH 7.0)
50% Formamide
0.1% Tween20
50μg/ml Heparin
100μg/ml sonicated denaturated salmon sperm DNA

Staining solution
1ml AP buffer
4.5μl NBT (Roche)
3.5μl BCIP (Roche)

Transmission electron microscopy (in collaboration with Marianne Braun)

Adult *Drosophila melanogaster* flies were anesthetized with CO_2 and transferred into 70% EtOH for 30s. In PBS *Drosophila* heads were cut off using straight and sharp Spring scissors Cohan-Vannas (Fine Science Tools). After removing the proboscis, the heads were transferred into fixative (2.5% glutaraldehyde in PBS) over night. Fly heads were postfixed in Dalton solution (containing 1% Osmiumtetroxide, 1% Kaliumbichromat and 0.85% Natriumchlorid) and further dehydrated and embedded in Epon. Semi-thin sections (1μm) were stained with Toloidinblue. Ultra-thin sections (70nm) were obtained with an Ultracut Ultramicrotome (Reichert-Jung) and counterstained with Uranylacetat and Leadcitrat. Images with a magnification of 6000x were taken using a Zeiss EM 10 and JEOL TEM 1230.

3 Results

3.1 Gogo is required for R axon pathfinding

Adult animals in which photoreceptor (R) neurons are specifically homozygous for *gogo* mutation (*gogo*$^-$ *ey*FLP flies) show a number of defects in all R axon types. They display incomplete medulla rotation, combined with the formation of abnormal bundles through an ectopic chiasm at the posterior side of the lamina (Figure 3-1A, A'). Although R1-6 axons correctly target the lamina, the overall lamina structure shows mild irregularities (Figure 3-1B, B'). The projection pattern of R7 axons is generally disrupted, resulting in crossings and a low frequency of undershooting the medulla layer M6 (Figure 3-1C, C'). R8s have the most striking defects among the R cell axons: they cross and bundle, they often overshoot their correct target layer (M3) and mistarget to the R7 target layer M6 (Figure 3-1D, D'). Moreover, R8s often stall at the temporary layer (M1) and fail to innervate the medulla (Figure 3-1D' arrowheads).

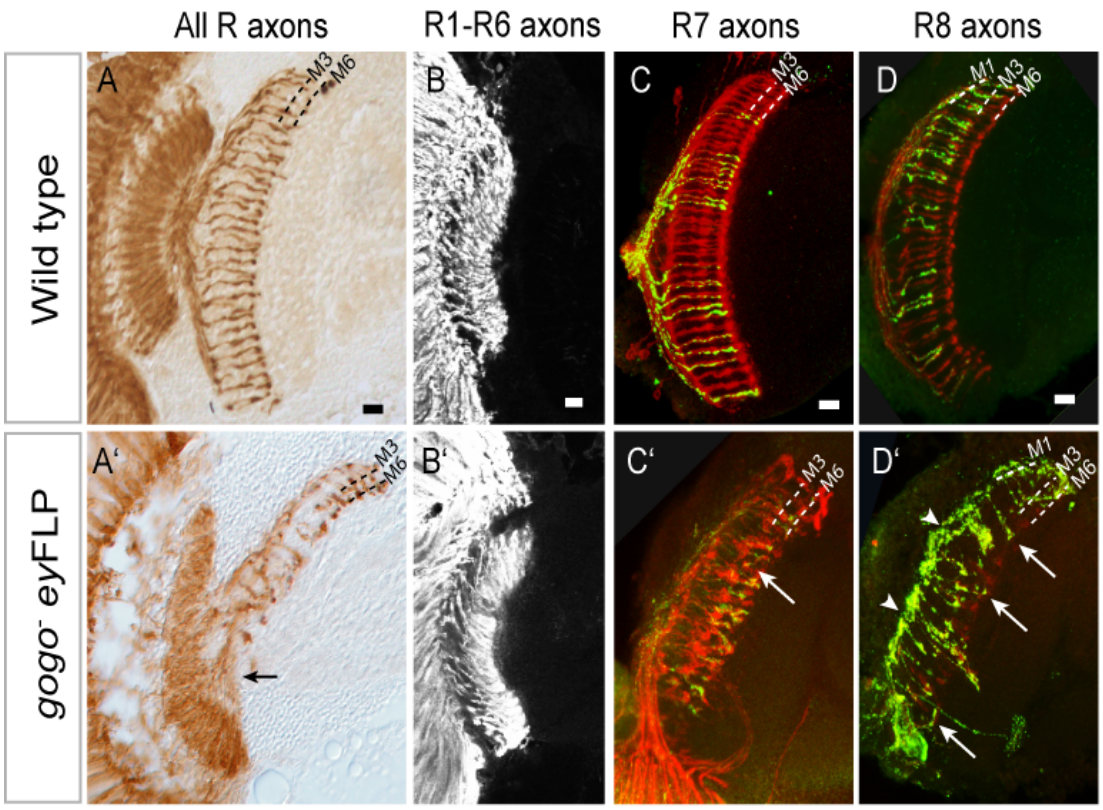

Figure 3-1 Pathfinding defects of *gogo* mutant R axons.
(**A-D**) Horizontal cross section images of the adult fly heads: wild type (A-D), *gogo*^{D869} *ey*FLP mutant (A'-D'). Flies expressing *gl-lacZ* marker in R1-R8, stained with anti-β-galactosidase (A, A'); *Rh1-τlacZ* expressed in R1-R6, stained with anti-β-galactosidase (B, B'); flies expressing the R7 marker *Rh4*-mCD8GFP (C, C') or R8 marker *Rh6*-mCD8GFP (D, D'), stained with mAb24B10 (red) and anti-GFP (green). Mainly R axons that target the medulla (R7 and R8) exhibit striking phenotypes. They form a second chiasm (arrow in A'), bundles and mutual crossings. R7 undershoot their correct target layer (arrow in C') and R8-overshooting phenotypes (arrows in D') were observed at low frequency. R8s often stall at their temporary layer (M1) and fail to innervate the medulla (arrowheads in D'). Scale bars 10μm

All three isolated mutant *gogo* alleles, which induce a premature translation stop before the transmembrane domain (Figure 1-7), were considered as null alleles, as they exhibit the same phenotype of R axon projections in *ey*FLP mosaics, in sporadic survivors of trans-allelic combinations (transheterozygous flies) and over a deficiency uncovering *gogo* locus (Df(3L)ED4858) (Figure 3-1, Figure 3-4; and data not shown).

To look for the onset of axon pathfinding defects in *gogo* mutants, R8 axons were specifically labeled using *ato-τmyc* (*myc* tagged bovine Tau protein expressed under the R8-specific promoter *atonal*; Senti et al., 2003) in *gogo*$^-$ *ey*FLP third instar larvae. In wild type, R8 axons are evenly spaced (Figure 3-2A, A*i*), whereas in *gogo* mutants, bundles and gaps appear between adjacent R8 axons in the medulla (Figure 3-2B, B*i*). Interestingly, the defect seems to set in after R8 axons have passed through the lamina and reach the medulla. This erroneous pathfinding suggests that the proper interaction between *gogo*$^-$ R8 axons is lost, most likely at the stage when R axons enter the medulla.

The maturation of optic lobes requires proper R cell differentiation and innervation from the compound eye (Huang and Kunes, 1996; Meyerowitz and Kankel, 1978; Selleck et al., 1992). However, since all photoreceptors were present and properly located in the tangential sections of *gogo*$^-$ *ey*FLP compound eyes (Figure 3-2E, n=5, 648 ommatidia for [D1600]; n=3, 494 ommatidia for [H1675]), the observed phenotypes in *gogo* mutants are not due to defects in R cell fate specification. Moreover, neurons and glia show no developmental defects in the brain in larval *gogo*$^-$ *ey*FLP mutant brains (Figure 3-2C, D).

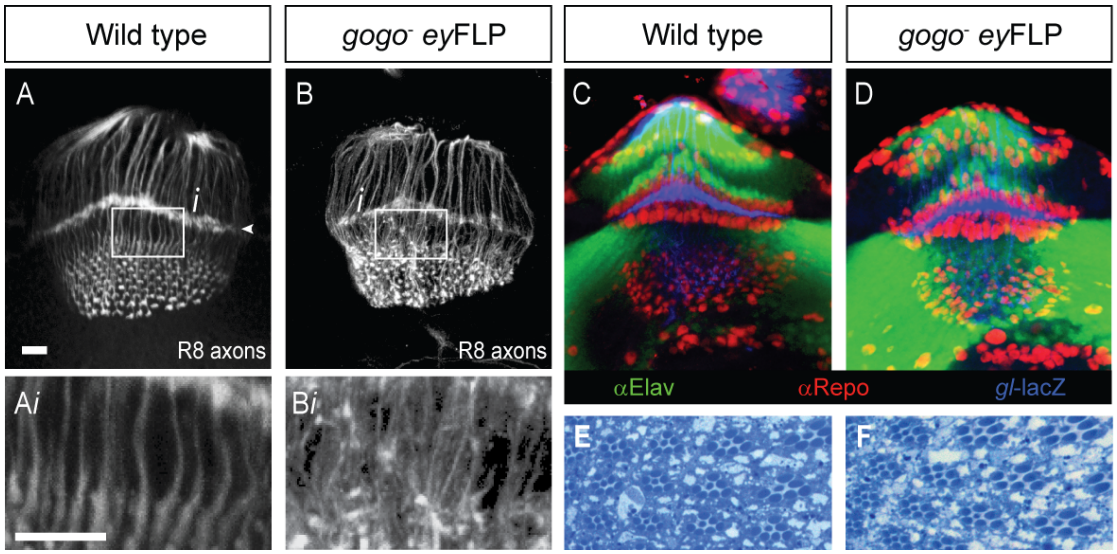

Figure 3-2 Onset of developmental defects

(**A-B**) R8 axons in the larval optic lobe expressing the *ato-τmyc* transgene stained with anti-Tau and anti-Myc antibody. WT R8 axons form parallel tracts and the growth cones are distributed evenly (A, A*i*). In *gogo*^{D869} *ey*FLP larvae, R8 axons show drastic defects in the medulla. Axons tangle and bundle to each other (B, B*i*). Magnified images are shown in A*i* and B*i*. Arrowhead: Lamina plexus. (**C-D**) The optic lobes of third instar larvae are shown. Flies express *gl-lacZ* marker in R1-R8. Neurons (anti-Elav; green), glia (anti-Repo; red) and R axons (anti-β-gal; blue) are stained. In *gogo*^{D869} *ey*FLP mutants, location and number of neurons and glia cells are indistinguishable from wild type. (**E-F**) Tangential sections of WT and *gogo*^{D1600} *ey*FLP retina were stained with Toloidinblue: The rhabdomeres of photoreceptor neurons develop normally in *gogo* mutants. Scale bars 10μm

3.2 Gogo is evolutionary conserved

Studies in vertebrate and invertebrate systems have revealed that the mechanism and the molecules that control axon guidance are highly conserved in evolution (Goodman, 1994). Since both the Tsp1 and the CUB domains are widespread across animals, the search for homologues was concentrated on the apparently uncharacterized N-terminal region (54-458aa, Figure 1-7). A series of PSI-BLAST searches within the NCBI non-redundant database was performed in collaboration with Alexander Schleiffer (IMP, Vienna). Homologues were not only identified in other insects, but also in nematodes and vertebrates.

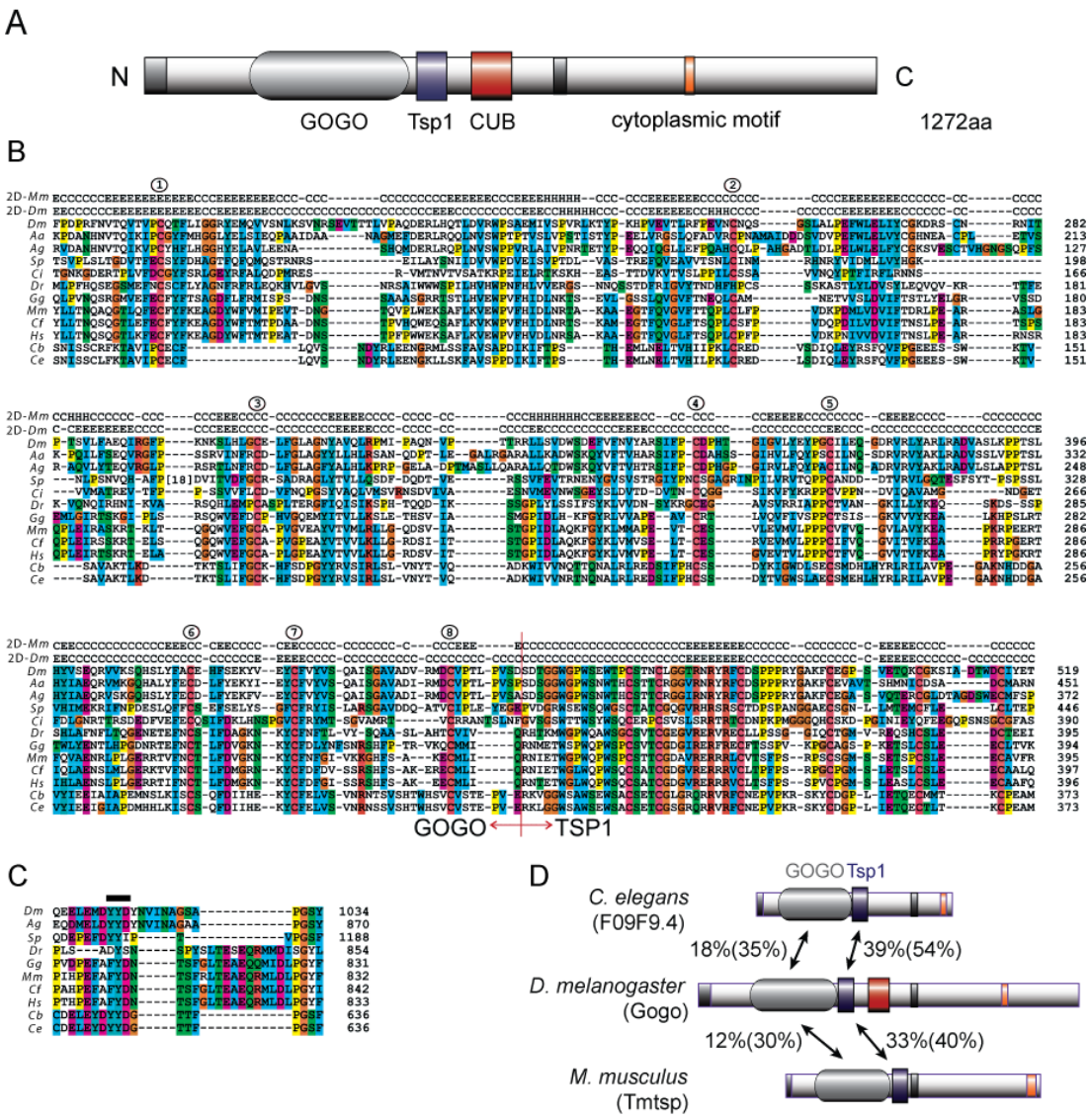

Figure 3-3 Evolutionary conserved Gogo domains

(**A**) Gogo protein structure. The colored boxes and ovals indicate: light grey, GOGO domain; purple, Tsp1 domain; red, CUB domain; dark grey, signal peptide; black, transmembrane domain. A conserved cytoplasmic motif is depicted in orange. (**B**) Multiple alignment of the GOGO and the TSP1 domain: *Drosophila* Gogo and selected orthologues were aligned using Probcons (Do et al., 2005), manually edited with GeneDoc (Nicholas and Jr., 1997) and colored using Clustal X (Jeanmougin et al., 1998). The secondary structures of *Dm* and *Mm* were predicted by PSIPRED and are shown above (H=helix, E=strand, C=coil) (Bryson et al., 2005). An 18 amino acids long unaligned region in *Sp* has been replaced by brackets. Eight conserved cysteines in the GOGO domain are marked with circles. The approximate border between the GOGO and the TSP1 domain is indicated by a red vertical line. (**C**) Multiple alignment of a conserved cytoplasmic motif. The YYD tripeptide motif is marked with a black bar. *Dm*, *Drosophila melanogaster*; Aa*, Aedes aegypti*; Ag, *Anopheles gambiae*, Sp; *Strongylocentrotus purpuratus*; Ci, *Ciona intestinalis*; Dr; *Danio rerio*; Gg, *Gallus gallus*; Mm, *Mus musculus*; Cf, *Canis familiaris*; Hs, *Homo sapiens*; Cb, *Caenorhabditis briggsae*; Ce, *Caenorhabditis elegans*. (**D**) Comparison of the molecular structures of *Drosophila* Gogo, mouse Tmtsp and *C. elegans* F09F9.4, indicating the similarity of protein organization between the different homologue candidates. Numbers indicate the amino acid identity and similarity (in brackets) between the GOGO and Tsp1 domains.

All homologue candidates contain a so far uncharacterized conserved region, which was named the GOGO domain (depicted as a light grey box in Figure 3-3A). The GOGO domain encodes eight conserved cysteines and a secondary structure of mainly beta strands (Figure 3-3B). This amino acid sequence is predicted to assemble an Ig-like fold.

All homologous proteins sharing the GOGO domain have a Tsp1 domain directly adjacent (Figure 3-3D). The CUB domain is missing in vertebrate and nematode *gogo* orthologues. Although there is no overall conservation within the cytoplasmic domains of different species, a motif specific for the *gogo* orthologues was identified. The short sequence contains a highly conserved tripeptide motif, YYD that may serve as a putative regulatory site and/or protein interaction domain (Figure 3-3A, C).

3.3 Gogo requires the GOGO and Tsp1 domain

To assess the functional properties of Gogo's extracellular domains, a series of rescue experiments was performed using Gogo fragments lacking different extracellular domains (Figure 3-4A). All fragments were tagged with a *myc* epitope and were expressed in all photoreceptor types using a direct fusion to the R neuron specific promoter, GMR (glass multiple reporter). In all rescue experiments, three independent insertions for each construct were tested in two different alleles of *gogo* ([D869] and [D1600]). The expression of the full length protein (GogoFL) completely rescued *gogo*$^{-}$ *ey*FLP mutants (Figure 3-4B). In further rescue experiments, Gogo was non-functional whenever the Tsp1 domain or parts of the GOGO domain was deleted, (Figure 3-4A, B). However, a fragment containing the GOGO and Tsp1 domain was sufficient to rescue the phenotype (ΔN-G in Figure 3-4A, B), showing the importance of the newly identified domain. The expression and localization of the expressed transgenes was assessed by Myc staining in the larval retina and optic lobe (Figure 3-4C). Extracellular deletion constructs showed no difference to the rescuing full-length construct, indicating that the extracellular domain is not required for Gogo membrane insertion and localization.

These results suggest that the GOGO domain and the Tsp1 domain, but not the CUB-like domain, constitute the minimal extracellular fragment necessary and sufficient for Gogo function. Since the Tsp1 domain interacts with numerous cell-cell communication and extracellular matrix proteins (Adams and Tucker, 2000), these domains may serve as extracellular interaction domains.

Figure 3-4 Structure-function analysis

(**A**) Full length and truncated *gogo* transgenes fused to four C-terminal c-myc epitopes are expressed under the control of the GMR promoter for rescue experiments. The left column illustrates the structure of the different *gogo* transgenes lacking defined domains. The colored boxes and ovals indicate: light grey, GOGO domain; purple, Tsp1 domain; red, CUB domain; yellow, signal peptide; black line, transmembrane domain. The column on the right indicates whether these transgenes rescue the R axon projection defects in *gogo*$^{-}$ *ey*FLP mosaics. (+), rescued; (-), non-rescued. (**B**) Anti-β-galactosidase stainings of horizontal adult head sections of *gogo*^{D869} *ey*FLP mosaics carrying the indicated GMR transgene and the *glass-lacZ* reporter, both are expressed in R1-R8 neurons. The targeting defects of *gogo* mutants (*ii*) are almost completely rescued with GogoFL (*iii*) compared to WT (*i*), but were not rescued by GogoΔC (*iv*). Truncated proteins lacking either parts of the GOGO domain (GogoΔN-H (*viii*)) or the Tsp1 domain in (GogoΔN-E (*v*)) fail to rescue, whereas the presence of the GOGO domain and the Tsp1 domain is sufficient to rescue *gogo*$^{-}$ *ey*FLP flies (GogoΔN-F and -G (*vi*, *vii*)). (**C**) The myc tagged GMR *gogo* transgenes were expressed in all photoreceptor types in wild type flies, detected by anti-Myc antibody. Expression of the transgenes can be observed in the cross section images of developing photoreceptors within the eye disc (left panels) and in axons and growth cones innervating the optic lobe (right panels). Independent of their rescuing abilities, transgenes clearly localize to the membrane of photoreceptors (white arrows) and more importantly to the growth cones (arrowheads). The yellow arrow indicates GogoΔC accumulation in the cell bodies.

(**D**) GogoFL::GFP and GogoΔC::GFP transfected S2 cells were stained with Gogo antibody against the N-terminus of the protein (red) without (left columns) or after (right columns) a treatment of detergent TritonX. Both constructs clearly show the surface staining of Gogo on the plasmamembrane of the cells (red). Staining against GFP is shown in green. The mCD8::GFP construct was used as a negative control to show that the Gogo antibody is specific to Gogo expression. Scale bars 10μm

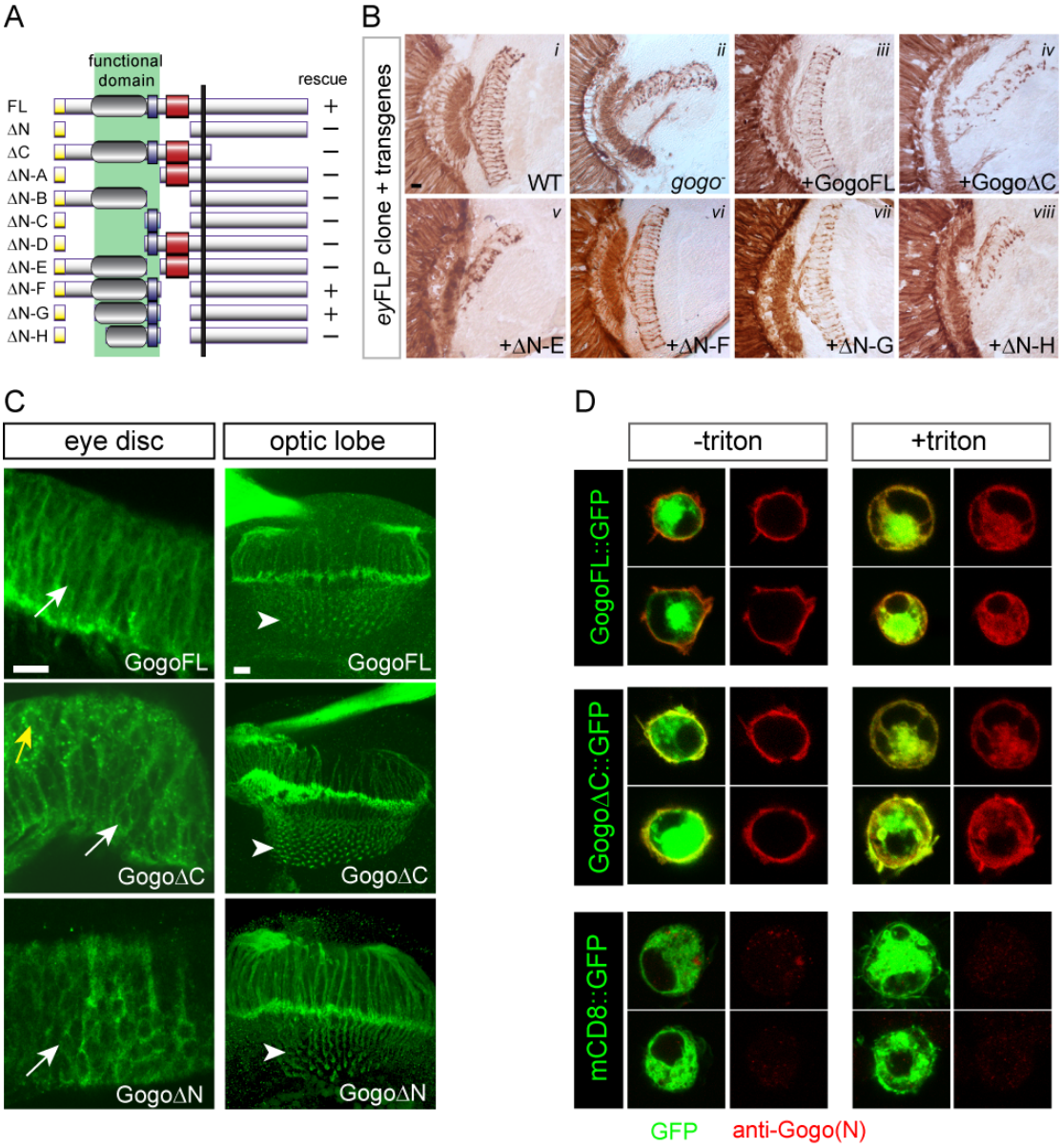

3.4 Gogo requires the cytoplasmic domain for its function

In a rescue experiment similar to the one described above, the deletion of the entire cytoplasmic domain (GogoΔC) did not rescue the *gogo*$^{-}$ *ey*FLP mutant (Figure 3-4A, B). To show proper membrane insertion of the GogoΔC fragment, its localization was checked in eye discs, optic lobes and in transfected S2 cells. In S2 cells, surface labeling without detergent clearly showed that both full length and ΔC constructs localized to the surface of the cells (Figure 3-4D). In eye discs and optic lobes, both proteins were localized to the cell membrane and enriched at the growth cone (Figure 3-4C). A more punctate staining accumulated in the cell body of R neurons expressing the ΔC construct (yellow arrow in Figure 3-4C) compared to other non-rescuing constructs, such as GogoΔN (Figure 3-4C). Nevertheless, localization to the membrane, along R axons and to their growth cones, appears comparable to the rescuing full length construct. Thus, the performed rescue experiment shows that the cytoplasmic domain of Gogo is required for its molecular activity.

3.5 Gogo is dynamically expressed in the developing visual system

To investigate Gogo's role in axonal pathfinding, its expression during visual system development was assessed by *gogo in situ* hybridization performed by Satoko Suzuki and antibody staining performed together with Takashi Suzuki. *gogo* mRNA expression was detected both in the eye disc and the brain of third instar larvae. In eye discs, the region posterior to the morphogenetic furrow, where differentiating R neurons reside, is stained in a dotted manner (Figure 3-5A). The dotted expression in the eye disc was investigated in more detail by double staining of *gogo* mRNA and Elav antibody which labels all R cell types. *gogo* mRNA is detected predominantly in the center of each ommatidium, where R8 is located (Figure 3-5B-B*i'*). The single *gogo* expressing cell in the ommatidial center was identified as R8 by double staining using the R8 specific marker Senseless (Sens). The R8 nuclei stained by Senseless are nicely enclosed by *gogo* mRNA, localizing to the cytoplasm of the cell (Figure 3-5D-D*i'*). In addition to photoreceptor expression, presumed medulla neurons, whose cell bodies lie outside the crescent shape formed by innervating R7/8 neurons (Figure 3-5C), showed high levels of *gogo* mRNA expression.

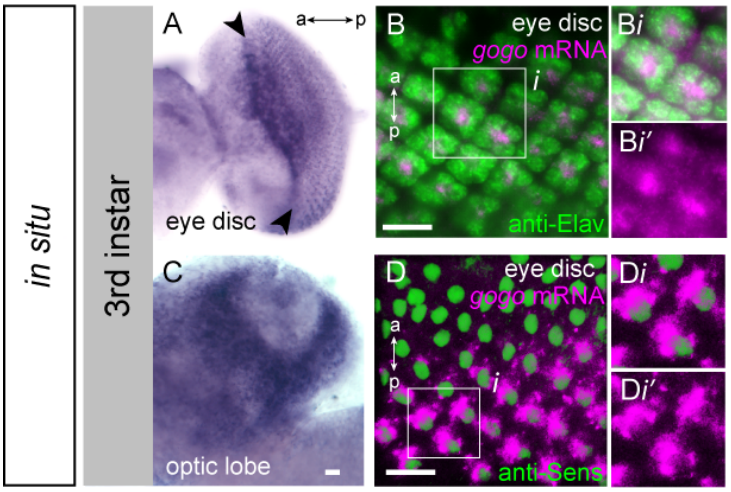

Figure 3-5 *gogo in situ* staining in eye discs and optic lobes
(**A-D**) *in situ* hybridization of *gogo* in third instar larvae. In the eye-disc (A,B,D), *gogo* mRNA is expressed in developing photoreceptors posterior to the morphogenetic furrow (arrowheads) (A). Staining of *gogo* mRNA (magenta) and Elav protein (green) shows that *gogo* mRNA is expressed in one cell per ommatidium (B). In the optic lobe, *gogo* mRNA is expressed in a crescent shape surrounding the optic lobe center (C) A 3D image of simultaneous staining *gogo* mRNA (magenta) and Senseless protein (green) shows that *gogo* mRNA is localized around the Senseless positive nuclei of R8s (D). Magnifications: merge (D*i*); magenta (D*i'*). a; anterior, p; posterior. Scale bars 10µm

A Gogo antibody was generated against the extracellular domain by Takashi Suzuki. This Gogo antibody labels R axons, shown by colocalization with labeled R axons. R cells were specifically labeled with mKOrange (monomeric Kusabira Orange) (Karasawa et al., 2004) under the control of the GMR promoter. In third instar larvae, Gogo seems to be absent in the lamina, which is innervated by R1-R6 (Figure 3-6B-B'), but highly expressed in R axons in the medulla (R7 and/or R8). As the majority of R axons innervating the medulla are R8 axons at this stage of development, this staining is consistent with the *in situ* which shows strong *gogo* expression in R8s in the eye disc. In particular, antibody staining at the tip of axons is clearly visible (Figure 3-6A-A*i*' arrows), suggesting a role for Gogo in navigating growth cones. The most outer axons (arrowhead in Figure 3-6A), which represent the youngest in-growing axons show the strongest Gogo expression along the axon. Strong staining is also observed below the lamina plexus (Figure 3-6A, B, bracket), in the lobula and in the lobula plate. Since the *in situ* also shows robust expression in the region outside the medulla crescent where medulla neurons arise, it is very likely that the antibody staining in the lobula/lobula plate is mainly caused by the localization of Gogo to the processes of unidentified medulla neurons.

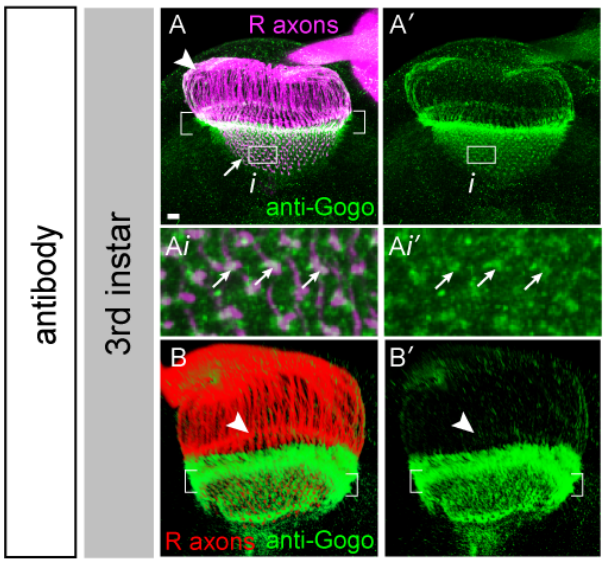

Figure 3-6 Gogo expression during larval development

(**A-B**) Gogo antibody staining of WT third instar optic lobes (A). Gogo (green) localizes predominantly along the axon (arrowhead in A) and at the growth cones of R7/8 (arrow in A). The staining in the medulla colocalizes with the growth cones marked by GMR-mCD8mKOrange, stained with anti-KO (magenta); arrows in A*i*, A*i*). 3D projection image (using the software AMIRA) shows that Gogo expression is not observed on R1-R6 axons, which terminate in the lamina (arrowhead). R axons are stained using GMR-mCD8mKOrange (red) and Gogo antibody (green) (B-B'). Scale bars 10μm

During early pupal stages, Gogo expression is unambiguously detected in all photoreceptor types stained with mKOrange. At 24APF (24hr after puparium formation), Gogo is observed in R8 axons and the axonal termini of R7 and R1-6 (Figure 3-7A-A*ii*'). Thus, Gogo is expressed in all the photoreceptors at this stage (Figure 3-7H, H'). Interestingly, at 40APF, when R1-6s are still involved in lamina cartridge formation, Gogo is expressed on all R1-6 axons (Figure 3-7C, C', D, D').

From the mid-pupal stage onward, Gogo expression becomes reduced in the photoreceptor axons. At 40APF faint staining can be observed around the M3 layer (Figure 3-7E-E*i*'). Since the Gogo staining and R axons do not overlap perfectly, it is likely that the staining derives from lamina neurons or higher order neurons.

Similarly, in late stages of pupal development Gogo seems to be present in R neurons at a very low level only. At 72APF, Gogo can be rarely seen on the axons of R7/8, together with a faint staining of supposedly lamina or medulla neurons (Figure 3-7F-F*i*'). In contrast to the observed protein reduction in photoreceptor axons, Gogo protein levels seem not to be altered in the photoreceptor cell bodies. In the retina Gogo protein was detected in all photoreceptor types throughout pupal development (Figure 3-7G-L'). This observation rather suggests the presence of a mechanism regulating Gogo protein level within the axon or growth cone rather than transcriptional regulation.

The specificity of the generated Gogo antibody was confirmed in *gogo*$^{-}$ *ey*FLP larval mosaics and by labeling small heterozygous WT clones in an otherwise homozygous *gogo* mutant retina during pupal development. Anti-Gogo staining is not detected in *gogo* mutant retinal cells at 24APF, 40APF and 48APF (Figure 3-7B-B' and data not shown).

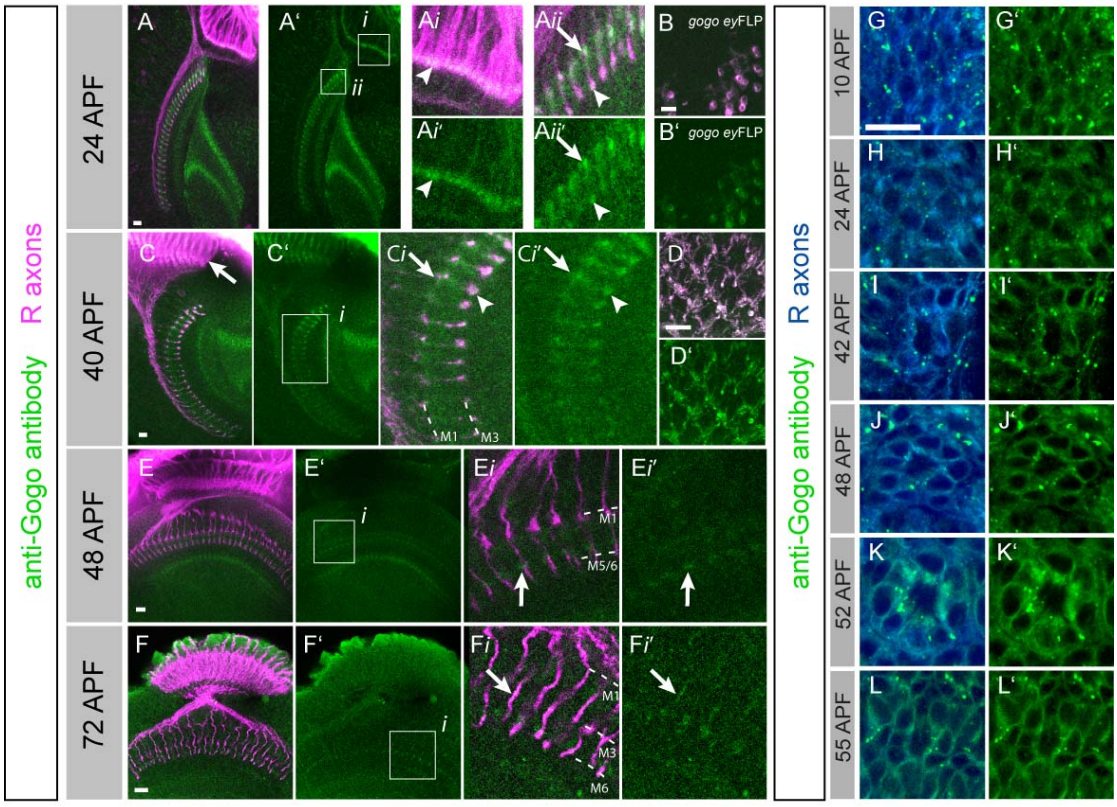

Figure 3-7 Gogo is dynamically presented on R axons during pupal stages

Anti-Gogo staining is shown in green (A-L) and R axons are visualized by GMR-mCD8mKOrange in magenta (A-F) or blue (G-L), respectively. (**A-B'**) The optic lobe (A-A*ii'*) and the retina (B-B') of 24APF pupae. (A) Strong Gogo expression is observed on R axons in the lamina (*i*) and the medulla (*ii*). Magnifications of the lamina (A*i*, A*i'*) and the medulla (A*ii*, A*ii'*). In the lamina, Gogo localizes to the termini of R1-6 (arrowheads in A*i*, A*i'*). In the medulla, Gogo strongly overlaps with the termini of R7 (arrowheads in A*ii*, A*ii'*) and R8 (arrows in A*ii*, A*ii'*). In *gogo*^{H1675} *ey*FLP retina, WT R cells marked with GMR-mCD8mKOrange (magenta) completely overlap with Gogo positive cells (green), whereas gogo^{-} cells lack Gogo protein (B, B'). (**C-F*i'***) The optic lobe at 40APF (C-D'), 48APF (E-E*i'*) and 72APF (F-F*i'*): At 40 APF termini of R7 and R8 show Gogo staining (R7, arrowheads; R8, arrows in C*i* and C*i'*). Gogo is strongly localized to the R1-6 axons during lamina cartridge formation (D, D'). At 48APF, overall expression of Gogo becomes reduced. Punctate Gogo is seen around the M3 layer to which R8 extends its filopodia at this stage (arrows in E*i*, E*i'*). Gogo expression can be vaguely detected on R axons at 72APF (arrow in F*i*, F*i'*). Medulla layers are indicated in C*i*, E*i*, and Fi. (**G-L'**) In contrast all photoreceptor cell bodies are Gogo protein positive during the pupal stages 10APF, 24APF, 42APF, 48 APF, 52 APF and 55 APF. Scale bars 10μm.

3.6 *gogo* brain expression is not required for R axon guidance

Since expression of Gogo protein is also detected in an undefined population of medulla neurons in the Gogo antibody staining, the question whether brain expression of Gogo is required for R axon pathfinding arose. To test this, GogoFL was specifically expressed in R neurons in transheterozygous *gogo*$^-$ survivors, which lack Gogo in the whole animal, including the brain. Therefore, Gogo expressing R axons project into optic lobes mutant for *gogo*. Transheterozygous animals were rescued to the same extent as observed in the *gogo*$^-$ *ey*FLP mutant background after expression of GMR-GogoFL (Figure 3-8A-F). Early pathfinding defects during larval development were rescued (Figure 3-8B), as well as the adult projection pattern (Figure 3-8E). Therefore, Gogo is exclusively required in R axons, but not in the brain for R axon pathfinding. This result strongly argues against homophillic (Gogo-Gogo) interactions between R axons and target cells, but does not exclude homophilic axon-axon interactions among R cells.

In order to assess whether Gogo shows the ability to bind homophilically, Xiuye Chen transfected *Drosophila* culture S2 cells with GFP-tagged GogoFL or GogoΔC, and checked whether the cells form aggregates. As a positive control, the homophilic cadherin Flamingo (Fmi) was used. It was shown that the expression of full-length Fmi protein induced strong aggregation of S2 cells (Usui et al., 1999). Also in our positive control experiment, cells transfected with Flamingo showed a very strong aggregation (Figure 3-8G). In contrast, neither the GogoFL nor GogoΔC expressing cells showed any aggregation (Figure 3-8H, I) in all triplicate experiments. Since the S2 aggregation assay is considered a robust assay to assess homophilic interactions, the result suggests that Gogo has no ability for homophilic binding.

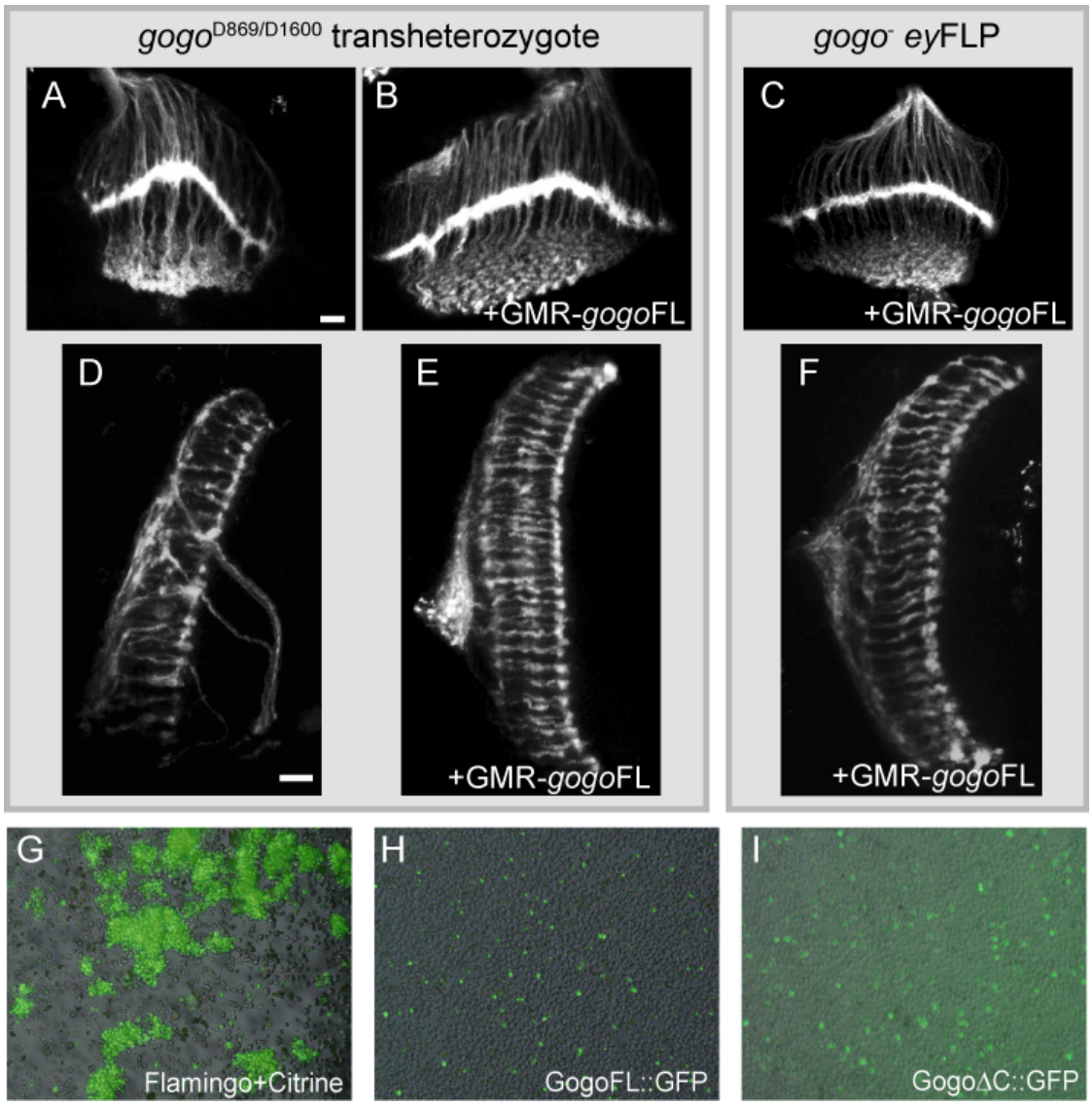

Figure 3-8 Gogo is autonomously required in R axons

(A-F) Whole-mount confocal images visualizing R cell projections with mAb24B10. (A-C) larval phenotypes (D-F) adult phenotypes (**A, D**) *gogo*$^{D869/D1600}$ trans-heterozygous mutant (**B, E**) *gogo*$^{D869/D1600}$; GMR-*gogo*FL: (**C, F**) *gogo*^{D869} *ey*FLP; GMR-*gogo*FL. GogoFL rescues both *gogo* trans-heterozygous and *gogo*^{D869} *ey*FLP phenotypes (**G-I**) S2 cells were cotransfected with actin-GAL4 and UAS-Flamingo (*fmi*) +UAS-Citrine (left), UAS-GogoFL::GFP (middle), or UAS-GogoΔC::GFP (right). Cells transfected with *flamingo* formed aggregates of more than 20 cells. GogoFL or GogoΔC transfected cells do not aggregate. Scale bars 10μm.

3.7 Identification of the *gogo* enhancer fragment

Previous experiments have demonstrated that Gogo is autonomously required for R axon guidance in visual system development. *In situ* and antibody staining of Gogo confirm this role in R axons. In addition, the performed stainings revealed Gogo expression in a population of unidentified neurons in the developing optic lobe. *gogo in situ* staining applied to Drosophila embryos revealed further expression in the CNS of the embryo (data not shown). However, investigating Gogo's role in these neurons appears difficult as the identity of the cells can hardly be dissected with the quality of stainings obtained so far.

One possible strategy to identify these cells can be the identification of the *gogo* enhancer fragment. Using the Gal4/UAS system, *gogo*-specific expression of marker proteins, which can either be localized to the nucleus or to axons, can be highly amplified in comparison to endogenous *gogo* expression.
Four different fragments (*gogo*1-4) were cloned upstream of the *gal4* gene (Figure 3-9A). The obtained *gogo*1-4-Gal4 lines were combined with UAS-GFP:lacZnls (nls, nuclear localization signal) and analyzed for expression in 3rd instar larval eye discs. For each construct three independent transgenic insertion lines were examined. *gogo*2-Gal4 showed a striking similar expression pattern compared to the *gogo in situ* (Figure 3-9B), whereas none of the other cloned Gal4 lines gave any signal (data not shown). UAS-GFP:lacZnls expression driven by *gogo*2-Gal4 was almost restricted to one R cell lying in the middle of each ommatidium (Figure 3-9B, B*i*). Only few ommatidia contained one or two additional cells with faint expression (Figure 3-9B, B*i*). The cells lying in the middle of each ommatidium were identified as R8 by colocalization with the R8 marker Sens (Figure 3-9C, C´, C´´). In contrast to the *in situ*, now a perfect overlap was obtained. The expression pattern was also investigated in the optic lobe by expressing the axonal marker UAS-mCD8GFP under the control of *gogo*2-Gal4 (Figure 3-9D, D´). R8 axons projecting into the medulla are nicely stained. Consistent with previous results, almost no staining was observed within the lamina. Therefore, the obtained expression pattern of *gogo*2-Gal4 seems to resemble the endogenous *gogo* expression within R axons during larval development. In pupae, R7 and R8 showed *gogo*2-Gal4, UAS-GFP:lacZnls expression (Figure 3-9E). In addition, one or two R1-R6 cells showed stainings. One of the cells could be identified as R3 due to its position within the ommatidium. The pupal expression of the *gogo2* enhancer fragment only partially reflects the

endogenous expression pattern observed in antibody stainings. Thus, the fragment does not contain the entire *gogo* enhancer. Also no staining is observed below the lamina plexus, in the lobula and lobula plate in the larval stainings (Figure 3-9D, D´), whereas using the Gogo antibody strong stainings were detected in these regions (compare Figure 3-6A, B, bracket). Nevertheless, expression of *gogo*2-Gal4 expression could be detected in the CNS of 3rd instar larvae (Figure 3-9F).

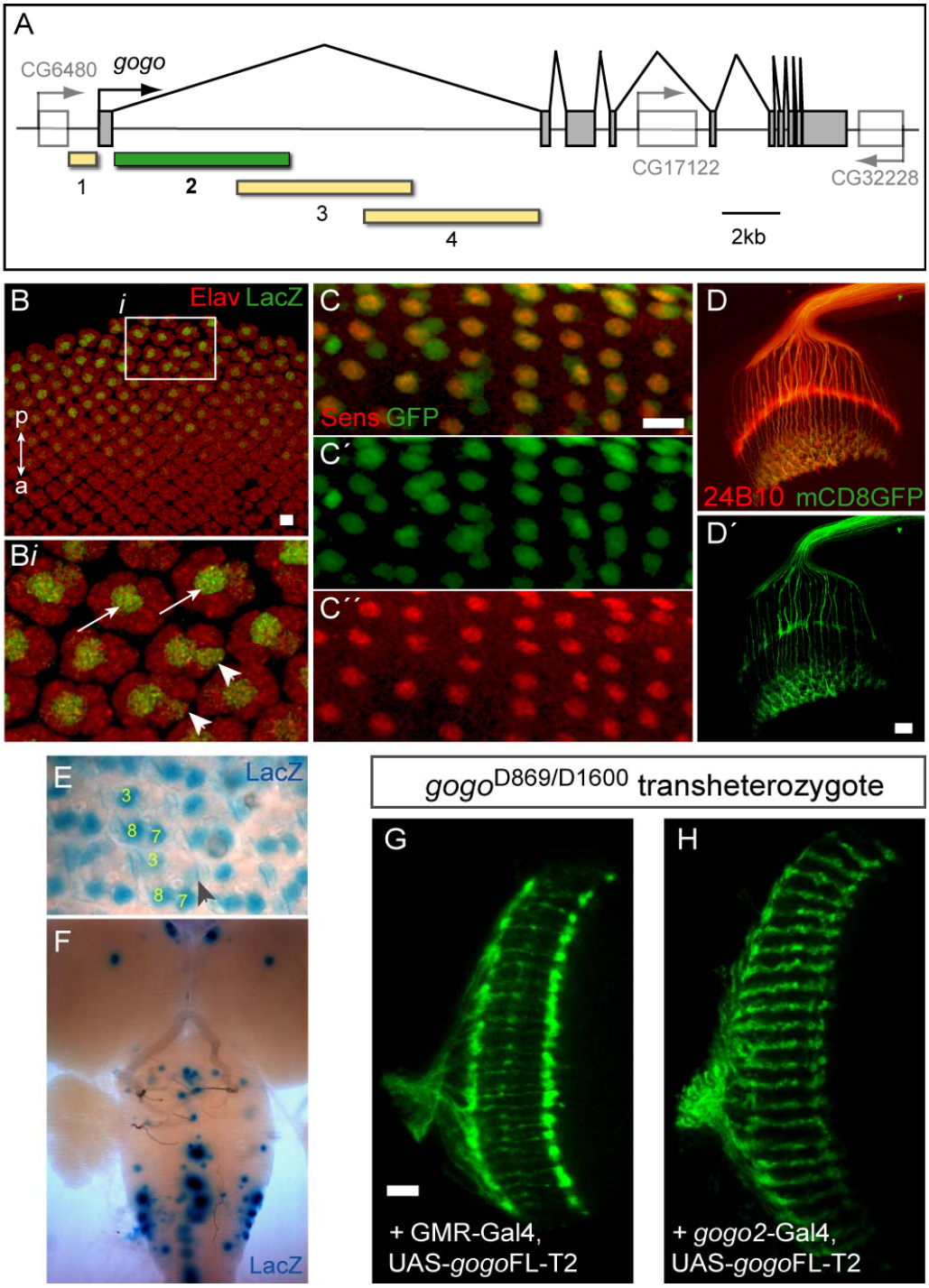

Figure 3-9 *gogo* enhancer fragment bashing

(**A**) Four different fragments were cloned upstream of the *gal4* gene: Fragment 1 derives from the intergenic region upstream of the *gogo* coding sequence; Fragment 2, 3 4 are overlapping 6kb fragments spanning the entire first *gogo* intron. (**B, B*i***) *gogo*2-Gal4 drives the expression of UAS-GFP:lacZnls detected by LacZ antibody staining (green) in eye discs. R1-R8 cells were stained with anti-Elav antibody. *gogo*2-Gal4 is strongly expressed in one R cell lying in the middle of each ommatidium (arrows). Few ommatidia contain one or two additional cells with faint expression (arrowheads). (**C, C´, C´´**) *gogo*2-Gal4 drives the expression of UAS-GFP:lacZnls detected by GFP antibody staining (green) in eye discs. R8 cells were labeled with anti-Sens antibody. *gogo*2-Gal4 expression is strongest in R8 axons. (**D, D´**) UAS-mCD8GFP is expressed under the control of *gogo*2-Gal4. UAS-mCD8GFP is detected by GFP antibody staining (green). R1-R8 axons were stained with. The expression in the optic lobe is restricted to R axons which project into the medulla, but no expression is detected below the lamina plexus in the lobula or lobula plate. (**E**) *gogo*2-Gal4 UAS-GFP:lacZnls expression is detected by LacZ staining in R7, R8 and R3 in the pupal retina at 48APF. In some of the ommatidia an additional cell showed faint expression (arrowhead) (**F**) *gogo*2-Gal4 UAS-GFP:lacZnls expression detected by LacZ staining the CNS of 3rd instar larvae. (**G, H**) *gogo*$^{D869/D1600}$ adult flies, R axons are visualized with mAb24B10 antibody. As a positive control UAS-*gogo*FL-T2 was expressed under the control of GMR-Gal4 (F). *gogo*2-Gal4 UAS-*gogo*FL-T2 expression rescues the axon guidance defect of R7 and R8 axons (G). Scale bars 10μm.

To test if *gogo*2-Gal4 expression is sufficient to rescue the *gogo* mutant phenotype in R axons, UAS-*gogo*FL-T2 was expressed in transheterozygous *gogo* mutants (Figure 3-9H). The projection pattern of R7 and R8 was fully rescued, suggesting that the identified enhancer fragment fulfills all functional requirements at least for R7 and R8 cells. In addition, it partially reflects the temporal dynamics of endogenous expression, starting from R8s during larval development and then expanding to R7s and some R1-R6 cells during pupal development. For this reasons, there is a high chance that the *gogo* enhancer fragment could be a useful tool in future experiments examining Gogo's function in the CNS.

3.8 *gogo* is required for the assembly of lamina cartridges

The strong *gogo* expression in all R1-R6 photoreceptors shown by antibody staining during pupal suggests a possible requirement of Gogo in theses cell types. Although R1-6 axons in *gogo ey*FLP flies correctly target the lamina and do not overshoot into deeper neuropils, the overall lamina structure shows mild irregularities (Figure 3-1B'). Gogo antibody staining revealed its expression in R1-R6 during mid pupal stages (Figure 3-7D). During this time, R1-R6 axons start extending to their final targets, the lamina neurons, to form lamina cartridges. As the observed lamina irregularities in *gogo* mutants could be caused by defects in cartridge formation, the ultra structure of the lamina was analyzed using transmission electron microscopy (TEM).

The lamina of wild type *ey*FLP controls displays a highly regular array of evenly sized cartridges that mainly consist of six R1-R6 terminals surrounding the lamina neurons L1 and L2 in the center (Figure 3-10A). In *gogo*$^{-}$ *ey*FLP mosaics this array was generally disrupted, containing cartridges of variable sizes (Figure 3-10B-C).

In order to quantify missorting of R1-R6 termini into cartridges, montages of electron micrographs covering the lamina were analyzed and quantified excluding the most outer lamina regions (Figure 3-10D). In wild type controls the majority (89.7%) of the cartridges contained six R terminals (29 cartridges, n=2). Only 10.3% showed aberrant numbers ranging from 5 to 7 terminals per cartridge. In contrast, the number of determined R1-R6 terminals within each cartridge ranged from 1 to 9 terminals per cartridge in *gogo*$^{-}$ *ey*FLP flies, indicating a severe missorting defect. In total, 79.1% of the cartridges were affected (43 cartridges, n=2). Despite the missorting defect, *gogo* mutant R terminals contained characteristic structures, as capitate projections (glial invaginations) (Fabian-Fine et al., 2003) or T-bar-shaped dense structures. These features suggest the formation of functional synapses in *gogo* mutant R terminals (Figure 3-10A-B*i*) (Bazigou et al., 2007). Since the *ey* enhancer fragment present in *ey*FLP shows expression in a small proportion of brain cells including lamina neurons, the experiment was repeated using a recently published 100% eye-specific fragment *ey*$^{3.5}$ (Bazigou et al., 2007). In *ey*$^{3.5}$FLP mosaics the majority of R cells are homozygous mutant, whereas the target cells are reliably WT. Using *ey*$^{3.5}$FLP, a only slightly weaker phenotype was obtained compared with *gogo*$^{-}$ *ey*FLP mosaics (Figure 3-10C).

In summary, these results indicate that Gogo mediates interactions between R1-R6 growth cones within the target region. Nevertheless, the defects in projections could

be secondary, reflecting an earlier role in R8 or defects in axon fascicle ordering before reaching the lamina.

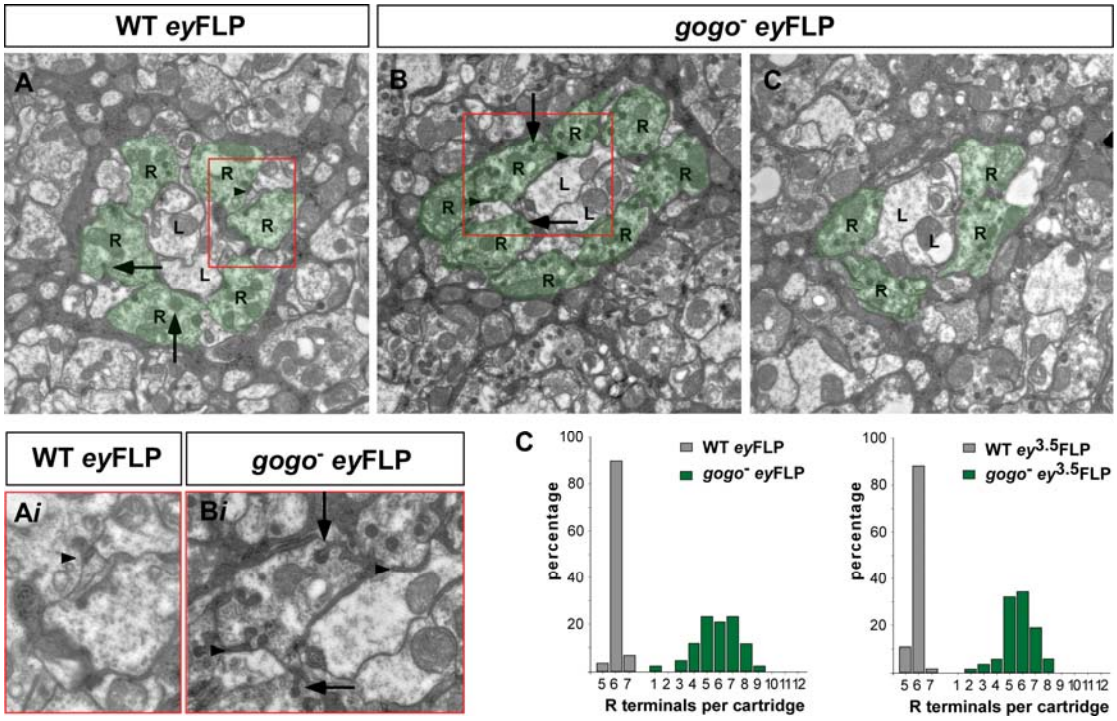

Figure 3-10 Lamina cartridge formation in *gogo* mutants

(**A-C**) TEM of adult lamina cartridges: In wild type *ey*FLP controls six R cell terminals (R highlighted in green) are arranged around the lamina neurons L1 and L2 in the center (A). In $gogo^{D1600}$ *ey*FLP flies the number of terminals varies (B and C). Representative images show cartridges with 8 terminal (B) and 4 terminals per cartridge (C). R cells contain glia capitate projections (arrows in A, A*i*, B, B*i*). R axons from T-bar shaped synapses (arrowheads in A, A*i*, B, B*i*).

(**D**) Quantification of R cell terminals per cartridge in *ey*FLP (left panel) and $ey^{3.5}$FLP mosaics (right panel). The distribution of *gogo* mutant R cells per cartridge (green) is wider compared to WT (gray). WT *ey*FLP: n=2, 29 cartridges; $gogo^{D1600}$ *ey*FLP: n=2, 43 cartridges; WT $ey^{3.5}$FLP: n=2, 66 cartridges; $gogo^{D1600}$ $ey^{3.5}$Flp: n=2, cartridges 91.

3.9 *gogo* functions in R8 but not in R7 axons

During larval development R7 axons fasciculate with pioneering R8 axons and simply follow their trajectories. Nevertheless, Gogo is expressed strongly in R7s in early-mid pupal stages when R7 axonal termini have already segregated from R8s. Thus, it is possible that Gogo has an autonomous function in R7 axonal pathfinding during pupal development.

To test Gogo's requirement in R7, *gogo* mutant clones were generated specifically in R7, but not in R8 cells using the GMR-FLP MARCM system (Figure 3-11A) (Clandinin et al., 2001; Lee et al., 2001; Maurel-Zaffran et al., 2001). This experiment was performed together with Takashi Suzuki. The GMR-FLP strategy takes advantage of the fact that different R cell types are generated in temporally separated mitoses. R2–R5 and R8 derive from mitotic divisions occurring anterior to the morphogenetic furrow. R1, R6 and R7 derive from mitotic divisions occurring posterior to the morphogenetic furrow. To induce mitotic recombination the GMR enhancer, which is expressed posterior to the furrow, drives Flipase expression. Although all R cell types will express the Flipase, only mitoses happening posterior to the furrow, namely in R1, R6 and R7 will induce mitotic recombination, resulting in approximately 15% of R1s, R6s, and R7s being homozygous for a particular chromosomal arm. To label exclusively mutant R7s the MARCM method (mosaic analysis with a repressible cell marker) was used (see chapter 2.13) (Lee and Luo, 1999). The UAS-synaptobrevin-GFP reporter is expressed under the control of the R7-specific PANR7-Gal4 in homozygous mutant R7s only, but dominantly repressed by Gal80 in heterozygous R7s.

Out of 130 *gogo* mutant R7 axons assessed, not a single R7 showed an abnormal phenotype (Figure 3-11B). Due to the possibility that *gogo*$^-$ R7 axons may exhibit stronger phenotypes only in *gogo* mutant R7 populations, clones composed of more than two adjacent *gogo*$^-$ R7 axons were analyzed. Out of 25 clones, no aberrant phenotype was observed, neither in R7 axons nor their termini (arrows in Figure 3-11B), indicating that R7 specific loss of *gogo* does not result in autonomous projection defects in R7.

In addition, the Gal4-UAS system was applied to test if R7-specific *gogo* expression is sufficient to rescue the R7 targeting defects in *gogo ey*FLP mutants. R7-specific UAS-*gogo*FL-3B expression, using PM181-Gal4 (Lee et al., 2001), did not rescue the *gogo*$^-$ *ey*FLP phenotype (Figure 3-11C). In contrast, GMR-Gal4 driven UAS-*gogo*FL-3B expression was able to rescue *gogo*$^-$ *ey*FLP flies (data not shown).

Is R7 pathfinding dependent on the R8 axon? To address this question UAS-*gogo*FL-T2 was expressed in *gogo eyFLP* mutants using a combination of two independent R8-specific Gal4 lines, 109-68-Gal4 (White and Jarman, 2000) and *caps*-Gal4 (Shinza-Kameda et al., 2006). Although R7 was still mutant for *gogo*, R8 specific *gogo* expression was sufficient to rescue targeting defects of both, R8s and R7s (Figure 3-11D). Using a single R8-specific Gal4 did not rescue or only partially rescued *gogo eyFLP* flies (data not shown). This could be explained by the differential expression timing and levels. Therefore, this experiment clearly shows the autonomous requirement of Gogo in R8 axons. In contrast, the disruption of R7 axons in *gogo* mutants is a consequence of secondary defects deriving from abnormally guided R8s.

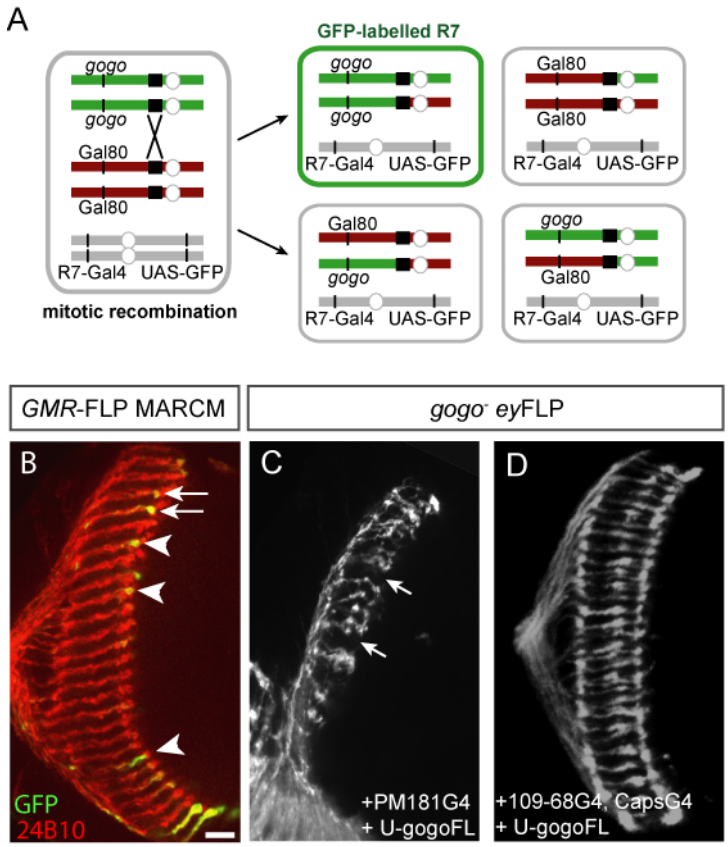

Figure 3-11 *gogo* functions in R8 axons, but not in R7

(**A**) Schematic summary of selective labeling of single *gogo* mutant R7 axons in adult flies using GMR-FLP MARCM system (adapted from Lee et al., 2001). White circles indicate the centromere, black bars FRT sites. (**B**) *gogo* mutant R7 axons generated by the GMR-FLP MARCM method terminate in the correct layer of the medulla (arrowheads). Also, R7 clones composed of more than two adjacent axons did not show defects (arrows). mAb24B10 (red) labels all R7 and R8 axons, irrespective of their genotype; Synaptobrevin-GFP specifically labels $gogo^{D869}$ mutant R7 axon termini (green). All R8 axons (and unlabeled R7 axons) are $gogo^{+}$. (**C**) R7-specific expression of *gogo* induced by PM181-Gal4; UAS-*gogo*FL-3B does not rescue the R7 $gogo^{D869}$ *eyFLP* phenotype (arrows) (**D**) R8-specific Gogo expression, induced by the combination of 109-68-Gal4 and *caps*-Gal4 to drive the expression of UAS-*gogo*FL-T2, instead rescued both R8 and R7 targeting defects completely in $gogo^{D869}$ *eyFLP* flies. R7 and R8 axons were labeled with mAb24B10 (C, D). Scale bars 10μm.

3.10 In larvae *gogo*$^{-}$ R8 axons lose repulsive interactions

The strong *gogo* expression in R8 photoreceptors shown by *in situ* in larval eye discs and the intense R8 bundling observed in *gogo*$^{-}$ *ey*FLP larvae (Figure 3-2B, B*i*) suggests a requirement of Gogo in outgrowing R8 photoreceptor axons. The formation of axon bundles and gaps within the medulla of *gogo*$^{-}$ *ey*FLP larvae indicates that the proper interaction between *gogo*$^{-}$ R8 axons is lost, most likely at the stage when R axons enter the medulla. Since most of the R neurons were mutant for *gogo* in these animals, it was unclear whether the cause of spatial gaps and bundles was the lack of attraction or repulsion among mutant axons.

Small patches of homozygous mutant cells (small clones) were generated expressing FLP recombinase under the control of the weak eye-specific promoter *ey*1x FLP.Exel (Shinza-Kameda et al., 2006) without introducing a recessive cell lethal mutation on the wild type chromosome (see chapter 2.13). The resulting homozygous *gogo* mutant axons were labeled with GFP using the MARCM method (Lee and Luo, 1999). To distinguish wild type (including heterozygous) axons the GMR-mKOrange transgene was introduced as a marker onto the wild type chromosome arm. We refer to this modified method as complementary MARCM (cMARCM) (see chapter 2.13), established by Satoko Suzuki. This method clearly distinguishes *gogo* mutant axons, labeled with GFP (inserted on the mutant chromosome) and wild type (WT) axons, labeled with mKOrange (inserted on the wild type chromosome).

Figure 3-12 Schematic summary of methods to generate mosaic animals

Schematic showing cMARCM (A) and the strategy to specifically label mutant and WT R8 axons (B). For both methods, the weak eye-specific promoter *ey*1x FLP.Exel was used to drive Flipase expression and to induce mitotic recombination in a small fraction of R cells. White circles indicate the centromere, black bars FRT sites. (**A**) Left panel: Heterozygous flies carry GMR-mKO, which is expressed in all R axons and the Gal80 repressor on one chromosome, in trans the *gogo*^{D869} mutation. In heterozygous flies the expression of UAS-GFP by the neuronal driver *elav*-Gal4 is repressed by Gal80. Right upper panel: upon recombination the GMR-mKO marker and Gal80 are lost. UAS-GFP expression is no longer repressed in homozygous mutant cells. Right lower panel: in heterozygous cells all R cells are labeled with mKO, GFP expression is repressed. In the rescue cMARCM experiments either UAS-gogoFL or UAS-gogoΔC was recombined to the right arm of the mutant chromosome to be expressed in homozygous mutant cells upon mitotic recombination. (**B**) Left panel: The *gogo*^{D869} mutant chromosome arm carries the R8-specific marker *ato*-τmyc, in trans the GMR-mKO marker. Right upper panel: Homozygous mutant R8 cells lose mKO expression, but carry instead two copies of *ato*-τmyc resulting in strongly labeled R8 axons. Right lower panel: Heterozygous R8 cells are still labeled with mKO and carry only one copy of *ato*-τmyc, resulting in faint R8 marker staining.

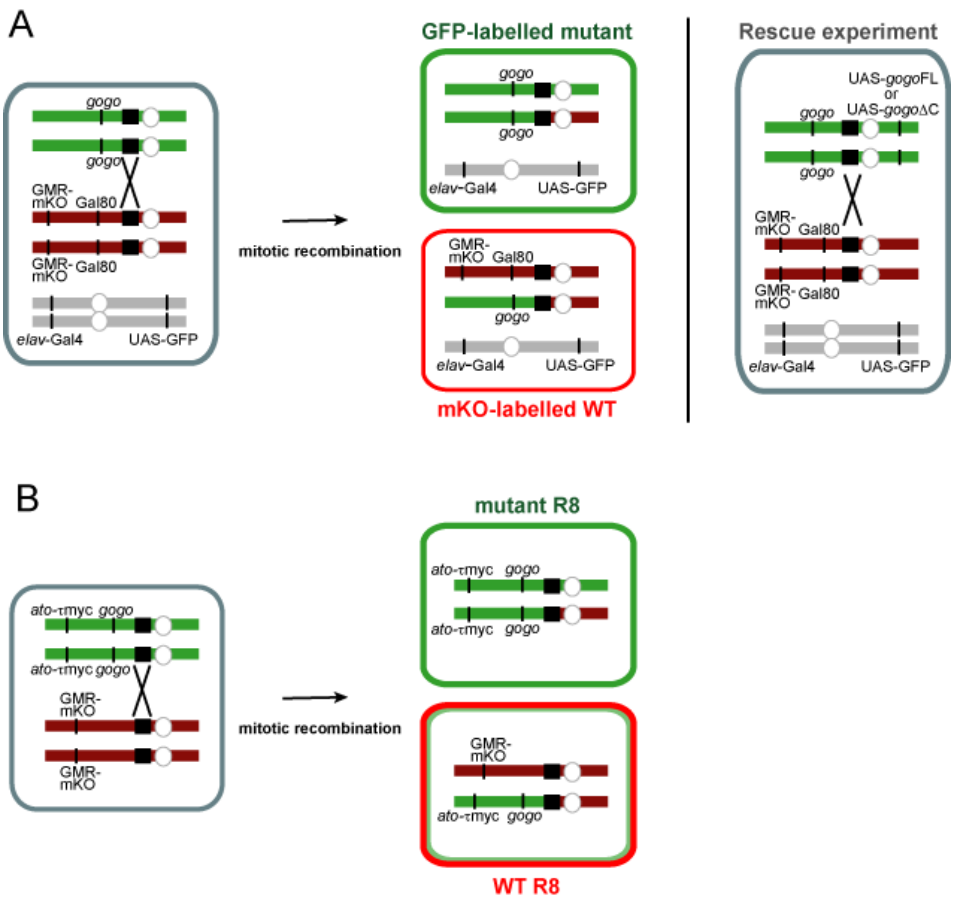

The cMARCM analysis was performed together with Satoko Suzuki. In the wild type mosaic control, green WT R7/8 axons do not bundle with their green WT neighbors (Figure 3-13A-A" and F). In contrast, *gogo* mutant axons start to form bundles with neighboring *gogo* mutant axons (Figure 3-13B, B' and F). Interestingly, the red WT axons adjacent to the *gogo*$^{-}$ clone barely seem affected (Figure 3-13B" and F). When "single" *gogo* mutant axons are generated, no visible abnormalities can be detected in these mutant axons (Figure 3-13C-C" and F), suggesting that the pathfinding error of *gogo* mutants mainly occurs among mutant axons, but not among mutant and WT axons. Pathfinding errors are rescued by reintroducing GogoFL protein within the mutant clone, but can not be rescued by reintroducing GogoΔC (Figure 3-13D- E').

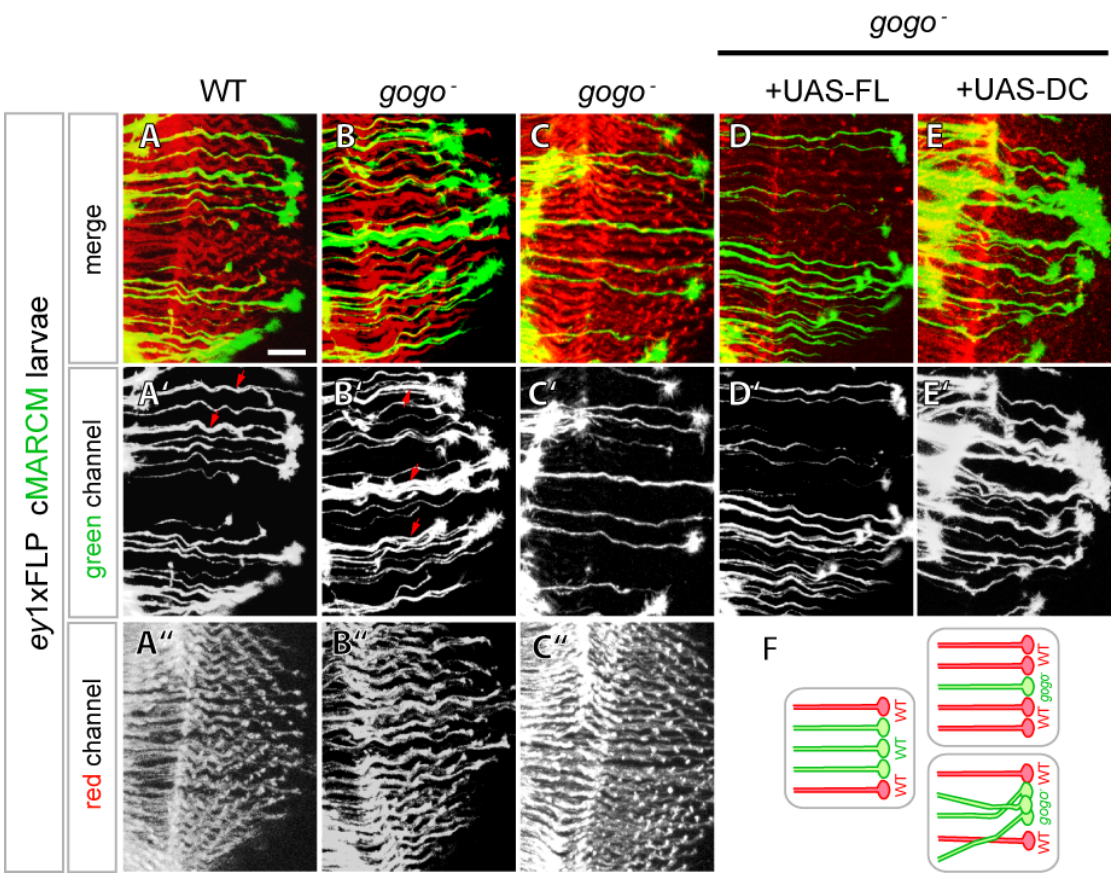

Figure 3-13 Axon bundling in small *gogo* mutant clones

(**A-E**) Larval optic lobes of mosaic animals generated by cMARCM. Axons from small clones induced by ey1xFLP.Exel are labeled with anti-GFP (green in A-E), and remaining WT axons are labeled with a mixture of anti-Myc and anti-KO (red in A-C), or anti-KO alone (red in D and E). In the control, *gogo*$^{+}$ axons do not bundle and run in parallel to each other (A, A'). A few thick stainings are presumably R7/8 fascicles deriving from the same ommatidium (red arrows in A'). In *gogo*^{D869} mutant mosaics (B and C), *gogo*$^{-}$ axons from the small clone bundle to each other (red arrows in B'), while single isolated *gogo*$^{-}$ axons do not show any abnormalities (C'). In these animals, surrounding WT axons are hardly affected (B" and C"). The *gogo*$^{-}$ phenotype is rescued by UAS-*gogo*FL-3B (D), but not by the UAS-gogoΔC-3B construct (E). (**F**) Schematic drawings showing that *gogo*$^{-}$ axons lose repulsive axon-axon interaction and bundle within the clone, but rarely affect surrounding WT axons. Single *gogo*$^{-}$ axons extend normally. Scale bars 10μm.

Although the majority of R axons within the medulla at this time of development derive from R8 cells and only few R7 axons have arrived in the medulla, the result would be more conclusive if the behaviour of R8 axons was specifically examined. To assess the behaviour of mutant R8 axons in detail, the R8 marker *ato-τmyc* was recombined on the same chromosomal arm as the *gogo* gene (left arm of 3rd chromosome). Homozygous *gogo* mutant R8 axons can therefore be distinguished by stronger R8 marker expression and by the lack of mKOrange, which labels only WT R7/8 axons. This method clearly distinguishes *gogo* mutant R8 axons strongly expressing *ato-τmyc* (inserted on the mutant chromosome arm), from wild type R8 axons labeled with mKOrange (inserted on the wild type chromosome arm).

In small mutant clones, neighboring *gogo*⁻ R8 axons tend to form bundles (Figure 3-14B-B" red arrows), whereas the surrounding WT axons are not affected. In some cases, *gogo*⁻ R8 axons that were clearly separated come closer and bundle to each other (Figure 3-14B-B" yellow arrows). This suggests that *gogo* mutant R8 axons attract each other over a relatively short distance. For quantification clone borders between *gogo*⁻ and WT axons were examined whether the mutant R8 axon at the border favors the adjacent *gogo*⁻ axon (Figure 3-14Db) or adjacent WT axon (Figure 3-14Dc), or does not form bundles at all (Figure 3-14Da). In total, 71% of *gogo*⁻ R8 axons (75 cases observed) bind to another *gogo*⁻ R8 axon, whereas none binds to the adjacent WT R8 (Figure 3-14C, D). This strongly suggests that Gogo mediates repulsive interactions among R8 axons.

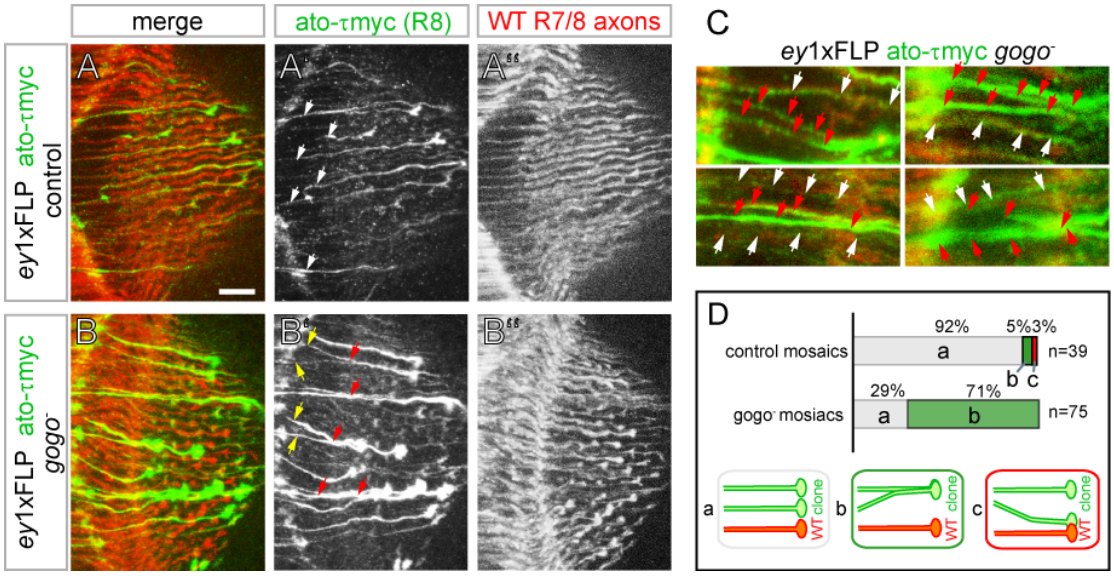

Figure 3-14 Larval *gogo*⁻ R8 axons lose axon-axon repulsion

(A-C) Axons from small clones induced by ey1xFLP.Exel. R8 axons labeled with *ato-τmyc* are visualized by anti-Tau (green). WT axons labeled with mCD8KOrange are stained with anti-mCD8 (red). Since the *ato-τmyc* marker is on the same arm as the *gogo* gene, strongly stained green axons without red staining are *gogo*⁻ R8 axons. (**A-A"**) Wild type control clone: *ato-τmyc* FRT/ GMR-mCD8KO FRT. Axons do not form bundles (white arrows in A'). (**B-B"**) *gogo*^{D869} clone: *ato-τmyc gogo*⁻ FRT/ GMR-mCD8KO FRT. Mutant axons bundle (red arrows in G'). Mutant R8 axons that were clearly separated form bundles (yellow arrows in B'). (**C**) *gogo*^{D869} clone: *ato-τmyc gogo*⁻ FRT/ GMR-mCD8KO FRT. Representative sample images of the clone border which was used for quantification in (D). *gogo*⁻ R8 axons (red arrows) bundle within the clone but adjacent WT axons (white arrows) are barely affected. (**D**) Quantification of the phenotype. The R8 *gogo*⁻ axon or the R8 control axon at the border of the clone was examined to see whether it does not a form bundle (a), bundles to adjacent R8 clone axon (b), or to the adjacent WT R8 axon (c). Out of 75 clone borders investigated, 71% of *gogo*⁻ axons bind to the *gogo*⁻axon, and none binds to the WT. In WT control clones, 92% of the R8 axons observed at the clone border do not form bundles (n=39). Scale bars, 10μm.

3.11 R8 target recognition is impaired in *gogo* mutants

In addition to the aberrant R8 phenotype in *gogo* mutant larvae we observed an additional R8-specific mutant phenotype in adult flies. The expression of the adult R8-specific marker *Rh6*-mCD8GFP revealed that several R8 axons did not extend their processes, but rather stalled at the R8 temporary layer (arrowheads in Figure 3-1). The stalling behavior of R8 axons was closer investigated by Takashi Suzuki in order to reveal a possible *gogo* function in axon-target interaction. The R8 marker *Rh6*-mCD8GFP was used to label the majority (70%) of R8s in adult flies regardless of their genotype. In order to distinguish WT and *gogo*$^-$ axons, small clones of WT axons were labeled with mKOrange. In large *ey*FLP clones mutant R8 axons (green only) stopped at the temporary layer (Figure 3-15B-B' red arrows), whereas single remaining WT R8s (green and red) managed to correctly extend to the M3 layer. The percentage of mutant R8 axons stalling at the temporary layer was quantified indirectly. Serial image stacks were taken along the dorsal-ventral axis through *gogo*$^-$ *ey*FLP and wild type *ey*FLP control clones. For quantification, the non-stalling *Rh6*-GFP positive R8 axons were counted within confocal stacks with defined thickness. WT and mutant non-stalling axons can be easily distinguished by the presence or absence of the mKOrange expression. In the control animals, 280.5 mKOrange negative R8 axons per 100μm section (animals: n=6, 201.5μm in total) correctly innervated beyond the temporary layer (Figure 3-15A, C). In *gogo* mutant mosaics, the number of extending *gogo* mutant R8 axons is reduced to 114.9 axons per 100 μm section (n=8, 354.2μm in total, Figure 3-15B, B', C). These numbers suggests that around 60% of *gogo*$^-$ R8s are stalling before entering the medulla (Figure 3-15C), most likely at the R8 temporary layer.

Interestingly, similar numbers of mKOrange-positive R8 axons entered the medulla columns both in *gogo* mosaics and wild type mosaics (38.7 R8 axons in control and 36.2 axons in mutant clones per 100μm; Figure 3-15C), indicating that the final targeting of WT axons is not affected by surrounding mutant axons. Two representative images show examples (arrowheads in Figure 3-15B) of isolated WT R8 axons surrounded by *gogo* mutant axons, which are able to innervate the medulla in a normal manner. These observations strongly suggest that *gogo* has an autonomous function in R8 to regulate axon-target interactions.

We also detected overshooting of R8 axons to the R7 layer (white arrows in Figure 3-15B'). The quantification of the overshooting phenotype showed that 8.5 R8 axons

per 100 μm inappropriately targeted the R7 layer (n=8, 354.2μm in total), which was a clearly smaller fraction than the number of stalling R8 axons.

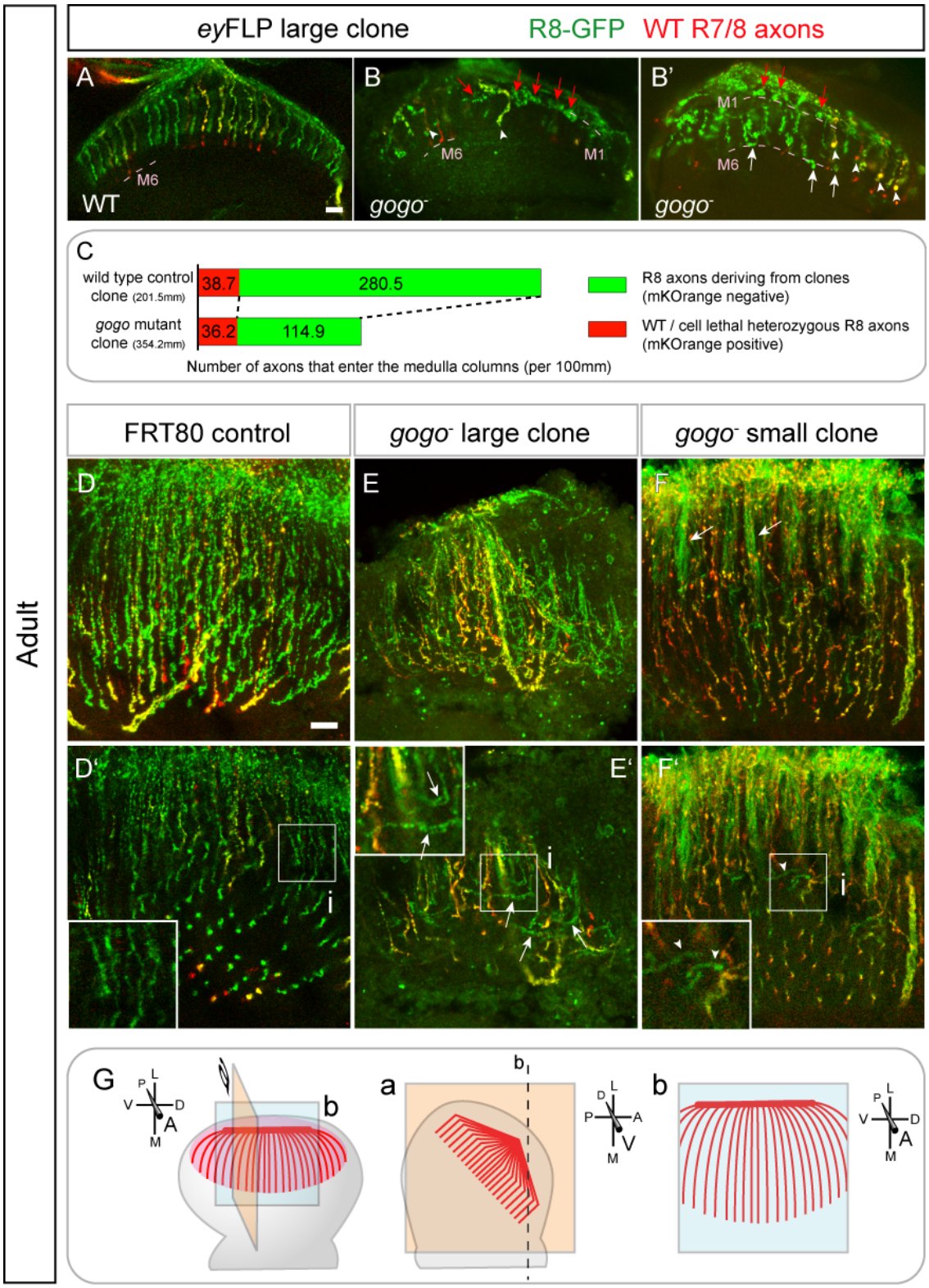

Figure 3-15 *gogo* mutant R8 axons show target recognition defects

(**A-B**) Images of *ey*FLP mosaic medulla in horizontal view (plane a in G). Adult R8 axons are labeled with *Rh6*-mCD8GFPmyc and visualized with anti-GFP (green). WT axons are labeled with GMR-mCD8mKOrange (red). (A) Wild type control clone. (B-B') Some *gogo*$^-$ R8 axons overshoot to the M6 layer (white arrows in B') and many *gogo*$^-$ R8 axons stall at the R8 temporary layer (red arrows in B, B'). Note that wild type R8 axons innervate the medulla (white arrowheads in B). (**C**) The quantification of the R8 axons innervating deeper medulla layers in wild type control (top bar) and *gogo*^{D869} mutant clone (bottom bar). The number of control or *gogo* mutant R8 axons (mKOrange negative; green bar) and the number of WT R8 axons (mKOrange positive; red bar) that enter the medulla were quantified per 100μm thickness. The difference in axon number (280.5 -114.9) represents the R8 axons which failed to enter the medulla in the mutant mosaics. The number of red+green axons is equivalent in *gogo* mutant and control animals (red bars). (**D-F**) Images in frontal view from the anterior of the adult optic lobe (plane b in G). (D, E, F) Projection of a 14μm-thick confocal stack: (D', E', F') Single focal plane image from (D, E, F). Higher magnifications of the boxed areas (*i*) are shown within each panel. In wild type *ey*FLP control clones, finely-organized parallel axonal tracts are observed (D, D'). In large *gogo*$^-$ *ey*FLP clones, *gogo*$^-$ R8 axons often form bundles with other *gogo*$^-$ axons (E,E') and make a sharp turn at the surface of medulla (arrows in E'). The "stray" phenotype at the surface can also be observed in a single focus plane (E'). (F, F') small *gogo*$^-$ clones were created using *ey*FLP without cell lethal mutation. Axon bundling can be observed within the *gogo*$^-$ clones (arrows in F). While most of the neurons send their axons in parallel to each other in a organized way, a small fraction of axons (green without red), which are *gogo*$^-$, turn towards the dorsal-ventral axis within the surface of medulla (arrowheads in F'). (**G**) Schematic drawing of the adult medulla to demonstrate the orientations of the views.
Scale bars, 10μm.

Next the same samples were observed from the anterior of the adult optic lobe (Figure 3-15D-F'). In this orientation, R8 axonal projections are seen at the temporary layer from the top view (plane b in Figure 3-15G). In a 14μm-thick confocal projection, wild type control axons are organized in parallel axonal tracts in the wild type control (Figure 3-15D). However, in *gogo* mutant *ey*FLP clones, *gogo*$^-$ R8 axons often make a sharp turn at the surface of the medulla and stray at the surface (Figure 3-15E). We confirmed this "straying" phenotype at the surface by taking only one confocal section image (Figure 3-15E'). In contrast to WT axons, which normally turn into the medulla and target the M3 layer which lies underneath, a certain fraction of *gogo*$^-$ R8 axons aberrantly turns in the wrong direction and strays at the surface. We examined this phenotype in smaller clones, since this abnormal phenotype can be a community effect of a large fraction of misguided axons. Strikingly, we observed the same phenotype in smaller *ey*FLP *gogo* mutant clones without cell lethal mutation (see chapter 2.13, Figure 3-15F, F'). While most of the wild type axons are parallel to each other in a highly organized way, *gogo*$^-$ axons make an inappropriate turn towards the dorsal-ventral axis within the surface of the medulla, qualitatively the same phenotype as we observe in the large *gogo*$^-$ clones (compare with Figure 3-15E-E'). This straying phenotype is striking, since it appears that *gogo*$^-$ axons fail to detect pathfinding cues to enter the deeper medulla layers, and that, as a consequence, they are misguided and straying along the medulla surface.

3.12 Gogo functions in R8 target layer selection

During larval development *gogo*$^-$ axons form bundles which can still be observed in adult flies (Figure 3-15F, arrow). Although the striking R8 phenotype in adults suggests an autonomous role in later targeting decisions, the targeting defect in *gogo*$^-$ adults could also reflect a secondary defect, caused by intense axon bundling during larval stages. In order to exclude a secondary defect, small *gogo* clones were created to investigate the behavior of single/few *gogo*$^-$ R8 axons in the absence of strong bundling defects. In addition, the preserved overall projection pattern within these small mosaics allows a better identification of the respective layers within the medulla.

First mosaic animals were observed during mid-pupal stages at 55APF. At this stage the final target layer choice of R8s has already been made. R8s have already extended their axons to the M3 layer and started to establish their firm connections (Figure 1-6A, Figure 3-16A, Ting et al., 2005) Small clones of *gogo*$^-$ axons were created by *ey*1xFLP.Exel. Mutant R8 axons were labeled as described in chapter 3.10 (Figure 3-12B). All *gogo* mutant R8 axons strongly express *ato-τmyc*, whereas wild type axons are specifically labeled with mKOrange. Small populations of mutant R8 axons showed bundling before the M1 layer, but managed to separate before reaching the M1 layer (Figure 3-16B, B'). Nevertheless, *gogo* mutant R8s often fail to extend their axons to M3 and stay at the M1 layer instead. This defect can be observed also in single isolated *gogo*$^-$ R8 axons that have not formed bundles (arrows in Figure 3-16C-D').

In adult flies, small clones were created using *ey*FLP recombination without using a cell lethal mutation (see chapter 2.13). The R8 marker *Rh6*-mCD8GFP was used to label the majority (70%) of R8s. WT axons were specifically labeled with mKOrange. The majority of wild type axons create a normal overall projection pattern, which precisely defines the position of the medulla layers of interest M1, M3 and M6 (indicated with dashed lines in Figure 3-16E-G'). In addition to prematurely stopping and straying axons (arrowheads in Figure 3-16E, F), M6 layer overshooting of *gogo*$^-$ R8 axons was also observed in the small clones (arrow in Figure 3-16G).

These results strongly indicate that Gogo mediates axon-target interaction independent of larval axon-axon interaction.

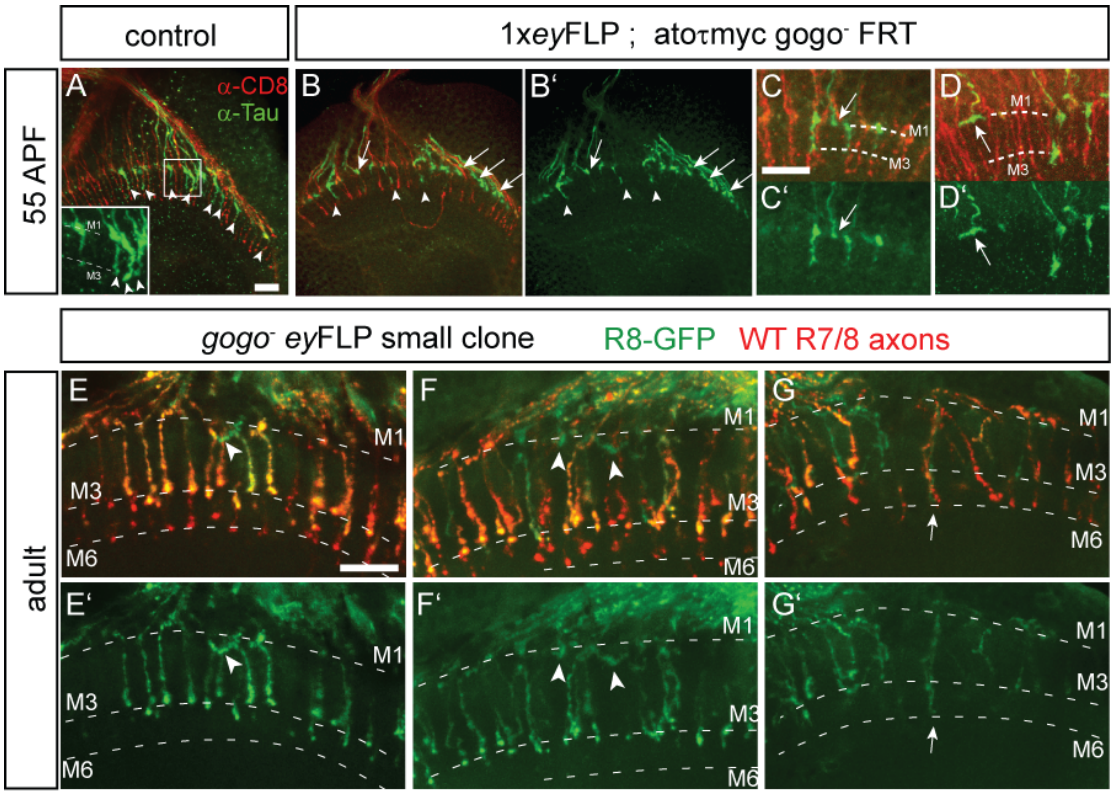

Figure 3-16 Gogo functions in R8 axon-target recognition

(**A-D'**) Small populations of wild type (A) or *gogo*^{D869} R8 axons (B-D) were created by ey1xFLP.Exel at 55APF. *gogo*^{D869} clone: *ato-τmyc gogo*$^{-}$ FRT/ GMR-mCD8KO FRT. R8 axons labeled with *ato-τmyc* are visualized by anti-Tau (green). WT axons labeled with mCD8KOrange are stained with anti-mCD8 (red). Note that some *gogo*$^{-}$ R8 axons (strong green without red) extend normally (arrowheads), whereas a significant amount of mutant R8 axons shows defects (arrows) (B,B'). Single isolated *gogo*$^{-}$ R8s often fail to extend their axons to M3 (C-C', arrows) or even stray at the M1 layer (D-D', arrows).
(**E-G'**) Adult medulla targeting phenotype of *gogo*^{D869} R8 axons in small clones. R8 axons are labeled with Rh6-mCD8GFP, and wild type axons are labeled with GMR-mKOrange. Mosaic clones were generated by *ey*FLP without using a cell lethal mutation. As observed in larger clones, *gogo*$^{-}$ R8 axons often stay at the M1 layer and do not innervate the medulla column (arrowheads in E-F'). The phenotype can be seen autonomously either in a single cell clone (E-E') or in a small cluster of neurons (F-F'). Occasionally the *gogo*$^{-}$ R8 overshoot the correct M3 layer and target the M6 layer (arrow in G, G'). Medulla layers are indicated with dashed lines. Scale bars, 10μm.

3.13 Gogo mediates axon-target recognition at the R8 temporary layer

The straying phenotype at the M1 layer infers a possible role of Gogo in the proper recognition of the intermediate target layer. In previous experiments only time points after the extension phase of R8 from M1 have been analyzed, as shown for 55APF or adult flies in chapter 3.12. In order to examine *gogo* mutant R8 axons during the phase of M1 intermediate target layer selection and position maintenance until the extension phase at 50APF, R8s were labeled in large *ey*FLP clones with the R8 specific marker *ato*-τmyc and investigated during pupal stages at 17APF, 35APF and 50APF.

In wild type flies the segregation of R7 and R8 growth cones into distinct medulla layers can be observed at 17APF (Figure 3-17A-A'). Also in *gogo*$^-$ eyFLP flies two distinct layers are formed (Figure 3-17E-E'). However, R8 axons display a slightly different morphology, as their growth cones appear elongated compared to wild type R8 axons.

In wild type flies at 35 APF, the temporary layers of R8 and R7 are more distant, but the relative position of R8 to R7 is maintained (Figure 3-17B-B'). R8s are still anchored at the M1 layer without showing visible extensions. In contrast, several *gogo* mutant axons have prematurely started extending from the M1 layer at this stage (Figure 3-17F-F'). The early extended axons show a highly irregular pattern lacking a strict columnar organisation. Nevertheless R7 and R8 axons seem to remain separated, as no complete overlap of R7 and R8 termini was observed.

At 50 APF when R8s and R7s normally start extending to their final targets (Figure 3-17D-D'), most of the mutant R8 axons, which have remained at the temporary layer, now fail to extend filopodia (Figure 3-17G-G'). Extended R8 axon terminals are not restricted to their proper target layer M3 as in WT. In some cases *gogo*$^-$ R8 axons even overshoot to the M6 target layer of R7.

The number of R8 axons which prematurely extended beyond the M1 layer was quantified within confocal stacks of defined thickness (Figure 3-17I). In the WT control animals, 0 (17APF) and 0.9 (35APF) R8 axons showed thin extensions per 50μm section earlier than 50 APF (n=2, 28μm and n=3, 56μm respectively). At 50 APF 104.2 extensions per 50μm were quantified in wild type (n=4, 48μm), showing that the final extension of R8s does not occur in WT before this time point (Ting et al., 2005). In the *gogo* mutant mosaics, only 0.7 R8 axons showed a slightly different

position in deeper medulla layers at 17APF (n=4, 69μm), indicating that the primary segregation of R8 and R7 is not affected. Nevertheless, R8 axons fail to immobilize until 50 APF, as 34.4 premature R8 axonal extensions are displayed per 50μm at 35 APF (n=5, 106μm). At 50 APF the number of extending mutant R8 axons is only slightly increased to 40.0 axons per 50μm (n=5, 130μm). Strikingly, these 40 axons exactly constitute 40% of the quantified extended wild type axons at 50APF, reflecting the quantified stalling phenotype in adult (see chapter 3.11).

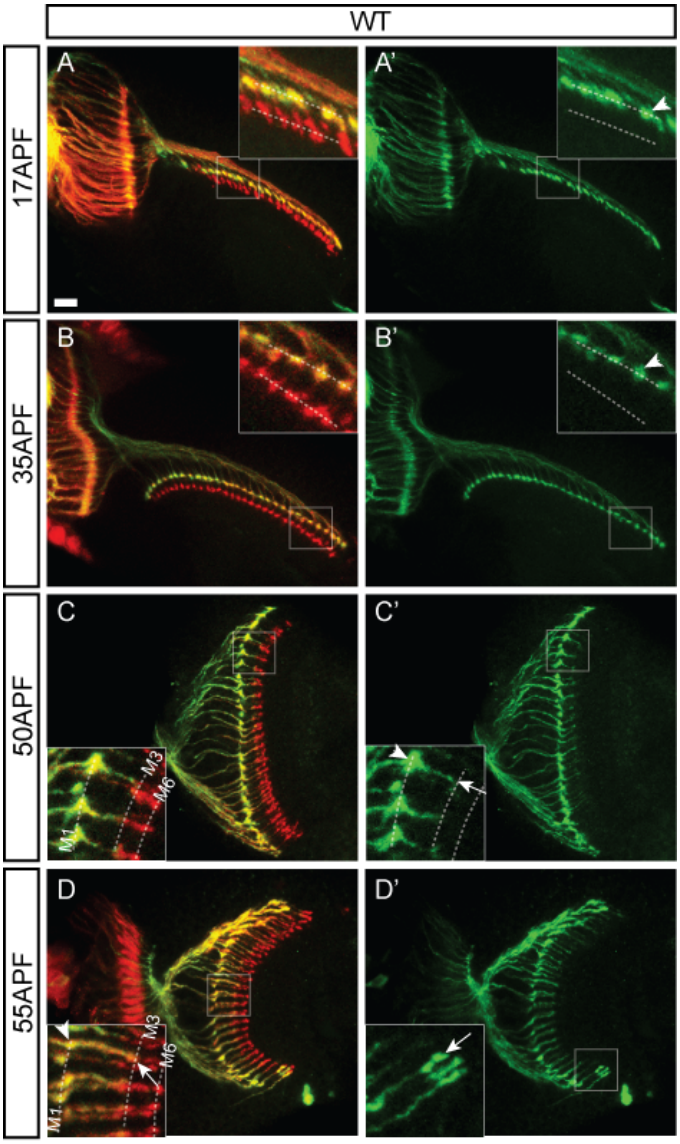

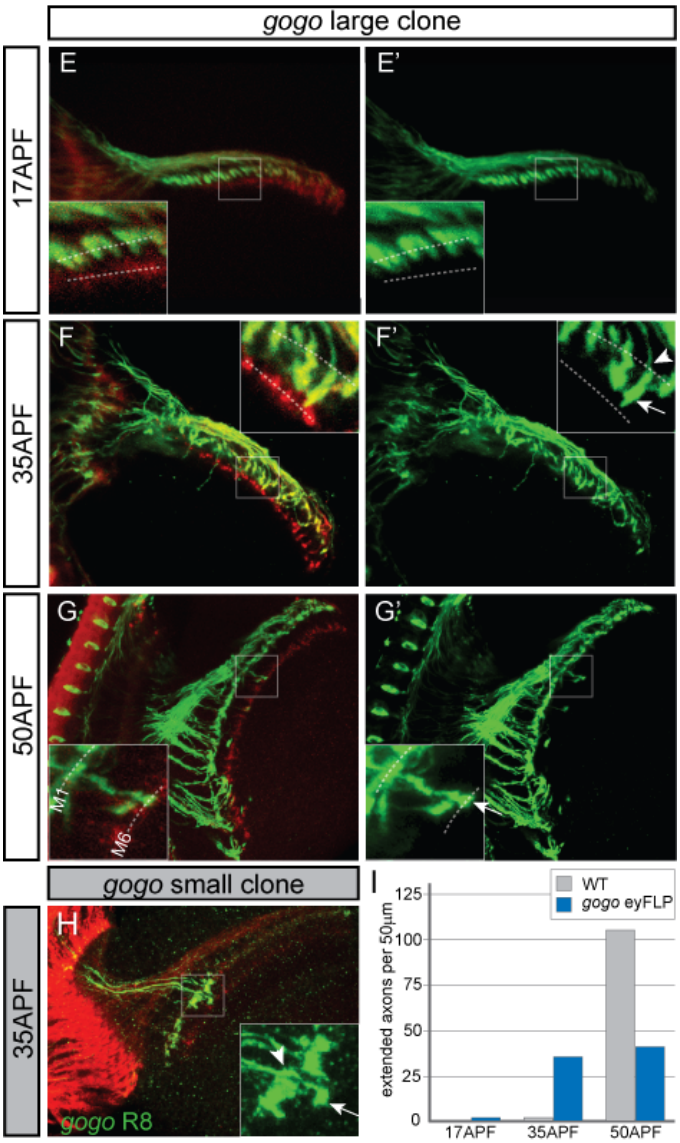

Figure 3-17 *gogo* R8 axons prematurely extend from their temporary targets

(**A-G'**) R8s were labeled in large *ey*FLP clones with the R8 specific marker ato-τmyc (green). R7 and R8 axons were stained with mAb24B10 (red). Axonal projections were investigated during pupal stages at 17APF, 35APF, 50APF and 55APF. (**A-D'**) WT control clones: At 17APF R8 (arrowhead) and R7 terminals are separated in two distinct layers (indicated by dashed lines) (A, A'). At 35APF R8 axons remain anchored to their temporary target layer (arrowhead) (B, B'). At 50 APF R8 axons extend thin filopodia (arrow) to the M3 layer, while bulb-like structures remain at the M1 layer (arrowhead). The two final targeting layers M3 and M6 can be easily distinguished (dashed lines) (C, C'). At 55 APF thickened R8 terminals appear at the M3 layer (arrow) (D, D´), while the bulb-like structures at the M1 layer slowly start to vanish (arrowhead) (D). (**E-G'**) *gogo* clones: At 17 APF R8 and R7 are separated in two distinct layers (indicated by dashed lines), but R8 terminals show a distinct morphology compared to WT (E, E'). At 35 APF prematurely extending R8 axons can be observed. They display thickened axonal terminals (arrow). At the same time, the bulb-like structure at the M1 layer seems to be lost (arrowhead). R7 and R8 terminals still form separated layers (F, F'). At 50 APF some R8 axons overshoot to the R7 target layer M6. In contrast to WT, all extended axons display thickened terminals (arrow). The majority of R8 axons fails to extend from the M1 layer (G, G') (**H**) Small clone of *gogo*$^{-}$ R8 axons created by ey1xFLP.Exel at 35APF. The *gogo*^{D869} clone: *ato-τmyc gogo*$^{-}$ FRT/ GMR-mCD8KO FRT. R8 axons labeled with *ato-τmyc* are visualized by anti-Tau (green). WT axons labeled with mCD8KOrange are stained with anti-mCD8 (red). A single *gogo*$^{-}$ R8 axon (strong green without red) prematurely extends and looses its bulb-like structure at the M1 layer (arrowhead). The extended axon displays a thickened terminal (arrow). Magnifications of the boxed areas are shown within each panel. (**I**) Quantification of extending axons during pupal development. Scale bars, 10µm.

In addition, the structures of premature extensions clearly contrast the proper extensions in wild type flies. At 50 APF, wild type R8 axons start extending thin filopodia to deeper medulla layers, while thick bulb-like structures remain at the M1 layer (Figure 3-17C'). Thickened R8 axon terminals do not appear at the M3 target layer before 55 APF (Figure 3-17D'). At the same time, the bulb-like structures at the M1 layer slowly disappear in WT. However, in *gogo*$^-$ *ey*FLP mutants the premature extended axons already display thickened terminals, structures different from filopodia and seem to lack bulb-like structures at the M1 layer (Figure 3-17F', G'). For closer investigation of the premature extensions small *gogo*$^-$ R8 clones were created by *ey*1xFLP.Exel and investigated at 35APF (Figure 3-17H). In addition to the thickened terminals, premature extending axons lack the thick bulb-like structures remaining at the M1 layer.

These results indicate that at least some R8 axon terminals completely loose contact to binding sites at the M1 layer and continue to grow out inappropriately. The proper recognition of the intermediate target layer and position maintenance until mid pupal stages seems to be required to allow R8 axons to enter their correct medulla columns and recognize their correct target layer.

3.14 Gogo overexpression anchors R8s at the M1 layer

If Gogo is sensing pathfinding cues at the temporary target layer of the medulla, then how does Gogo respond to these cues (adhesive/attractive, or repulsive)? To distinguish between these possibilities the *gogo* gain-of-function (GOF) phenotype was assessed by overexpressing full length Gogo in R axons. To achieve a higher level of expression throughout development, we used GMR-Gal4 to drive UAS-*gogo* expression. Strikingly, 100% of R8s form large bulb-like structures and terminate at the M1 layer after overexpression of the transgenic line UAS-*gogo*T2 (Figure 3-18C, C') (animals: n=5, 196.56μm in total, more than 600 R8 axons estimated). The array of large bulbs in the UAS-*gogo*-T2 GOF (Figures 7B, B', D) is in clear contrast to the uncoordinated turning and stalling in *gogo* loss-of-function (LOF) (Figure 3-15). The R8-specific GOF phenotype strongly argues against a simple artifact, as Gogo is overexpressed in R7s as well. In addition, the expression of UAS-*gogo*-T2 under the control of GMR-Gal4 in a *gogo* mutant background was able to rescue the overall projection pattern of R8 and R7, however resulted in R8 axons terminating at the M1 layer (see large bulbs at the M1 layer in Figure 3-9G).

Milder overexpression phenotypes were observed in different UAS-*gogo* insertion lines (UAS-*gogo*T1, UAS-*gogo*2B,-3A,-3B,-3C, Figure 3-18B, B' and data not shown). By overexpression of intermediate transgenes large bulb-like structures were maintained to a certain extent at the M1 layer, which normally disappear until adulthood in wild type flies (Figure 3-18A). Only few stalling axons were identified in different transgenes (quantified for UAS-*gogo*-T1, Figure 3-18D). However, in contrast to UAS-*gogo*T2 the majority of R8s managed to extend processes to the M3 layer (Figure 3-18B, B', C').

The variability in phenotypical expressivity could be a consequence of different expression levels among the insertion lines used. Expression levels of all available myc-tagged UAS-*gogo* lines (generously provided by Stephan Ohler) were analyzed by Western blot at different stages throughout development. The construct with the strongest expressivity UAS-*gogo*-T2 showed the highest expression levels throughout all stages investigated. This result points towards a possible correlation between expression level and the observed phenotypical strength.

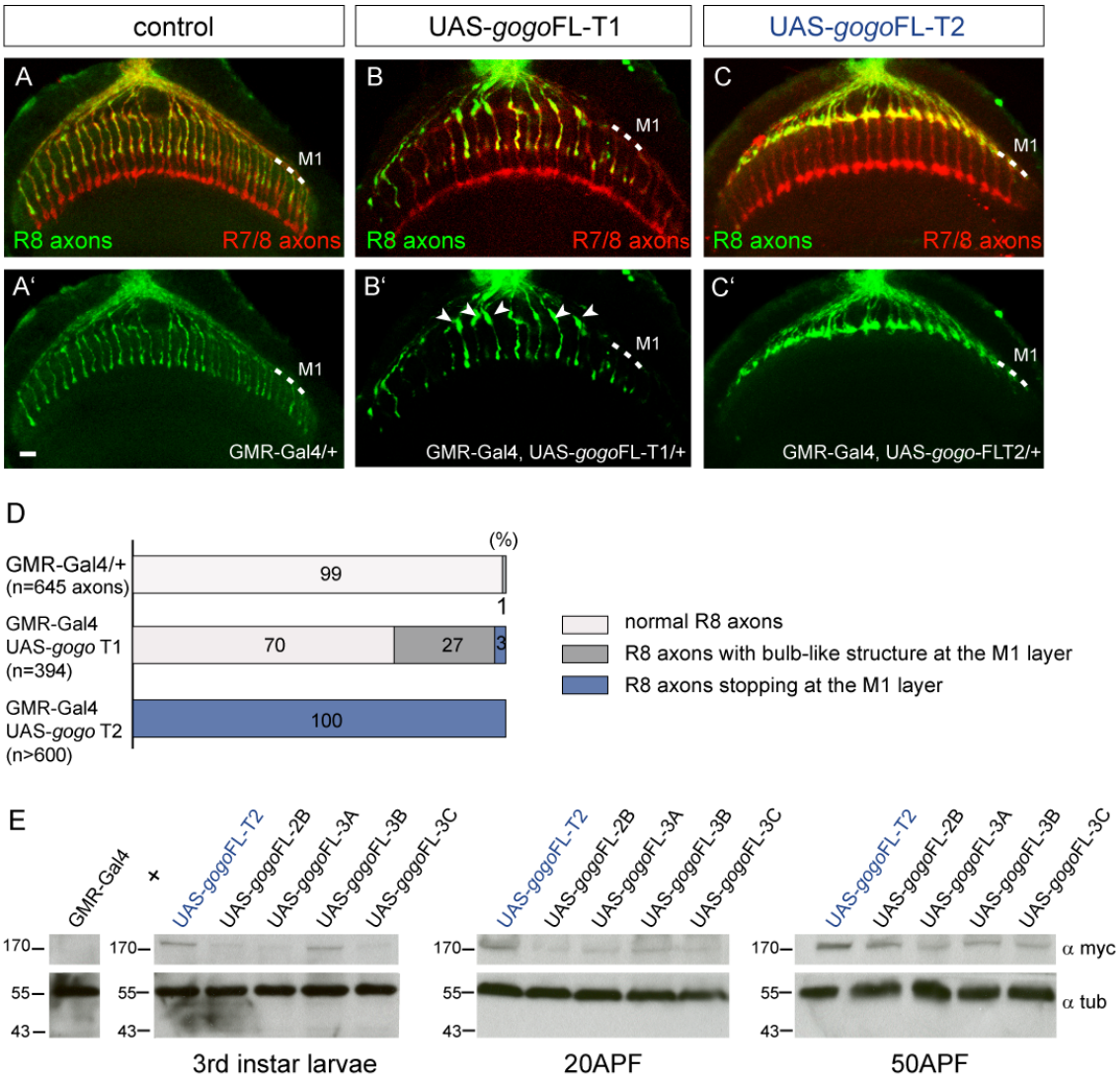

Figure 3-18 Gogo overexpression phenotype

(**A-B**) Images of the adult flies: All R cell projections (red; mAb24B10) and R8 axons (green; *Rh6*-mCD8GFP with anti-GFP) are visualized in the GMR-Gal4/+ control (A, A') and GMR-Gal4, UAS-*gogo*FL-T1/+ (B, B') and GMR-Gal4, UAS-*gogo*FL-T2/+ medulla (C, C'). In the *gogo* overexpression using the UAS-*gogo* T1 line, large bulb-like structures are seen at the M1 layer (arrowheads in B') and few R8 stops. The majority of R8s, however, still managed to extend their processes to the M3 layer. We consider this as a mild overexpression phenotype. The UAS-*gogo* T2 transgene results in a much stronger overexpression phenotype. R8 axons terminate at the M1 layer (C'). Note that R7 axons are completely normal (B, C'). (**D**) The quantification of the GMR-Gal4 UAS-*gogo* overexpression experiment. UAS-*gogo*T1 shows a mild *gof* phenotype, whereas T2 shows a highly penetrant *gof* phenotype. (**E**) Western analysis of overexpressed Gogo protein. Left panel: GMR-Gal negative control. Five different UAS-*gogo* insertions tagged with myc were expressed using GMR-Gal4. 3rd instar larval brains and whole pupae at 20APF and 50APF were analyzed. Gogo protein was detected using αmyc antibody. Tubulin levels assessed by an anti-tubulin (α tub) antibody served as a loading control. Scale bars, 10μm.

The striking GOF phenotype suggests two different possibilities: either, Gogo is sensing a repulsive cue from layers deeper than M1 layer, so that higher activation of Gogo repels R8 axons from the M3 layer, or Gogo regulates the attraction/adhesion by a cue from the M1 layer temporarily, and abnormally high Gogo levels result in permanent anchoring of R8 at the M1 layer. The LOF data supports more the latter option, as straying and premature extension of *gogo*$^-$ R8 axons can be explained by the presence of attractive/adhesive cues from the M1 layer.

Thus, it is highly intriguing that *gogo* function is not only mediating repulsive interaction among outgrowing R8 axons, but also has a qualitatively different function during pupal development, which appears to involve proper target recognition between R8 axon and the milieu at the temporary layer, M1. We propose that this second mechanism ensures that the R8 axons locate and maintain the position at the correct temporary target site until the proper developmental time point and thereby allows the axons to enter the appropriate column in the medulla.

4 Discussion

4.1 Autonomous receptor function in photoreceptor cells

The single transmembrane protein Gogo, which is expressed in photoreceptor cells, is required in the retina for axon-axon repulsive interactions and appropriate column and target layer selection in the optic lobe of the *Drosophila* brain. The evolutionary conservation of this molecule across different species implies a high functional relevance.

The protein structure of Gogo, comprising protein interaction domains present in other axon guidance receptors, strongly indicates a function as a receptor or cell adhesion molecule. Within the extracellular domain, two conserved regions were shown to be essential and sufficient for Gogo function in photoreceptor axons, the Tsp1 and the newly identified GOGO domain (Chapter 3.3). Both domains show the ability for protein interaction. Eight conserved cysteines within in the GOGO domain possibly form four disulfide-bonds to assemble immunoglobulin-like protein interaction domains (Takayanagi et al., 2006). Also, the Tsp1 domain shows the ability to interact with multiple cell-surface or extracellular proteins, including matrix glycoproteins and proteoglycans (Adams and Tucker, 2000).
So far, there is no evidence that Gogo's extracellular domain is able to promote homophilic binding among Gogo proteins, as shown in S2 cell aggregation assays (chapter 3.6). In addition, homophilic interactions are neither required for the repulsion among R8 axons nor in axon-target interaction (chapter 3.6, 3.10). All results obtained suggest a heterotypic interaction, in which Gogo could act in response to an as yet unidentified ligand.

The strict requirement of the cytoplasmic domain, which was demonstrated in rescue experiments in two different stages during development, axon-axon interaction in larvae (chapter 3.10) and axon-target interaction in adults (chapter 3.3), argues against a merely adhesive role of Gogo. In contrast, it was shown for some adhesion molecules (such as N-Cad) that the cytoplasmic domain is not needed for homophilic adhesion and functionality. Therefore, their function can be achieved without intracellular signaling (Yonekura et al., 2007). The opposite is known for repulsive guidance receptors, such as Eph receptors or Dscam. Although the physical binding

of the extracellular domains to their ligands can be achieved without the cytoplasmic domain, still the repulsive response triggered by these receptors strictly requires the cytoplasmic domain for intracellular signal transduction (Feldheim et al., 2004; Labrador et al., 1997; Matthews et al., 2007; Wojtowicz et al., 2004; Zhu et al., 2006). The requirement of Gogo's cytoplasmic domain argues against a simple adhesive role and implies that cytoplasmic signaling is required for Gogo function. The lack of an intracellular catalytic domain (as for example a kinase domain) does not contradict intracellular signaling events, as shown for the well described family of Robo receptors. Similar to Gogo, Robo proteins contain a poorly conserved cytoplasmic domain without any obvious catalytic activity (Kidd et al., 1998). But they contain short conserved cytoplasmic sequence motifs, which are thought to be binding sites for various signaling proteins, as for example Abl/Ena/Vasp, Dock/Nck or the Rho GAPs (GTPase activating proteins) Vilse/crGAP (Bashaw et al., 2000; Fan et al., 2003; Hu et al., 2005; Lundstrom et al., 2004; Wong et al., 2001).

Similarly, there is no overall conservation within the Gogo cytoplasmic domain, except for a specific short motif, which is shared by all Gogo orthologues (chapter 3.2). The short sequence contains a highly conserved tripeptide motif, Tyr-Tyr-Asp (YYD) that may serve as a putative regulatory site through phosphorylation of the Tyrosine and/or protein interaction domain. It was shown that a similar tripeptide motif Asp-Arg-Tyr (DRY) is conserved in mammalian odorant receptors, which belong to the family of G protein coupled receptors (GPCRs). Olfactory sensory neurons expressing odorant receptors mutant for the DRY motif are deficient in both axon targeting and G protein coupling (Imai et al., 2006). In principle, it is feasible that the highly conserved Gogo tripeptide also holds the potential to trigger an intracellular signaling pathway which could even be conserved across different species. For this reason, it would be interesting to investigate a possible functional role of this short cytoplasmic motif. Rescue experiments using either deletions of the motif or site-directed mutagenesis manipulating the potential phosphorylation-sites could be applied in order to investigate this question.

Although Gogo expression was detected in brain neurons other than R cells by *in situ* and antibody staining (chapter 3.5), the *gogo* transheterozygous mutants were rescued by the exclusive Gogo expression in R neurons (chapter 3.6). R axon targeting is therefore not dependent on Gogo expression within the brain. This result not only excludes the possibility of homophilic axon-target interaction, but also shows the autonomous requirement in R cells. In addition, a cell-autonomous function of Gogo was shown for single axons in mosaic animals. Also in pupae, single *gogo* mutant R8 axons show defects and fail to extend into the medulla column (Figure 3-16). Vice versa, single isolated WT R8 axons, which are surrounded by misprojecting and stopping *gogo* mutant axons, constituting a reverse MARCM situation, correctly innervate the medulla (Figure 3-15B). All these examples nicely demonstrate that Gogo acts in a cell-autonomous manner in R8 axons.

Both lines of evidence, the autonomous function and the requirement of the cytoplasmic domain, provide a strong argument that Gogo could act as a novel receptor in axon guidance.

4.2 R8 axon-axon interaction

In eye-specific *gogo*$^-$ mosaics, larval axons do not manage to maintain their relative positions within the medulla. They entangle each other and form bundles (chapter 3.10). This disrupts the formation of the retinotopic map, an important feature in visual system wiring which allows the continuous representation of visual space in the brain. Studies investigating the establishment of topographic maps have proposed two basic principles to be involved in the formation of the neuronal map during development. The first principle is the existence of positional labels in gradients across the projecting and target areas, as shown for ephrin-A/EphA, ephrin-B/EphB, Wnt3 and En-2 (Brunet et al., 2005; McLaughlin and O'Leary, 2005; Schmitt et al., 2006). In addition to a role for specific graded labels, axon-axon mediated competition is thought to be the second key principle (Reber et al., 2004). In *Drosophila* both principles, long-range positional cues and local R axon-axon interactions, are thought to be involved in topographic mapping along the dorsoventral axis. As positional cues, Eph receptor tyrosine kinase gradients in the medulla and DWnt4 positional cues were shown to be required for topographic map formation (Dearborn et al., 2002; Sato et al., 2006). Futhermore, independent guidance of R axons involving axon-axon competition was proposed (Kunes et al., 1993; Senti et al., 2003). Interestingly, the homophilic cell adhesion molecule Flamingo was shown to be required for competitive or inhibitory interactions between adjacent R8 growth cones (Senti et al., 2003). However, the underlying mechanism has not been investigated yet.

The observed *gogo* mutant phenotypes in larvae suggest that during the extension phase *gogo* mutant axons lose repulsive interactions within the medulla, resulting in strong axonal bundling. Larval Gogo expression which was present mainly in R8s (chapter 3.5) hinted at a function in R8 pioneers, allowing correct spacing of parallel outgrowing axons. In small *gogo* mutant clones R8 mutant axons were shown to exclusively form bundles with other R8 mutant axons, while surrounding WT axons are not affected (chapter 3.10). This implies an axon-axon repulsive effect among R8 axons mediated by Gogo. Homophilic interaction with brain cells was excluded by the transgenic expression of Gogo in R axons. Gogo expression in R axons which project into transheterozygous *gogo* brains is sufficient to restore normal axonal

spacing (chapter 3.6). As a consequence, Gogo resembles a novel regulator of axon-axon competition in the larval visual system.

How does Gogo prevent inappropriate adhesion or bundling among R8 axons through repulsive interaction? In our model, we favor the idea of competitive interactions among R8 axons. The idea is that Gogo acts as a heterotypic receptor mediating repulsive interactions among R8 axons, but at the same time competes with possible adhesive forces among R8 axons (Figure 4-1). Adhesive interactions can be the result of expressed homophilic cell adhesion molecules which are required for target layer selection and binding, but have to be suppressed during axon outgrowth in order to inhibit inappropriate axon-axon interactions. Possible candidates for regulated cell adhesion molecules could be for example N-Cadherin, as well as the R8-specific expressed adhesion molecule Capricious (Caps). The proposed competitive-forces model also explains why single isolated *gogo*$^-$ axons fail to form bundles in the absence of other mutant axons and surprisingly project without defects (Figure 4-1).

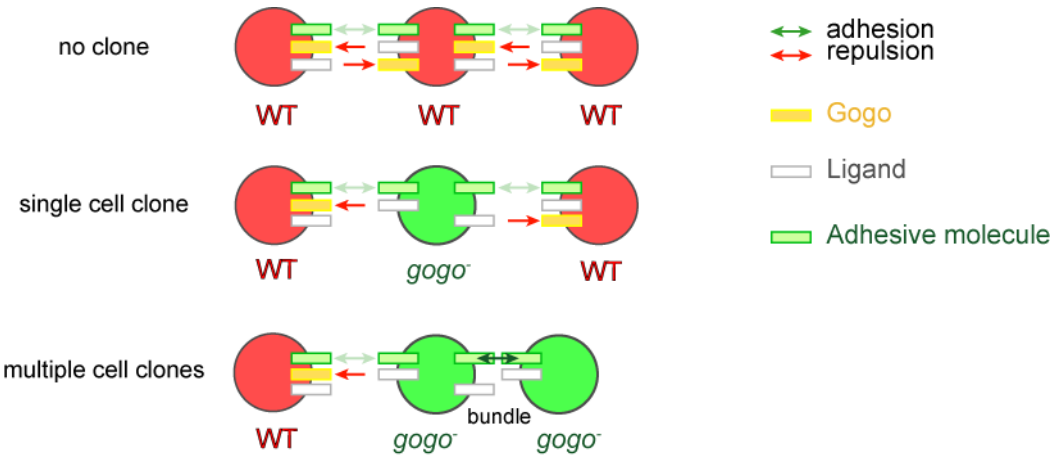

Figure 4-1 Model for competitive axon-axon interactions

Model for axon-axon interaction; Gogo may be a heterotypic receptor that mediates repulsive interaction among R8 axons. In the wild type situation, both attractive and repulsive interactions constitute the balanced force between the axons (top). In a single cell mutant clone, the balance between the forces is still maintained so that no bundles are formed (middle). When a cluster of axons is mutated, the repulsive force is weakened within the clone, so that mutant axons form bundles (bottom).

A different competitive model has been proposed for the topographic map formation of retinal ganglion cells (RGC) in the mouse. But in contrast to our competitive forces model, the RGC–RGC axon-axon competition is governed by comparisons of internal EphA receptor repulsive signaling intensities within neighboring axons (Reber et al., 2004). A difference in signaling intensities between younger and older R8 axons could also be true for Gogo, as antibody staining revealed highest protein localization to the youngest in-growing axons (chapter 3.5). Nevertheless, no real Gogo gradient was observed across R8 axons. Interestingly, also Fmi shows a strikingly similar expression pattern during larval development (Lee et al., 2003).

4.3 Axon-target interaction

In addition to defects in larval axonal projections, aberrant phenotypes are displayed in *gogo* mutant adult flies in all types of photoreceptors (chapter 3.1), indicating an additional requirement in the establishment of proper axonal connections with target cells. This was supported by antibody stainings showing Gogo expression in all photoreceptor types during certain stages of pupal development (chapter 3.5). Expression was observed in R1-R6 axons during the phase of cartridge formation, as well as in R7 and R8 axons during the first medulla targeting step, involving the time of intermediate target layer recognition and position maintenance. However, Gogo expression was not detected in photoreceptor axons during the second targeting step in R7 and R8 axons, as well as in R1-R6 axons after 40APF. The dynamic expression pattern and regulation of Gogo protein within the axon during pupal development argues for a possible function in specific targeting steps.

Initially, R1-6 axons of *gogo ey*FLP flies correctly target the lamina and do not overshoot into deeper neuropils during larval development, but then fail to assemble proper lamina cartridges (chapter 3.8). Although the observed phenotype indicates a functional role of Gogo in sorting R1-R6 axons to their correct cartridges, experimental evidence is required to exclude secondary defects due to the R8 mistargeting. The possible influence of R8s on R1-R6 projections is based on the sequential axon outgrowth during larval development; in which R1-R6 strongly depend on the trajectories formed by R8 pioneer axons (chapter 1.3). Observing cartridge formation in a R8-specific rescue background (compare chapter 3.9) could easily demonstrate that *gogo* is indeed autonomously required for the choice of postsynaptic partners in R1-R6 axons, in addition to the function shown for R8s. Furthermore, it would be possible to perform single cell mosaic analysis in R1-R6 neurons to investigate cell-specific mutant phenotypes.
Already at this stage of investigations, two arguments make an autonomous function in R1-R6 most likely. First, the observed bundling phenotype among mutant R8 axons is only observed in the medulla when axons have already passed the lamina, indicating that the retinotopic map and overall projection is still intact within the lamina (chapter 3.1). Second, also *fmi* has been shown to affect R8 and R1-R6 independently. In the absence of *fmi*, bundling of R8 axons is induced, similar to the *gogo* (lof). Despite the defect in R8s an independent role in R1-R6 was demonstrated

(Lee et al., 2003; Prakash et al., 2005). Again, the mutant phenotype observed in R1-R6 axons of *fmi* mutants is comparably similar to the missorting observed in *gogo* mutants (chapter 3.8) (Lee et al., 2003).

Mutant R7 axons also display targeting defects in adult flies (chapter 3.1). In *gogo eyFLP* flies, R7 axons do not show a strict columnar restriction, reflected by frequent crossings. In addition, a small number of axons fail to connect to their proper target layer M6 and mistarget to the R8 target layer M3 instead. In contrast to R8s, no stalling of R7 axons was observed at the superficial layer of the medulla. In total, R7s display a much milder mutant phenotype in comparison to R8 axons. The R7-specific *gogo* mutant clones and the R8-specific rescue experiment disproved an autonomous Gogo function in R7 (chapter 3.9), showing that R7s are highly dependent on the trajectories formed by R8 axons during larval development. As R7 axons manage to correctly separate from R8 axons to reach their intermediate target layer underneath the R8 temporary layer (chapter 3.13), a fasciculation defect can be excluded as the cause for mistargeting. Additional evidence for the lack of Gogo function in R7 is provided by the Gogo overexpression experiments (chapter 3.14), in which R7s show no targeting defects despite highly elevated Gogo levels.

In addition to Gogo's early function in R8 axon-axon interaction during larval development, the observed *gogo* mutant phenotype in adults suggested a second independent role in R8 axon-target interaction during pupal development. Interestingly, several mutants were identified that have striking R-axon guidance phenotypes in larvae but less severe phenotype in adults (Berger et al., 2008). The shown transience of defects strongly suggests the existence of different mechanism underlying the development of larval and adult systems. Vice versa, it is likely that the same gene is independently involved in the development of both systems. However, also limitations to the existence of completely unrelated mechanism exist as shown in our rescue experiment, which argues for a R8-dependent projection pattern of R7.

Nevertheless, two important observations suggest a second, unrelated and independent role of Gogo in R8 axon target interaction: First, the majority of R8 axons fails in properly entering the medulla column and strays at the surface of the medulla (chapter 3.11). This phenotype could be reproduced in single *gogo* mutant axons, proving a R8-specific cell-autonomous function in axon-target interaction (chapter 3.12). Second, R8 axons overexpressing Gogo permanently terminate at the surface layer, whereas R7s remain unaffected (chapter 3.14).

In our model (Figure 4-2) we propose that Gogo positively regulates the adhesion of R8 axons with the M1 temporary layer during early pupal development and thereby prevents R8 axons from prematurely extending from the M1 layer until their proper extension time point at 50APF. However, the final R8 targeting step might require Gogo removal during mid-pupal stages in order to allow axon extension to the final target layer M3. The observation that Gogo protein is detected during the first step of R8 targeting, intermediate target layer recognition and position maintenance, but can not be detected during the second targeting step, the extension to the M3 layer, supports this idea. In the Gogo overexpression situation, high Gogo protein levels are present in photoreceptors until late pupal stages due to the amplification using the Gal4/UAS system in combination with the very strong promoter GMR. The overexpression results in permanent anchoring of R8 axons to the M1 layer (chapter 3.14).

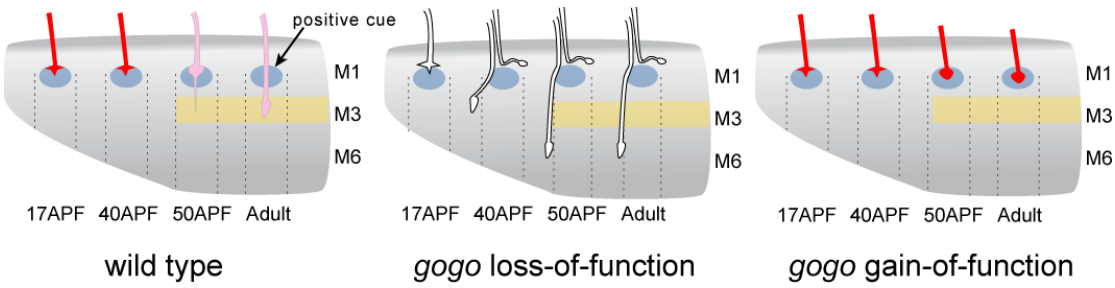

Figure 4-2 Model for R8 axon-target interaction
Model showing Gogo function in R8 axons during pupal development: In **WT** Gogo is required for the M1 layer recognition of R8 axons and position maintenance until 50APF. Gray spots indicate a possible pathfinding cue which acts positively on the R8 axons at the M1 layer. A proper intermediate target layer interaction allows R8 axons to retain their position. The decrease in the intensity of red in R8 axons suggests the down-regulation of Gogo levels after the mid-pupal stage. After Gogo down-regulation, R8 axons target to their proper target layer within the correct medulla column. Medulla column are indicated by dashed lines. In **gogo (lof)** axons are not able to sense the positive cue at the intermediate layer. Axons stray and prematurely extend into deeper medulla layers without showing columnar or M3 layer restriction. In **gogo (gof)** R8 protein levels are not down-regulated. R axons become permanently anchored at the M1 layer.

The R8 mutant phenotype suggests that the proper interaction with the temporary targets is lost. However, the position maintenance seems to be absolutely required to allow proper entry of R8 axons into medulla columns. The observed straying of mutant R8s along the medulla surface in adult flies clearly supports this idea (chapter 3.11). In addition, it was observed during pupal development that several R8 axons fail to maintain their position at their intermediate target layer until their proper extension time point at 50APF (chapter 3.13). Structural differences of prematurely extending mutant axons, which lack bulb-like structures shown by WT axons at the

M1 layer, in deed indicate that these axons have completely lost contact to their temporary targets. Premature extensions during pupal development were not restricted to invade the deeper medulla, but also extended along the medulla surface (chapter 3.12). Therefore, the loss of temporary target layer interaction during pupal development is very likely the cause for the observed straying phenotype in adult flies.

Mutant axons that prematurely extend into deeper medulla layers do not oblige columnar nor target layer restriction. Their thickened terminals clearly contrast the highly coordinated WT R8 outgrowth to the M3 layer, which is initiated by the extension of thin filopodia (Figure 4-2).

Considering the fact that the medulla undergoes dramatic developmental changes from the time R8 axons arrive at their intermediate targets until the time point they finally start extending to their final targets, the chaotic behavior of premature R8 axons does not come as a surprise. Each mature medulla column is the result of the sequential in-growth of at least 50-60 different neurons processes arranged in defined layers (Fischbach and Dittrich, 1989). The extension of R8 axons to their final targets has to be exactly timed to the maturation of the medulla neuropil and its target layer. It was shown that stereotyped and dynamic interplay between different axons during medulla development are involved in forming these precise patterns (Nern et al., 2008; Ting et al., 2005). A recent study suggests that the precise packing of axon terminals in the medulla is neither a consequence of targeting to pre-existing layers nor an exact sequence of afferent interactions (Nern et al., 2008). Instead it was suggested that layer-specific connectivity emerges through the coordinated execution of multiple neuron-specific targeting programs, which also depend on each other.

Interestingly, the photoreceptor cells themselves seem to play an active role in shaping their target environment. A recent study proposed that R cell axons release Jelly belly (Jeb) to activate Anaplastic lymphoma kinase (Alk) signaling in the brain, probably their target neurons (Bazigou et al., 2007). These anterograde signaling events are then supposed to regulate late events of R8 axon-target maturation, as loss of Jeb/Alk signaling affects the expression of guidance molecules in the R8 recipient layer M3. Interestingly, one of the altered molecules within the M3 layer is Fmi. In addition, loss of *fmi* in the target region causes R8 targeting effects, similar to *fmi ey*FLP but also to *gogo ey*FLP flies. This indicates that anterograde signaling coordinates the timing of R8 cell growth cone extension with local expression of cell-adhesion molecules in the M3 layer which are required for R8 axon targeting.

As the maturation of the R8 target layer seems to be concerted to photoreceptor development, it would be very interesting to investigate the importance of proper temporary target layer interaction in this context. Up to date, there is not much known, neither about the function of intermediate R8 targeting nor about the process of intermediate target layer recognition. However, the identification of the *gogo* gene, which is required in the process, now allows performing further experiments to approach these open questions.
For example, a possible connection between temporary target layer interaction and M3 target layer maturation could be easily tested in *gogo ey*FLP flies by investigating Fmi expression in the brain. In the same way, the effect of Gogo OE in R axons on the Fmi expression within the M3 layer could be analyzed. In the Gogo OE situation, R8 axons correctly target their temporary layer, but than fail to extend to the M3 layer. The formation of a mature M3 layer in this context would suggest that in deed Gogo has to be removed to allow axon extension from the M1, whereas the lack of a mature M3 layer would imply that the removal of Gogo could be correlated to anterograde Jeb/Alk signaling initiation in R8 axons.

Another interesting observation is the fact that mutant R8s transiently stop at the M1 layer during early pupal development. R7 axons, which arrive later, manage to overtake and separate into a layer distinct from R8s which have arrived and stopped in the medulla several hours before. The two distinct layers which can be observed at 17APF (chapter 3.13) highly suggest that the quality of the intermediate target layer itself or of the environment changes after 17APF allowing mutant axons to be released from their stopping position and to proceed extending. These supposed changes raise the question if Gogo could be actively or indirectly involved in shaping the mid-pupal temporary target layer or allowing proper connection to the M1 layer after 17APF.
In this context, R8 axons mutant for *caps* show a striking similar phenotype compared to *gogo*$^{-}$ flies (Shinza-Kameda et al., 2006). In *caps* mutant flies, R8 axons initially manage to stop at the M1 layer during early pupal development, however, during mid-pupal development gaps emerge within the M1 layer, suggesting the detachment and premature extension of R8 axons from the M1 layer. Unfortunately, the behaviour of R8 axons was not sufficiently investigated in the study by using R8-specific markers. Interestingly, in the Caps OE situation, some R7 axons, which have successfully separated from R8s and reached their temporary target layer in early pupae, then started retracting to the R8 temporary layer M1 during mid-pupal stages. The Caps OE phenotype clearly contrasts the Gogo OE, where R7 remain

completely unaffected despite the increased Gogo levels. These results highly suggest that only the combination of Gogo and Caps allows the continuous interaction of R8 axons at the M1 layer after 17APF, but both are not required for the initial recognition. Caps overexpressing R7 axons, which endogenously express Gogo at the same time, then retract to the R8 temporary target layer M1. Two experiments could reveal if Gogo and Caps are both required in R8 axons for maintaining the growth cones at the M1 layer: First, Caps OE in a *gogo ey*FLP mutant background should abolish the retraction of R7 axons to the M1 layer, and second, co-overexpression of Caps and Gogo should increase the number of R7 axons retracting to the R8 temporary layer M1. The retargeting of R7 axons to the R8 temporary layer is intriguingly fascinating for a second reason, as in the Caps OE situation several R7 axons then seem to behave like R8s during the final targeting step and terminate in M3 (Shinza-Kameda et al., 2006). This implies also a possible role of intermediate targeting also in defining final target connections. In this sense, the co-overexpression of Caps and Gogo could also result in permanent anchoring of R7s at the M1 layer.

What are the possible candidate cells serving as temporal targets of R8 axons during pupal development? It is known that the processes of lamina neurons L1-L5 innervate along the R7 and R8 axons and sequentially enter the corresponding medulla columns in early pupal stages (Ting et al., 2005). However, by expressing the dominant negative form of EGFR in lamina neurons, in which the differentiation of L1-L5 is blocked, R8 and R7 still appear to show normal axonal projection at mid-pupal stage (Ting et al., 2005). Nevertheless it is important to note that the corresponding study has not used R8-specific markers in order to properly dissect R8 axonal behavior. Recently, it has been reported that the abnormality in axonal tiling of L1-5 in *Dscam2* mutants caused the pathfinding defects of R7/8 axons (Millard et al., 2007). It is possible that the abnormally guided processes of L1-5 result in a different outcome than the simple loss of L1-5. Other possible candidates are the medulla neurons, which send their processes into the columnar structure of the M1-M6 layers in the outer medulla. Since the mechanism of differentiation and development of these neurons and their processes is largely unknown, it will be intriguing to explore the role of Gogo in possible interactions between R axons and lamina/medulla neuron processes and the contribution of known regulators of R axon guidance in this process. Especially the role of broadly expressed Cadherins in these specific connections would be of great interest.

4.4 Possible genetical interaction with the cadherin Flamingo

Our results define two distinct and specific functions for Gogo in R axon targeting. First, it facilitates competitive or inhibitory interactions between adjacent R8 growth cones and second, it promotes R8 axon-target interactions. In order to allow these completely different functions, it is very likely that Gogo genetically interacts with other cell surface molecules, thereby allowing selective interactions first among R axons and second with target cells. One promising candidate for such an interaction is the protocadherin superfamily member, Fmi. Evidence in support of this idea comes from the similarity of their visual system phenotypes and their expression patterns (Lee et al., 2003; Senti et al., 2003).

The similarity in the expression pattern is striking. Both Gogo and Fmi are expressed in all R neuronal types. In 3rd instar larvae both proteins show the strongest expression along axons of newly developed (young) axons in the optic stalk and optic lobe (Figure 3-5 and data not shown) (Lee et al., 2003). In addition, both proteins are expressed in R1-6 axons during cartridge formation in mid-pupal stages (Figure 3-7) (Lee et al., 2003). One of the differences in the expression pattern is the strong Fmi expression in lamina neurons and medulla cortical neurons. These stainings strongly overlap with the target layers of R8 and R7s in larval and pupal stages (Lee et al., 2003; Senti et al., 2003), while Gogo expression is hardly detectable in the proximal lamina and medulla (Figure 3-7).

Both *gogo* and *fmi* mutants show loss of repulsive interaction between adjacent R8s, resulting in a bundling of R8 axons in the larval stage. It is noteworthy that Fmi does not serve as an ordinary adhesion molecule in this context. In addition, *fmi* mutants display a very similar R1-R6 missorting phenotype during lamina cartridge formation (Lee et al., 2003). Recently it was shown that individual R1-R6 growth cones are sensitive to differences in Fmi activity through opposing interactions between neighboring cells and require these interactions to be balanced in order to extend along the appropriate trajectory during lamina cartridge formation (Chen and Clandinin, 2008). These results make it very likely that Fmi levels have to be highly regulated within the growth cone of R1-R6 axons. But most important, in *fmi* mutants R8s also stop at the superficial layer of the medulla (Senti et al., 2003). Further investigations of the fmi mutant phenotype could reveal additional similarities. Especially the *fmi* mutant phenotype during pupal development has not been

investigated yet. Fmi's role in homophilic axon-target interaction and the possible involvement of Gogo in this process is particularly interesting, as Fmi is expressed within several medulla layers in the brain. Most important, Fmi expression has been shown to be required in the M3 layer for proper R8 target layer recognition (Bazigou et al., 2007).
Genetical epistasis and overexpression experiments could clarify if the two molecules are acting within the same pathway or hint towards a possible regulation of Fmi by Gogo. Especially the latter would be of great interest, as it provides new insights in the regulation of specific interactions by using broadly expressed homophilic adhesion molecules.

In addition to its role in axon guidance, Flamingo was shown to control dendritic morphogenesis in the *Drosophila* embryonic peripheral nervous system (PNS). Due to the implied genetical interaction with *gogo* in photoreceptor axon guidance, it would be also interesting to have a closer look at the dendritic development of the PNS in a *gogo* mutant background. In general, the similarities and differences to the regulation of axon guidance in R axons might facilitate the understanding of the basic molecular specificity underlying neuronal connections.

4.5 Outlook

Both axon-axon and axon-target interactions have been demonstrated to play critical roles in the formation of visual and olfactory circuits in flies and mammals (Brown et al., 2000; Lattemann et al., 2007; Lee et al., 2001; Lee et al., 2003; Maurel-Zaffran et al., 2001; Prakash et al., 2005; Senti et al., 2003; Shinza-Kameda et al., 2006; Sweeney et al., 2007; Yamagata et al., 2002). However, the underlying molecular mechanisms have not been sufficiently elucidated.

Gogo is required for axon-axon and axon-target interaction in the fly visual system. Its conserved extracellular domain and cytoplasmic motif indicate an evolutionary conserved role in cell-cell communication. The obtained results provide a strong argument that Gogo could act as a novel receptor involved in heterotypic interaction with an as yet unidentified ligand. Thus, it will be important to identify the relevant Gogo ligand. Strong and specific axon pathfinding defects in both *gogo* LOF mutants and GOF transgenic flies make the *Drosophila* visual system an ideal model to search for a functionally relevant and probably conserved ligand for Gogo proteins.
However, it is also possible that Gogo does not act as classical axon guidance receptor. For example, Gogo could act as a co-receptor, which is not directly binding to ligands. In addition, one could imagine that Gogo could regulate the membrane localization of other guidance receptors or cell adhesion molecules.

In order to show that Gogo has a classic axon guidance receptor function, another important task for the future will be to elucidate the intracellular molecular mechanisms by which Gogo regulates R axon pathfinding. However, the hints to date have been limited. The cytoplasmic domain of homologues found in various species appears to have neither obvious catalytic domains or signaling modules, nor an overall conservation among species in its primary structure. However, a short cytoplasmic motif, shared by GOGO domain orthologues (Figure S4B), may serve as a protein interaction domain that binds to a conserved interaction partner. Rescue experiments using cytoplasmic deletion constructs or applying site-directed mutagenesis to the conserved tri-peptide can possibly give insights in its functional importance and the underlying intracellular mechanism. The identification of intracellular binding partners will shed light on the signaling pathway downstream of Gogo and its conservation in other species.

The mammalian homologue Tmtsp is the best characterized molecule of the Gogo family so far. It is expressed in endothelial cells and hematopoietic stem cells and the level of expression gradually declines as the cells differentiate. However, no obvious neuronal expression was reported (Takayanagi et al., 2006). Although Tmtsp may not have a functional role in axonal pathfinding in vertebrates, it might have the underlying molecular machinery analogous to *Drosophila* Gogo in the context of cell-cell communication. Therefore, elucidating exactly how Gogo regulates R axon pathfinding in *Drosophila* may also shed light on the function of *gogo* homologues in other species.

Bibliography

Adams, J.C., and Tucker, R.P. (2000). The thrombospondin type 1 repeat (TSR) superfamily: diverse proteins with related roles in neuronal development. Dev Dyn *218*, 280-299.

Altschul, S.F., and Koonin, E.V. (1998). Iterated profile searches with PSI-BLAST--a tool for discovery in protein databases. Trends Biochem Sci *23*, 444-447.

Bailey, T.L., and Gribskov, M. (1998). Methods and statistics for combining motif match scores. J Comput Biol *5*, 211-221.

Barbacid, M. (1995). Neurotrophic factors and their receptors. Curr Opin Cell Biol *7*, 148-155.

Bashaw, G.J., Kidd, T., Murray, D., Pawson, T., and Goodman, C.S. (2000). Repulsive axon guidance: Abelson and Enabled play opposing roles downstream of the roundabout receptor. Cell *101*, 703-715.

Bazigou, E., Apitz, H., Johansson, J., Loren, C.E., Hirst, E.M., Chen, P.L., Palmer, R.H., and Salecker, I. (2007). Anterograde Jelly belly and Alk receptor tyrosine kinase signaling mediates retinal axon targeting in Drosophila. Cell *128*, 961-975.

Berger, J., Senti, K., Senti, G., Newsome, T.P., Asling, B., Dickson, B.J., and Suzuki, T. (2008). Systematic Identification of Genes that Regulate Neuronal Wiring in the Drosophila Visual System PLOS Genetics *4*.

Bork, P., and Beckmann, G. (1993). The CUB domain. A widespread module in developmentally regulated proteins. J Mol Biol *231*, 539-545.

Brand, A.H., and Perrimon, N. (1993). Targeted gene expression as a means of altering cell fates and generating dominant phenotypes. Development *118*, 401-415.

Brown, A., Yates, P.A., Burrola, P., Ortuno, D., Vaidya, A., Jessell, T.M., Pfaff, S.L., O'Leary, D.D., and Lemke, G. (2000). Topographic mapping from the retina to the midbrain is controlled by relative but not absolute levels of EphA receptor signaling. Cell *102*, 77-88.

Brunet, I., Weinl, C., Piper, M., Trembleau, A., Volovitch, M., Harris, W., Prochiantz, A., and Holt, C. (2005). The transcription factor Engrailed-2 guides retinal axons. Nature *438*, 94-98.

Bryson, K., McGuffin, L.J., Marsden, R.L., Ward, J.J., Sodhi, J.S., and Jones, D.T. (2005). Protein structure prediction servers at University College London. Nucleic Acids Res *33*, W36-38.

Callahan, C.A., Muralidhar, M.G., Lundgren, S.E., Scully, A.L., and Thomas, J.B. (1995). Control of neuronal pathway selection by a Drosophila receptor protein-tyrosine kinase family member. Nature *376*, 171-174.

Campos-Ortega, J.A., and Hartenstein, V. (1997). The Embryonic Development of Drosophila
melanogaster. (Berlin and New York: Springer-Verlag).

Chan, S.S., Zheng, H., Su, M.W., Wilk, R., Killeen, M.T., Hedgecock, E.M., and Culotti, J.G. (1996). UNC-40, a C. elegans homolog of DCC (Deleted in Colorectal Cancer), is required in motile cells responding to UNC-6 netrin cues. Cell *87*, 187-195.

Chen, P.L., and Clandinin, T.R. (2008). The cadherin Flamingo mediates level-dependent interactions that guide photoreceptor target choice in Drosophila. Neuron *58*, 26-33.

Clandinin, T.R., Lee, C.H., Herman, T., Lee, R.C., Yang, A.Y., Ovasapyan, S., and Zipursky, S.L. (2001). Drosophila LAR regulates R1-R6 and R7 target specificity in the visual system. Neuron *32*, 237-248.

Clandinin, T.R., and Zipursky, S.L. (2002). Making connections in the fly visual system. Neuron *35*, 827-841.

Dearborn, R., Jr., He, Q., Kunes, S., and Dai, Y. (2002). Eph receptor tyrosine kinase-mediated formation of a topographic map in the Drosophila visual system. J Neurosci *22*, 1338-1349.

Dearborn, R., Jr., and Kunes, S. (2004). An axon scaffold induced by retinal axons directs glia to destinations in the Drosophila optic lobe. Development *131*, 2291-2303.

Dehal, P., Satou, Y., Campbell, R.K., Chapman, J., Degnan, B., De Tomaso, A., Davidson, B., Di Gregorio, A., Gelpke, M., Goodstein, D.M.*, et al.* (2002). The draft genome of Ciona intestinalis: insights into chordate and vertebrate origins. Science *298*, 2157-2167.

Desai, C.J., Gindhart, J.G., Jr., Goldstein, L.S., and Zinn, K. (1996). Receptor tyrosine phosphatases are required for motor axon guidance in the Drosophila embryo. Cell *84*, 599-609.

Dickson, B.J. (2002). Molecular mechanisms of axon guidance. Science *298*, 1959-1964.

Do, C.B., Mahabhashyam, M.S., Brudno, M., and Batzoglou, S. (2005). ProbCons: Probabilistic consistency-based multiple sequence alignment. Genome Res *15*, 330-340.

Eddy, S.R. (1998). Profile hidden Markov models. Bioinformatics *14*, 755-763.

Fabian-Fine, R., Verstreken, P., Hiesinger, P.R., Horne, J.A., Kostyleva, R., Zhou, Y., Bellen, H.J., and Meinertzhagen, I.A. (2003). Endophilin promotes a late step in endocytosis at glial invaginations in Drosophila photoreceptor terminals. J Neurosci *23*, 10732-10744.

Fan, X., Labrador, J.P., Hing, H., and Bashaw, G.J. (2003). Slit stimulation recruits Dock and Pak to the roundabout receptor and increases Rac activity to regulate axon repulsion at the CNS midline. Neuron *40*, 113-127.

Fannon, A.M., and Colman, D.R. (1996). A model for central synaptic junctional complex formation based on the differential adhesive specificities of the cadherins. Neuron *17*, 423-434.

Feldheim, D.A., Nakamoto, M., Osterfield, M., Gale, N.W., DeChiara, T.M., Rohatgi, R., Yancopoulos, G.D., and Flanagan, J.G. (2004). Loss-of-function analysis of EphA receptors in retinotectal mapping. J Neurosci *24*, 2542-2550.

Fischbach, K.F. (1983). Neural cell types surviving congenital sensory deprivation in the optic lobes of Drosophila melanogaster. Dev Biol *95*, 1-18.

Fischbach, K.F., and Dittrich, A.P.M. (1989). The optic lobe of Drosophila melanogaster. I. A Golgi analysis of wild-type structure. Cell Tissue Res. *258*, 441-475.

Fischbach, K.F., and Technau, G. (1984). Cell degeneration in the developing optic lobes of the sine oculis and small-optic-lobes mutants of Drosophila melanogaster. Dev Biol *104*, 219-239.

Fortini, M.E., and Rubin, G.M. (1990). Analysis of cis-acting requirements of the Rh3 and Rh4 genes reveals a bipartite organization to rhodopsin promoters in Drosophila melanogaster. Genes Dev *4*, 444-463.

Freeman, M. (1996). Reiterative use of the EGF receptor triggers differentiation of all cell types in the Drosophila eye. Cell *87*, 651-660.

Garrity, P.A., Lee, C.H., Salecker, I., Robertson, H.C., Desai, C.J., Zinn, K., and Zipursky, S.L. (1999). Retinal axon target selection in Drosophila is regulated by a receptor protein tyrosine phosphatase. Neuron *22*, 707-717.

Golic, K.G. (1991). Site-specific recombination between homologous chromosomes in Drosophila. Science *252*, 958-961.

Goodman, C.S. (1994). The likeness of being: phylogenetically conserved molecular mechanisms of growth cone guidance. Cell *78*, 353-356.

Halder, G., Callaerts, P., and Gehring, W.J. (1995). Induction of ectopic eyes by targeted expression of the eyeless gene in Drosophila. Science *267*, 1788-1792.

Hauck, B., Gehring, W.J., and Walldorf, U. (1999). Functional analysis of an eye specific enhancer of the eyeless gene in Drosophila. Proc Natl Acad Sci U S A *96*, 564-569.

Hay, B.A., Wolff, T., and Rubin, G.M. (1994). Expression of baculovirus P35 prevents cell death in Drosophila. Development *120*, 2121-2129.

He, Z., and Tessier-Lavigne, M. (1997). Neuropilin is a receptor for the axonal chemorepellent Semaphorin III. Cell *90*, 739-751.

Hedgecock, E.M., Culotti, J.G., and Hall, D.H. (1990). The unc-5, unc-6, and unc-40 genes guide circumferential migrations of pioneer axons and mesodermal cells on the epidermis in C. elegans. Neuron *4*, 61-85.

Hiesinger, P.R., Zhai, R.G., Zhou, Y., Koh, T.W., Mehta, S.Q., Schulze, K.L., Cao, Y., Verstreken, P., Clandinin, T.R., Fischbach, K.F.*, et al.* (2006). Activity-independent prespecification of synaptic partners in the visual map of Drosophila. Curr Biol *16*, 1835-1843.

Hu, H., Li, M., Labrador, J.P., McEwen, J., Lai, E.C., Goodman, C.S., and Bashaw, G.J. (2005). Cross GTPase-activating protein (CrossGAP)/Vilse links the Roundabout receptor to Rac to regulate midline repulsion. Proc Natl Acad Sci U S A *102*, 4613-4618.

Huang, Z., and Kunes, S. (1996). Hedgehog, transmitted along retinal axons, triggers neurogenesis in the developing visual centers of the Drosophila brain. Cell *86*, 411-422.

Huang, Z., Shilo, B.Z., and Kunes, S. (1998). A retinal axon fascicle uses spitz, an EGF receptor ligand, to construct a synaptic cartridge in the brain of Drosophila. Cell *95*, 693-703.

Imai, T., Suzuki, M., and Sakano, H. (2006). Odorant receptor-derived cAMP signals direct axonal targeting. Science *314*, 657-661.

Jarman, A.P., and Ahmed, I. (1998). The specificity of proneural genes in determining Drosophila sense organ identity. Mech Dev *76*, 117-125.

Jarman, A.P., Grell, E.H., Ackerman, L., Jan, L.Y., and Jan, Y.N. (1994). Atonal is the proneural gene for Drosophila photoreceptors. Nature *369*, 398-400.

Jeanmougin, F., Thompson, J.D., Gouy, M., Higgins, D.G., and Gibson, T.J. (1998). Multiple sequence alignment with Clustal X. Trends Biochem Sci *23*, 403-405.

Karasawa, S., Araki, T., Nagai, T., Mizuno, H., and Miyawaki, A. (2004). Cyan-emitting and orange-emitting fluorescent proteins as a donor/acceptor pair for fluorescence resonance energy transfer. Biochem J *381*, 307-312.

Keino-Masu, K., Masu, M., Hinck, L., Leonardo, E.D., Chan, S.S., Culotti, J.G., and Tessier-Lavigne, M. (1996). Deleted in Colorectal Cancer (DCC) encodes a netrin receptor. Cell *87*, 175-185.

Kidd, T., Brose, K., Mitchell, K.J., Fetter, R.D., Tessier-Lavigne, M., Goodman, C.S., and Tear, G. (1998). Roundabout controls axon crossing of the CNS midline and defines a novel subfamily of evolutionarily conserved guidance receptors. Cell *92*, 205-215.

Kolodziej, P.A., Timpe, L.C., Mitchell, K.J., Fried, S.R., Goodman, C.S., Jan, L.Y., and Jan, Y.N. (1996). frazzled encodes a Drosophila member of the DCC immunoglobulin subfamily and is required for CNS and motor axon guidance. Cell *87*, 197-204.

Kruger, R.P., Aurandt, J., and Guan, K.L. (2005). Semaphorins command cells to move. Nat Rev Mol Cell Biol *6*, 789-800.

Kunes, S., Wilson, C., and Steller, H. (1993). Independent guidance of retinal axons in the developing visual system of Drosophila. J Neurosci *13*, 752-767.

Labrador, J.P., Brambilla, R., and Klein, R. (1997). The N-terminal globular domain of Eph receptors is sufficient for ligand binding and receptor signaling. EMBO J *16*, 3889-3897.

Lattemann, M., Zierau, A., Schulte, C., Seidl, S., Kuhlmann, B., and Hummel, T. (2007). Semaphorin-1a controls receptor neuron-specific axonal convergence in the primary olfactory center of Drosophila. Neuron *53*, 169-184.

Lee, C.H., Herman, T., Clandinin, T.R., Lee, R., and Zipursky, S.L. (2001). N-cadherin regulates target specificity in the Drosophila visual system. Neuron *30*, 437-450.

Lee, R.C., Clandinin, T.R., Lee, C.H., Chen, P.L., Meinertzhagen, I.A., and Zipursky, S.L. (2003). The protocadherin Flamingo is required for axon target selection in the Drosophila visual system. Nat Neurosci *6*, 557-563.

Lee, T., and Luo, L. (1999). Mosaic analysis with a repressible cell marker for studies of gene function in neuronal morphogenesis. Neuron *22*, 451-461.

Leung-Hagesteijn, C., Spence, A.M., Stern, B.D., Zhou, Y., Su, M.W., Hedgecock, E.M., and Culotti, J.G. (1992). UNC-5, a transmembrane protein with immunoglobulin and thrombospondin type 1 domains, guides cell and pioneer axon migrations in C. elegans. Cell *71*, 289-299.

Lundstrom, A., Gallio, M., Englund, C., Steneberg, P., Hemphala, J., Aspenstrom, P., Keleman, K., Falileeva, L., Dickson, B.J., and Samakovlis, C. (2004). Vilse, a conserved Rac/Cdc42 GAP mediating Robo repulsion in tracheal cells and axons. Genes Dev *18*, 2161-2171.

Maniatis, T. (1986). Molecular cloning. A laboratory manual. (ed. New York: Cold Spring Harbor).

Martin, K.A., Poeck, B., Roth, H., Ebens, A.J., Ballard, L.C., and Zipursky, S.L. (1995). Mutations disrupting neuronal connectivity in the Drosophila visual system. Neuron *14*, 229-240.

Matthews, B.J., Kim, M.E., Flanagan, J.J., Hattori, D., Clemens, J.C., Zipursky, S.L., and Grueber, W.B. (2007). Dendrite self-avoidance is controlled by Dscam. Cell *129*, 593-604.

Maurel-Zaffran, C., Suzuki, T., Gahmon, G., Treisman, J.E., and Dickson, B.J. (2001). Cell-autonomous and -nonautonomous functions of LAR in R7 photoreceptor axon targeting. Neuron *32*, 225-235.

McFarlane, S., McNeill, L., and Holt, C.E. (1995). FGF signaling and target recognition in the developing Xenopus visual system. Neuron *15*, 1017-1028.

McLaughlin, T., and O'Leary, D.D. (2005). Molecular gradients and development of retinotopic maps. Annu Rev Neurosci *28*, 327-355.

Meinertzhagen, I.A., and Hanson, T.E. (1993). The Development of the Optic Lobe. In The Development of Drosophila melanogaster, M. Bate, and A. Martinez-Arias, eds. (Cold Spring Harbor: Cold Spring Harbor Laboratory Press), pp. 1363-1491.

Meinertzhagen, I.A., and O'Neil, S.D. (1991). Synaptic organization of columnar elements in the lamina of the wild type in Drosophila melanogaster. J Comp Neurol *305*, 232-263.

Meyerowitz, E.M., and Kankel, D.R. (1978). A genetic analysis of visual system development in Drosophilia melanogaster. Dev Biol *62*, 112-142.

Millard, S.S., Flanagan, J.J., Pappu, K.S., Wu, W., and Zipursky, S.L. (2007). Dscam2 mediates axonal tiling in the Drosophila visual system. Nature *447*, 720-724.

Mismer, D., and Rubin, G.M. (1987). Analysis of the promoter of the ninaE opsin gene in Drosophila melanogaster. Genetics *116*, 565-578.

Mitchell, K.J., Doyle, J.L., Serafini, T., Kennedy, T.E., Tessier-Lavigne, M., Goodman, C.S., and Dickson, B.J. (1996). Genetic analysis of Netrin genes in Drosophila: Netrins guide CNS commissural axons and peripheral motor axons. Neuron *17*, 203-215.

Miyatani, S., Shimamura, K., Hatta, M., Nagafuchi, A., Nose, A., Matsunaga, M., Hatta, K., and Takeichi, M. (1989). Neural cadherin: role in selective cell-cell adhesion. Science *245*, 631-635.

Morata, G., and Ripoll, P. (1975). Minutes: mutants of drosophila autonomously affecting cell division rate. Dev Biol *42*, 211-221.

Moses, K. (2002). Drosophila Eye Development. Springer Verlag Berlin Heidelberg *37*.

Moses, K., and Rubin, G.M. (1991). Glass encodes a site-specific DNA-binding protein that is regulated in response to positional signals in the developing Drosophila eye. Genes Dev *5*, 583-593.

Nern, A., Zhu, Y., and Zipursky, S.L. (2008). Local N-cadherin interactions mediate distinct steps in the targeting of lamina neurons. Neuron *58*, 34-41.

Newsome, T.P., Asling, B., and Dickson, B.J. (2000). Analysis of Drosophila photoreceptor axon guidance in eye-specific mosaics. Development *127*, 851-860.

Nicholas, K.B., and Jr., N.H.B. (1997). GeneDoc: Analysis and Visualization of Genetic Variation. http://www.cris.com/~Ketchup/genedoc.shtml.

Papatsenko, D., Nazina, A., and Desplan, C. (2001). A conserved regulatory element present in all Drosophila rhodopsin genes mediates Pax6 functions and participates in the fine-tuning of cell-specific expression. Mech Dev *101*, 143-153.

Poeck, B., Fischer, S., Gunning, D., Zipursky, S.L., and Salecker, I. (2001). Glial cells mediate target layer selection of retinal axons in the developing visual system of Drosophila. Neuron *29*, 99-113.

Prakash, S., Caldwell, J.C., Eberl, D.F., and Clandinin, T.R. (2005). Drosophila N-cadherin mediates an attractive interaction between photoreceptor axons and their targets. Nat Neurosci *8*, 443-450.

Raper, J.A. (2000). Semaphorins and their receptors in vertebrates and invertebrates. Curr Opin Neurobiol *10*, 88-94.

Ready, D.F., Hanson, T.E., and Benzer, S. (1976). Development of the Drosophila retina, a neurocrystalline lattice. Dev Biol *53*, 217-240.

Reber, M., Burrola, P., and Lemke, G. (2004). A relative signalling model for the formation of a topographic neural map. Nature *431*, 847-853.

Rutishauser, U. (1993). Adhesion molecules of the nervous system. Curr Opin Neurobiol *3*, 709-715.

Sato, M., Umetsu, D., Murakami, S., Yasugi, T., and Tabata, T. (2006). DWnt4 regulates the dorsoventral specificity of retinal projections in the Drosophila melanogaster visual system. Nat Neurosci *9*, 67-75.

Schmitt, A.M., Shi, J., Wolf, A.M., Lu, C.C., King, L.A., and Zou, Y. (2006). Wnt-Ryk signalling mediates medial-lateral retinotectal topographic mapping. Nature *439*, 31-37.

Schneider, I. (1972). Cell lines derived from late embryonic stages of Drosophila melanogaster. J Embryol Exp Morphol *27*, 353-365.

Schnorrer, F., and Dickson, B.J. (2004). Axon guidance: morphogens show the way. Curr Biol *14*, R19-21.

Selleck, S.B., Gonzalez, C., Glover, D.M., and White, K. (1992). Regulation of the G1-S transition in postembryonic neuronal precursors by axon ingrowth. Nature *355*, 253-255.

Senti, K.A., Usui, T., Boucke, K., Greber, U., Uemura, T., and Dickson, B.J. (2003). Flamingo regulates R8 axon-axon and axon-target interactions in the Drosophila visual system. Curr Biol *13*, 828-832.

Serafini, T., Kennedy, T.E., Galko, M.J., Mirzayan, C., Jessell, T.M., and Tessier-Lavigne, M. (1994). The netrins define a family of axon outgrowth-promoting proteins homologous to C. elegans UNC-6. Cell *78*, 409-424.

Shinza-Kameda, M., Takasu, E., Sakurai, K., Hayashi, S., and Nose, A. (2006). Regulation of layer-specific targeting by reciprocal expression of a cell adhesion molecule, capricious. Neuron *49*, 205-213.

Sodergren, E., Weinstock, G.M., Davidson, E.H., Cameron, R.A., Gibbs, R.A., Angerer, R.C., Angerer, L.M., Arnone, M.I., Burgess, D.R., Burke, R.D.*, et al.* (2006). The genome of the sea urchin Strongylocentrotus purpuratus. Science *314*, 941-952.

Steller, H., Fischbach, K.F., and Rubin, G.M. (1987). Disconnected: a locus required for neuronal pathway formation in the visual system of Drosophila. Cell *50*, 1139-1153.

Sweeney, L.B., Couto, A., Chou, Y.H., Berdnik, D., Dickson, B.J., Luo, L., and Komiyama, T. (2007). Temporal target restriction of olfactory receptor neurons by Semaphorin-1a/PlexinA-mediated axon-axon interactions. Neuron *53*, 185-200.

Takagi, S., Hirata, T., Agata, K., Mochii, M., Eguchi, G., and Fujisawa, H. (1991). The A5 antigen, a candidate for the neuronal recognition molecule, has homologies to complement components and coagulation factors. Neuron *7*, 295-307.

Takayanagi, S., Hiroyama, T., Yamazaki, S., Nakajima, T., Morita, Y., Usui, J., Eto, K., Motohashi, T., Shiomi, K., Keino-Masu, K.*, et al.* (2006). Genetic marking of

hematopoietic stem and endothelial cells: identification of the Tmtsp gene encoding a novel cell surface protein with the thrombospondin-1 domain. Blood *107*, 4317-4325.

Tessier-Lavigne, M. (1995). Eph receptor tyrosine kinases, axon repulsion, and the development of topographic maps. Cell *82*, 345-348.

Tessier-Lavigne, M., and Goodman, C.S. (1996). The molecular biology of axon guidance. Science *274*, 1123-1133.

Ting, C.Y., and Lee, C.H. (2007). Visual circuit development in Drosophila. Curr Opin Neurobiol *17*, 65-72.

Ting, C.Y., Yonekura, S., Chung, P., Hsu, S.N., Robertson, H.M., Chiba, A., and Lee, C.H. (2005). Drosophila N-cadherin functions in the first stage of the two-stage layer-selection process of R7 photoreceptor afferents. Development *132*, 953-963.

Usui, T., Shima, Y., Shimada, Y., Hirano, S., Burgess, R.W., Schwarz, T.L., Takeichi, M., and Uemura, T. (1999). Flamingo, a seven-pass transmembrane cadherin, regulates planar cell polarity under the control of Frizzled. Cell *98*, 585-595.

White, K., and Kankel, D.R. (1978). Patterns of cell division and cell movement in the formation of the imaginal nervous system in Drosophila melanogaster. Dev Biol *65*, 296-321.

White, N.M., and Jarman, A.P. (2000). Drosophila atonal controls photoreceptor R8-specific properties and modulates both receptor tyrosine kinase and Hedgehog signalling. Development *127*, 1681-1689.

Wojtowicz, W.M., Flanagan, J.J., Millard, S.S., Zipursky, S.L., and Clemens, J.C. (2004). Alternative splicing of Drosophila Dscam generates axon guidance receptors that exhibit isoform-specific homophilic binding. Cell *118*, 619-633.

Wong, K., Ren, X.R., Huang, Y.Z., Xie, Y., Liu, G., Saito, H., Tang, H., Wen, L., Brady-Kalnay, S.M., Mei, L.*, et al.* (2001). Signal transduction in neuronal migration: roles of GTPase activating proteins and the small GTPase Cdc42 in the Slit-Robo pathway. Cell *107*, 209-221.

Xu, T., and Rubin, G.M. (1993). Analysis of genetic mosaics in developing and adult Drosophila tissues. Development *117*, 1223-1237.

Yagi, T., and Takeichi, M. (2000). Cadherin superfamily genes: functions, genomic organization, and neurologic diversity. Genes Dev *14*, 1169-1180.

Yamagata, M., Weiner, J.A., and Sanes, J.R. (2002). Sidekicks: synaptic adhesion molecules that promote lamina-specific connectivity in the retina. Cell *110*, 649-660.

Yonekura, S., Xu, L., Ting, C.Y., and Lee, C.H. (2007). Adhesive but not signaling activity of Drosophila N-cadherin is essential for target selection of photoreceptor afferents. Dev Biol *304*, 759-770.

Zhu, H., Hummel, T., Clemens, J.C., Berdnik, D., Zipursky, S.L., and Luo, L. (2006). Dendritic patterning by Dscam and synaptic partner matching in the Drosophila antennal lobe. Nat Neurosci *9*, 349-355.

Zou, Y., and Lyuksyutova, A.I. (2007). Morphogens as conserved axon guidance cues. Curr Opin Neurobiol *17*, 22-28.

Acknowledgements

First of all, I want to thank my supervisor Takashi Suzuki. Thank you, for the great opportunity to do my PhD in your lab on such an interesting project, for your support, guidance, encouragement and the training especially at the beginning of my work. Thanks for your immediate help that was provided whenever needed. I also enjoyed it a lot to communicate my work on the conferences you enabled me to visit.

I am also very grateful to Rüdiger Klein and Iris Salecker, the members of my thesis committee, for their excellent advice that helped us shaping the project. Especially, I would like to thank Rüdiger for being my official Doktorvater.

For their contributions to the project, I would like to thank Satoko Suzuki for experiments and smart ideas, Stephan Ohler for providing me with transgenic fly lines and destination vectors, Alexander Schleiffer for the bioinformatics and Marianne Braun for the electron microscopy. Thanks to I. Salecker, J. Urban, H. Bellen and T. Uemura for sharing flies and reagents.

A big thank you goes to Harald Witte for his critical comments on my thesis. Your corrections were great! Thanks to Miriam Mann, for her generous support during the time I was injured with my knee. I would have been lost without your help.

I want to thank all members of the lab for their personal and scientific support. Especially I would like to thank Satoko for help and teaching, Franzi Götschel, Jing Shi, and Si-Hong Luu for all the funny moments we had in the fly room. Stephan, thank you for the scientific discussions, your help and friendship during the last three years. Our great adventures on the PhD retreat, in the Postalmklamm and around Kochel will be unforgettable.

Thanks to Jörg Polakowski for introducing me to the illustrator world. Also on a personal level, thank you for your constant support and the patient analytical examination of my problems and worries.

Ein ganz großes Dankeschön gilt meiner Familie, insbesondere meinen Eltern. Ohne eure Unterstützung und euer Veständnis wäre ich sicherlich nicht so weit gekommen.

Curriculum vitae

Personal Details

Name: Tatiana Tomasi
E-mail: t.tomasi@gmx.de
Date of birth: 19.03.1980
Place of birth: Rosenheim, Germany

Education

April 2005 – present	Ph.D. thesis in the laboratory of Dr. Takashi Suzuki (Axon Guidance and Neuronal Connectivity) at the Max-Planck-Institute of Neurobiology, Martinsried, Germany Title: The transmembrane protein Golden goal regulates retinal axon guidance in *Drosophila*
Nov. 2003 – Aug. 2004	Diploma thesis in the laboratory of Dr. Barbara Conradt at the Dartmouth Medical School, Hanover (NH), USA Title: Identification and characterization of genes involved in the specification of the sexually dimorphic CEMs in *C. elegans*
Nov. 1999 – Aug 2004	Diploma in Biology at the LMU, Munich, Germany Major subject: Cell biology Minor subjects: Genetics, Biochemistry and Ecology

Scientific communications and publications

- Tomasi, T., Hakeda-Suzuki, S., Ohler, S., Schleiffer, A., and Suzuki, T. (2008). The transmembrane protein Golden goal regulates R8 photoreceptor axon-axon and axon-target interactions. Neuron *57*, 691-704.
- Annual *Drosophila* Research Conference, Philadelphia (USA), 2007
- European *Drosophila* Research Conference, Vienna (Austria), 2007)
- CSHL Neurobiology of *Drosophila* meeting, Cold Spring Harbor (USA), 2007